

**Space Exploration Challenges:
Characterization and Enhancement of Space Suit Mobility and
Planetary Protection Policy Analysis**

by

Bradley Thomas Holschuh

B.S., Aerospace Engineering
Massachusetts Institute of Technology, 2007

Submitted to the Department of Aeronautics and Astronautics and the Engineering Systems Division
in Partial Fulfillment of the Requirements for the Degrees of

**Master of Science in Aeronautics and Astronautics
and
Master of Science in Technology and Policy**

at the
Massachusetts Institute of Technology
June 2010

©2010 Massachusetts Institute of Technology. All rights reserved.

Author
Department of Aeronautics and Astronautics and Engineering Systems Division
May 10, 2010

Certified by
Dava J. Newman, Ph.D.
Professor of Aeronautics and Astronautics and Engineering Systems
Thesis Supervisor

Accepted by
Dava J. Newman, Ph.D.
Professor of Aeronautics and Astronautics and Engineering Systems
Director, Technology and Policy Program

Accepted by
Eytan H. Modiano, Ph.D.
Associate Professor of Aeronautics and Astronautics
Chair, Committee on Graduate Studies

Space Exploration Challenges: Characterization and Enhancement of Space Suit Mobility and Planetary Protection Policy Analysis

by

Bradley Thomas Holschuh

Submitted to the Department of Aeronautics and Astronautics and the Engineering Systems Division on May 10, 2010 in Partial Fulfillment of the Requirements for the Degrees of Master of Science in Aeronautics and Astronautics and Master of Science in Technology and Policy

ABSTRACT

This thesis addresses two challenges associated with advanced space and planetary exploration: characterizing and improving the mobility of current and future gas-pressurized space suits; and developing effective domestic Planetary Protection policies for the emerging private space industry.

Gas-pressurized space suits are known to be highly resistive to astronaut movement. As NASA seeks to return to planetary exploration, there is a critical need to improve full-body space suit mobility for planetary exploration. Volume effects (the torque required to displace gas due to internal volume change during movement) and structural effects (the additional torque required to bend the suit materials in their pressurized state) are cited as the primary contributors to suit rigidity. Constant volume soft joints have become the design goal of space suit engineers, and simple joints like the elbow are believed to have nearly achieved such performance. However, more complex joints like the shoulder and waist have not yet achieved comparable optimization. As a result, it is hypothesized that joints like the shoulder and waist introduce a third, and not well studied, contributor to space suit rigidity: pressure effects (the additional work required to compress gas in the closed operating volume of the suit during movement).

This thesis quantifies the individual contributors to space suit rigidity through modeling and experimentation. An Extravehicular Mobility Unit (EMU) space suit arm was mounted in a -30kPa hypobaric chamber, and both volume and torque measurements were taken versus elbow angle. The arm was tested with both open and closed operating volumes to determine the contribution of pressure effects to total elbow rigidity. These tests were then repeated using a full EMU volume to determine the actual impact of elbow pressure effects on rigidity when connected to the full suit. In both cases, structural and volume effects were found to be primary contributors to elbow joint rigidity, with structural effects dominating at low flexion angles and volume effects dominating at high flexion angles; pressure effects were detected in the tests that used

only the volume of the arm, but were found to be a secondary contributor to total rigidity (on average < 5%). These pressure effects were not detected in the tests that used the volume representative of a full EMU. Unexpected structural effects behavior was also measured at high (> 75°) flexion angles, suggesting that the underlying mechanisms of these effects are not yet fully understood, and that current models predicting structural effects behavior do not fully represent the actual mechanisms at work. The detection of pressure effects in the well-optimized elbow joint, even if only in a limited volume, suggests that these effects may prove significant for sub-optimized, larger, multi-axis space suit joints. A novel, fast-acting pressure control system, developed in response to these findings, was found to be capable of mitigating pressure spikes due to volume change (and thus, pressure effects). Implementation of a similar system in future space suit designs could lead to improvements in overall suit mobility.

A second study, which focused on the implications of the development of the US private space industry on domestic Planetary Protection policy, is also presented. As signatories of the 1967 Treaty on Principles Governing the Activities of States in the Exploration and Use of Outer Space (commonly known as the Outer Space Treaty), the United States is responsible for implementing Planetary Protection procedures designed to prevent biological contamination of the Solar System, as well as contamination of the Earth by any samples returned from extra-terrestrial bodies. NASA has established policies and procedures to comply with this treaty, and has successfully policed itself independently and autonomously since the signing of the treaty. However, for the first time in the history of the American space program, private entities outside of NASA have developed the capability and interest to send objects into space and beyond Earth orbit, and no current protocol exists to guarantee these profit-minded entities comply with US Planetary Protection obligations (a costly and time-consuming process). This thesis presents a review of US Planetary Protection obligations, including NASA's procedures and infrastructure related to Planetary Protection, and based on these current protocols provides policy architecture recommendations for the emerging commercial spaceflight industry. It was determined that the most effective policy architecture for ensuring public and private compliance with Planetary Protection places NASA in control of all domestic Planetary Protection matters, and in this role NASA is charged with overseeing, supporting, and regulating the private spaceflight industry. The underlying analysis and architecture tradeoffs that led to this recommendation are presented and discussed.

Thesis Supervisor: Dava J. Newman

Title: Professor of Aeronautics and Astronautics and Engineering Systems; Director, Technology and Policy Program

Acknowledgements

MIT students love to pretend that their education is a battle against a faceless, relentless and unforgiving Institute located at 77 Massachusetts Avenue. The stomping grounds of Cambridge at times may feel like a theater of war, a constant rally against the seemingly unending onslaught of problem sets, projects, and the *dreaded* humanities requirement. Through an almost super-human propensity for productivity without adequate sleep, MIT students emerge from their time at the Institute with a sense of genuine victory, having slayed the beast and overcome the odds. And a funny thing tends to happen sometime during all that tooling and toiling – that battlefield, littered with punted problem sets and empty cans of highly caffeinated (and other) beverages, somehow becomes “home”.

Most will remember their time in Cambridge as a grueling but incredibly rewarding experience. For many undergrads, the title of “MIT Engineer” is rightfully earned in a whirlwind four years, at which point the Institute training grounds are usually abandoned for entirely new and formidable challenges. For the rest of us who choose to continue to call MIT home and fight the good fight as graduate students, the experience cannot be (and certainly is not) undertaken alone. Without the support and camaraderie of several individuals, Act II (years 5-7) of my battle might very well have been lost (or at least would have been far less enjoyable). I am thus forever indebted to several people for helping me through the trenches, each of whom has played an integral role not only in the professional development of this 3-year research effort, but also in the substantial growth I have experienced both as an engineer and as a person:

First and foremost I must thank my advisor (and mentor, and teacher), **Dava Newman**, for allowing me the academic freedom to explore new and interesting research ideas and for supporting me personally, professionally, and financially along the way. Her insights and guidance have helped transform me from a timid undergraduate to a seasoned researcher and experimentalist, and her perpetual energy and positive outlook have taught me to have confidence in myself and to always see the big picture in life. Without her generous support I would have never had the opportunity to fly weightless last summer, which was an experience I will absolutely never forget. And I am also forever grateful that she took the time to expose me to the Technology and Policy Program, in which I ultimately enrolled as a dual degree student: my participation in TPP has helped me grow as an engineer, as a policymaker, and as a leader, and has given me the chance to interact with a group of incredibly passionate, smart, and all-around fantastic individuals. None of this would have happened without her influence and support.

James Waldie, my friend and mentor, cannot be adequately thanked in only few lines of text. In addition to providing the foundational ideas for much of my professional work (including the original design of the prototype active pressure regulation system), he was right by my side in the trenches every day, helping me with everything from hardware design and fabrication to data collection and analysis. More importantly, though, he was a great friend: inviting me into his home; staying up late to play “stupid” video games; teaching me the nuances of Australian-New Zealand relations; and exposing me to the heaven incarnate otherwise known as Tim-Tams. If it weren’t for him I would have

never appeared on the Australian Nightly News donning a blue-power-ranger spandex suit, or found a justifiable way to incorporate arm-length veterinary latex gloves into space suit research, or had the memorable experience of midnight ghost-hunting in the basement of an unknown Savannah, GA, hotel. He also provided me with invaluable life advice during some pretty difficult times, and for that I will be forever grateful. James: expect a call the first time I finally set foot on your foreign soil.

Jeffrey Hoffman, who helped me craft this project from a series of loose concepts into a rigorous research effort, also deserves considerable credit. His advice and suggestions, based on his extensive experience as a 5-time shuttle astronaut, provided me with very real and practical information that helped me understand the issues related with human space exploration. Hearing his amazing (and entertaining!) experiences from the astronaut corps motivated and inspired me as I worked on this project, and his willingness to meet with me as often as necessary in the early stages proved invaluable in getting this project off the ground.

A substantial portion of the work presented here was completed over the summers of 2008 and 2009. I was financially supported over those summers by fellowships provided by the **Massachusetts Space Grant Consortium**, and I am very thankful for this support. Jeff Hoffman and **Helen Halaris** helped to make this support possible, so I owe them both a huge thank you for this as well.

Several industry experts provided me with guidance and support along the way, and without their help this project would not have been possible. **Ed Hodgson** and **Steve Dionne** at Hamilton-Sundstrand provided me with invaluable feedback as I struggled to identify the specific space suit problem I wanted to tackle, and also graciously loaned their actual space suit hardware to our lab for nearly a year and a half. Without their advice and their hardware (and their patience...), this study simply would not have happened. **Gary Harris**, whom I met at the 2009 ICES conference, graciously took the time to share his wisdom about the nuances of space suit garment design, and provided specific insight that helped me understand a phenomenon in my data that otherwise could have derailed my entire analysis. And **Karen Buxbaum**, with whom I serendipitously crossed paths thanks to her unique connection to MIT's TPP program, willingly spent her limited time to allow me to pick her brain on all things Planetary Protection, and also went above and beyond in subsequent weeks to connect me with important and difficult to reach individuals at NASA. My policy analysis would be substantially incomplete without her insight and recommendations.

Members of the constantly-evolving 16.62x faculty, including **Ed Greitzer**, **Sheila Widnall**, **Moe Win**, and **Jennifer Craig** deserve enormous thanks for allowing me to long overstay my welcome as Teaching Assistant for the class (now going on year 4...). Not only has this continued financial support made my graduate studies possible, but the opportunities I have had to work with (and learn from) each of them have been incredibly rewarding. They have helped me grow as a teacher and as a researcher, and my involvement in helping run the course has provided me with a welcome change of pace from the standard graduate student responsibilities. And in particular, I owe my

continued involvement with the course (and thus my ability to afford graduate school) to **Ian Waitz**, who after hearing about my struggles to find graduate school funding three years ago took it upon himself to ensure I was taken care of by specifically creating this graduate TA position and offering it to me. He certainly did not have to take such a personal interest in helping me, but I am forever grateful that he chose to do so. I will never forget the advice he gave me the day that he unexpectedly called me into his office to inform me of this perfect opportunity: he told me that there are many situations in life (including this one) where I would benefit by taking a little extra time to think things over, even if I thought I knew what I wanted immediately (and he forced me to wait 24 hours to give him a decision, even though I knew my answer the moment he made the offer). Rest assured his willingness to serve as a mentor and role model to me (in addition to serving as a professor and colleague) did not go unappreciated.

Todd Billings, **Dave Robertson**, and **Dick Perdichizzi** deserve special thanks for continuing for put up with me long after their official obligation to do so ended. Not only do they spice up the daily 62x experience, but they have time and again selflessly volunteered their energy and resources to help me with whatever design or fabrication problems I've come across as a graduate student (like helping my colleagues and I build a rig to break the world record for most rotations hanging from a power drill...). I just feel bad that they're stuck with me for another 3+ years.

From the TPP side of things, **Sydney Miller** and **Frank Field** deserve recognition for their tireless efforts both to educate me as a policy maker and to keep me on task and on schedule as a dual-degree student. They've made my TPP experience all the more memorable, and their efforts to ensure that I actually graduate are greatly appreciated. Similar recognition is certainly deserved for members of the Aero-Astro support staff, with whom I regularly interact: **Sally Chapman**, **Liz Zotos**, **Barbara Lechner**, **Marie Stuppard**, and **Beth Marois**.

It would perhaps be the understatement of the century to say that my graduate student experience has been improved by **my fellow lab mates at the MVL**. There are far too many of them to name, but suffice it to say that our shared experiences (everything from Warfish to Rock Band to beer brewing) will likely be what I remember and cherish most about my years as a graduate student at MIT. I look forward to the next several years of PhD study knowing that so many of them will be here with me.

Additionally, **Linnette Rivera**, a highly motivated visiting undergraduate student whom I had the pleasure of mentoring over the summer of 2009, deserves recognition for her help in creating many of the CAD models that appear in this document. Linnette: you have great potential, and I sincerely hope to cross paths with you again in the future.

I owe a large component of my continued sanity to the **MIT Varsity Ice Hockey program**, and in particular to Coaches (and brothers) **Mark**, **Jimmy**, and **Froggy O'Meara**. Through their dedication I learned much about the game of hockey, and thanks to them I had access to a fantastic outlet that I was able to use to escape from the daily stresses of MIT. Above and beyond the game of hockey, though, they helped me

grow as a man, and have given me far more than any other coach I've ever had (including the opportunity to help run the team on which I used to play). O'Mearas: thank you for the energy you have devoted to make the program what it is today, and for putting up with self-proclaimed nerd-athletes like me even though at times we make your life considerably more stressful.

To my partner in crime, Anna: you kept me going even when you probably didn't realize it. Thanks for everything – I couldn't have done this without you.

And last but certainly not least, my parents (Lee & Karin), my brothers (Jeff & Nick) and my grandparents (Reg & Lorine, and Jerry & Chris), deserve final recognition. There is not much that I can say to do justice to everything that you have done for me. Suffice it to say that I love you all very much, and you are the collective reason I am where I am today. This thesis is dedicated to you.

Ad Astra Per Aspera

Biographical Note

Bradley Holschuh was born in 1985 in Fargo, North Dakota. He was raised not far from there, across the Red River, in Moorhead, Minnesota. In 2003 he left the Midwest to attend the Massachusetts Institute of Technology in Cambridge, Massachusetts, graduating in 2007 with a Bachelor of Science degree in Aerospace Engineering with dual minors in Psychology and Earth, Atmospheric, & Planetary sciences. He spent the summer of 2006 participating in the NASA Academy program at the Goddard Space Flight Center (GSFC). He returned to MIT upon completing his undergraduate degree in the fall of 2007 to begin graduate study as a dual Master of Science degree candidate in Aeronautics and Astronautics, and Technology and Policy. As a graduate student, he served as Teaching Assistant for 16.62x for three academic years (2007-2010). Upon graduation he intends to continue studying in the MIT Aero/Astro department, working towards a PhD in the field of Aerospace Biomedical and Life Support Engineering.

Table of Contents

LIST OF ACRONYMS / DEFINITIONS	17
THESIS AIMS, FORMAT AND STRUCTURE	18
GAS-PRESSURIZED SPACE SUIT MOBILITY BACKGROUND, PREVIOUS WORK, AND MODELING	19
1.1 – INTRODUCTION	21
1.1.1 – Background	21
1.1.2 – Motivation and Objective	23
1.2 – LITERATURE REVIEW & PREVIOUS WORK	25
1.2.1 – Gas-Pressurized Space Suit History and Mobility Tradeoffs	25
1.2.2 – Mechanical Counter-Pressure to Improve Astronaut Mobility	29
1.2.3 – Descriptive Assessments of Suit Rigidity	30
1.2.4 – Physical Modeling of Suit Rigidity Components	31
1.2.5 – Summary	34
1.3 – LIMITATIONS OF PREVIOUS WORK & OPEN QUESTIONS	35
1.3.1 – Pressure, Volume, and Structural Effects Nomenclature	36
1.3.2 – Volume vs. Pressure Effects	37
1.4 – MODELING EFFORTS	38
1.4.1 – Isentropic Compression Model	38
1.5 – EXPERIMENTAL ASSESSMENT OF THEORY	41
1.5.1 - Characterization of the Components to Gas-Pressurized Space Suit Joint Rigidity	41
1.5.2 – Active Pressure Regulation as a Method to Improve Gas-Pressurized Space Suit Mobility	41
EXPERIMENTAL CHARACTERIZATION OF STRUCTURAL, VOLUME AND PRESSURE COMPONENTS TO GAS-PRESSURIZED SPACE SUIT JOINT RIGIDITY	43
2.1 - INTRODUCTION	45
2.1.1 - Conceptual Overview of Joint Torque Experiment	46
2.1.2 - Hypotheses	47
2.1.3 - Objectives	47
2.2 - EXPERIMENTAL HARDWARE AND SETUP	48
2.2.1 - Class III EMU Space Suit Arm Specimen and Hardware	48
2.2.2 - MVL Vacuum Chamber	49
2.2.3 - EMU Space Suit Arm Articulation Rig	51
2.2.4 – Space Suit Angle Measurement	56
2.2.5 - Torque Measurement	58
2.2.6 - Hardware Integration	59
2.3 - EXPERIMENTAL TEST PLAN AND METHODS	60
2.3.1 - Test Plan Overview	60

2.3.2 - Test Method 1: Unpressurized Arm Torque Tests	63
2.3.3 - Test Method 2: Pressurized, Open Volume Torque Tests	64
2.3.4 - Test Method 3: Pressurized, Closed Volume (Arm Only) Torque Tests	64
2.3.5 - Test Method 4: Pressurized, Closed Volume (Arm + Dummy Volume) Torque Tests	66
2.3.6 - Test Method 5: Pressurized, Uncapped Δ Volume Water Tests	67
2.4 - RESULTS	69
2.4.1 - Test 1: Unpressurized Elbow Flexion Torque vs. Angle Test	69
2.4.2 - Test 2: Pressurized, Open Volume Torque vs. Angle Test	70
2.4.3 - Test 3: Pressurized, Closed Volume (Arm only) Torque vs. Angle Test	72
2.4.4 - Test 4: Pressurized, Closed Volume (Arm + Dummy Volume) Torque vs. Angle Test	75
2.4.5 - Test 5: Pressurized, Uncapped Δ Volume Water Tests	81
2.4.6 - Structural, Volume, and Pressure Components to total Rigidity	83
2.5 – DISCUSSION	87
2.5.1 - Hypothesis Assessment and Conclusions	92
2.5.2 - Limitations	94
2.5.3 - Future Work	95
ACTIVE PRESSURE REGULATION AS A METHOD TO IMPROVE GAS-PRESSURIZED SPACE SUIT MOBILITY	97
3.1 - INTRODUCTION	99
3.1.1 - Conceptual Overview of Active Pressure System Experiment	100
3.1.2 - Hypothesis	101
3.1.3 - Objectives	101
3.2 – PRESSURE REGULATION ARCHITECTURE	102
3.2.1 – Pressure Regulation System Design Requirements	102
3.2.2 – Active Pressure Regulation Prototype Concept	102
3.3 – PROTOTYPE DEVELOPMENT	106
3.3.1 – Primary Chamber, HPR, and LPR Construction	106
3.3.2 – Plumbing	107
3.3.3 – HPR-LPR Pump	107
3.3.4 – Sensing and Control Architecture	107
3.3.5 – Pressure Sensors	109
3.3.6 – Solenoid Valves	111
3.3.7 – Solid State Relays	112
3.3.8 – DC Power Supplies	114
3.3.9 – Data Acquisition/Control Architecture	114
3.3.10 – Data Acquisition Board (DAQ)	115
3.3.11 – MATLAB Data Acquisition Toolbox and Simulink Modeling	116
3.3.12 – Vacuum Pump and Air Compressor	119
3.3.13 – System Integration	119
3.4 - EXPERIMENTAL TEST PLAN AND METHODS	120
3.4.1 – System Initialization and Calibration	120
3.4.2 – Syringe for Precise Primary Chamber Volume Change Control	120
3.4.3 - Test Plan Overview	121
3.4.4 - Test Method 1: Volume Change with No Regulation	122
3.4.5 - Test Method 2: Volume Change with Active Regulation	123
3.4.6 - Test Method 3: Multiple Volume Changes with Active Regulation	124
3.4.7 - Test Method 4: Multiple Volume Changes with Active Regulation, Reduced Stroke Speed	125

3.5 - RESULTS	126
3.5.1 - Test 1: Volume Change with No Regulation	126
3.5.2 - Test 2: Volume Change with Active Regulation	127
3.5.3 - Test 3: Multiple Volume Changes with Active Regulation	129
3.5.4 - Test 4: Multiple Volume Changes with Active Regulation, Reduced Stroke Speed	129
3.6 – DISCUSSION	132
3.6.1 - Hypothesis Assessment and Conclusions	134
3.6.2 – Limitations	135
3.6.3 - Future Work	136
US PLANETARY PROTECTION POLICY ANALYSIS FOR THE PRIVATE SPACEFLIGHT INDUSTRY	137
4.1 – INTRODUCTION	139
4.1.1 – Legal Basis for US Planetary Protection Obligations	140
4.1.2 – Categories of Planetary Protection	141
4.1.3 – Research Motivation	142
4.1.4 – Private Obligation to Uphold International Commitment	146
4.1.5 – Problem Statement	147
4.1.6 – Research Questions and Intended Audience	147
4.1.7 – Research Methods and Assumptions	148
4.2 – NASA PLANETARY PROTECTION METHODS	149
4.2.1 – Probabilistic Approach to Planetary Protection	149
4.2.2 – NASA Planetary Protection Methods	150
4.2.3 – NASA Planetary Protection Workforce	153
4.2.4 – European Planetary Protection Methods	154
4.2.5 – Analysis and Summary	155
4.3 – POLICY ARCHITECTURE ANALYSIS	156
4.3.1 – Policy Options and Metrics of Interest	156
4.3.2 – Policy Evaluation: NASA and the Private Sector Operate Autonomously	158
4.3.3 – Policy Evaluation: NASA Controls All Domestic Planetary Protection Efforts	161
4.3.4 – Policy Evaluation: NASA and the Private Sector are both Subject to External Review	164
4.4 – CONCLUSIONS	167
4.4.1 – Limitations and Recommendations for Future Work	168
THESIS SUMMARY AND CONTRIBUTIONS	170
APPENDICES	172
BIBLIOGRAPHY	189

Table of Figures

Figures 1a-b: Gas-pressurized space suits from the Apollo Program (A7L suit) and Shuttle Program (Extravehicular Mobility Unit, or EMU) taken from (NASA, 1969) and (NASA, 2009).....	22
Figures 2a-b: The XH-5 suit (with convolute elbow hip and knee joints) and Apollo A7LB suit (with convolute knee, elbow and thigh joints) taken from (Kozloski, 1994)	26
Figures 3a-b: The AX-2 suit (1968) and AX-5 suit (1988), which utilize hard joint segments separated by bearings to maintain constant volume during movement, taken from (Kozloski, 1994) (NASA, 1988)	27
Figures 4a-c (Clockwise from Top Left): The EMU HUT, EMU waist bearing and knee joints, and EMU shoulder and elbow joints, taken from (NASA, 2008).....	28
Figures 5a-b: MIT BioSuit™ concept and physical mock-up (photo credits: Dava Newman, Guillermo Trotti, Dainese, Donna Coveny)	29
Figure 6: EMU elbow and shoulder torque vs. angle data, taken from (Dionne, 1991)	30
Figure 7: EMU elbow torque vs. angle data, compared to the Beam Model, taken from (Schmidt, 2001) .	33
Figure 8: EMU elbow torque vs. angle data, compared to the Membrane Model, taken from (Schmidt, 2001).....	33
Figure 9: Pressure and Volume Effects in a hypothetical compression.....	37
Figure 10: One of two Class III EMU arm section provided by Hamilton Sundstrand (pictured with glove attached).....	48
Figures 11a-c (clockwise from left): EMU shoulder housing unit, shoulder housing unit cap, and EMU arm with wrist bearing plug (all pieces shown in gold)	49
Figure 12: MIT MVL vacuum chamber	50
Figure 13: Side-view schematic of the shoulder housing unit/vacuum chamber seal configuration (not to scale).....	51
Figure 14: Isometric- and top-view model of the EMU elbow articulation rig	53
Figure 15: Top-view schematic of the EMU Elbow Articulation Rig inside the MVL vacuum chamber (not to scale).....	54
Figure 16: Front and top view of the wrist plate attached to the wrist bearing plug and mounted on the brace rails on an EMU arm, respectively	55
Figure 17: Short and long radius angular scales on the MVL vacuum chamber (with forearm brace flexed to 90° visible in the background).....	57
Figure 18: Electronic torque wrench configured to the EMU articulation rig.....	58
Figure 19: Example of final hardware integration, with arm shown flexed between 75-90°	59

Figure 20: Unpressurized Arm Torque Test.....	63
Figure 21: Pressurized, open volume torque test (left).....	65
Figure 22: Pressurized, closed volume torque test (right).....	65
Figure 23: Pressurized, closed volume (arm + dummy volume) torque test.....	66
Figures 24a-c (clockwise from top left): Engineer measuring the total water required to fill the arm at 25° flexion; close-up views of the protective lining and leveling tool used to determine exact water levels at each angle.....	68
Figure 25: Baseline torque vs. angle of the arm/rig in its unpressurized state.....	69
Figure 26: Total torque vs. angle of the arm in its pressurized and open volume state, with gravity effects removed.....	70
Figure 27: Previous total torque vs. angle test of the EMU elbow in its pressurized state, conducted by MVL researchers, taken from (Schmidt, 2001).....	71
Figure 28: Total torque vs. angle of the arm in its pressurized and closed volume state, with gravity effects removed.....	72
Figure 29: Comparison of total torque vs. angle of the arm in its pressurized and open/closed volume states, with gravity effects removed.....	73
Figure 30: Magnification of the regime where pressure effects become significant in the pressurized, closed volume (arm only) EMU elbow.....	74
Figure 31: Test 2 data comparison between 6/08 and 6/09 tests, with gravity effects removed.....	75
Figure 32: Test 3 data comparison between 6/08 and 6/09 tests, with gravity effects removed.....	77
Figure 33: Repeat comparison of total torque vs. angle of the arm in its open and closed volume states, using 6/09 data, with gravity effects removed.....	78
Figure 34: Total torque vs. angle of the arm in its pressurized and closed volume state representative of a full EMU, with gravity effects removed.....	80
Figure 35: Comparison of total torque vs. angle of the arm in its pressurized and open/closed volume states, based on data from 6/09 tests with a representative EMU volume, with gravity effects removed.....	80
Figure 36: Pressurized EMU arm internal volume as a function of angle.....	82
Figure 37: Individual torque components vs. angle (closed volume, arm only), with gravity effects removed.....	84
Figure 38: Individual torque components vs. angle (closed volume, arm + pipe), with gravity effects removed.....	85
Figure 39: Hypothetical convolute joint in pressurized form (side view).....	89
Figure 40: C_p and restraint layer equilibrium in steady-state, pressurized form.....	90

Figure 41: Initial convolute deformation during small flexion, resulting in net torque acting in the opposite direction of flexion.....	90
Figure 42: Continued convolute deformation during moderate flexion, resulting in diminished net torque acting in the opposite direction of flexion.....	91
Figure 43: Significant convolute deformation during extreme flexion, resulting in net torque acting in the same direction of flexion as the C_p crosses the restraint layer threshold.....	91
Figure 44: Active pressure regulation system concept	103
Figure 45: System response to pressure increases due to volume reduction	104
Figure 46: System response to pressure decreases due to volume increase.....	104
Figure 47: System reservoir sustainability using an in-line pressure pump.....	105
Figure 48: Primary chamber, constructed from Schedule 40 PVC pipe.....	106
Figure 49: HPR and LPR, constructed from Schedule 40 PVC pipe.....	107
Figure 50: Sensing and control architecture block diagram	108
Figure 51: PX240A series pressure sensor, taken from (Omega.com, 2008).....	110
Figure 52: SV3300 series solenoid valve, taken from (Omega.com, 2008)	111
Figure 53: Example of a Crydom solid state relay, taken from (Digi-Key, 2008)	113
Figure 54: Solid state relay wiring configuration	113
Figure 55: USB-1408FS DAQ board from Measurement Computing Corp., taken from (Measurement Computing, 2008)	115
Figures 56a-h: Catalog of pertinent Simulink control blocks	118
Figure 57: Final Simulink control diagram	118
Figure 58: Fully integrated pressure regulation system prototype.....	119
Figure 59: 600 cm ³ syringe used for precise control of changes in internal volume (with the primary chamber visible at the bottom of the image).....	120
Figure 60: Pressure vs. time of the primary chamber without active regulation	126
Figure 61: Pressure vs. time of the primary chamber with active regulation	127
Figures 62a-b: Pressure vs. time of the HPR and LPR during active regulation	128
Figures 63a-c: Primary chamber, HPR and LPR pressure vs. time for 770 cm ³ /s stroke rate compression cycles (test 3)	130
Figures 64a-c: Primary chamber, HPR and LPR pressure vs. time for 210 cm ³ /s stroke rate compression cycles (test 4)	131

Figure 65: Relationship of 770 cm ³ /s stroke to HPR and LPR system activation for one cycle, leading to single large spike behavior (test 3).....	133
Figure 66: Relationship of 210 cm ³ /s stroke to HPR and LPR system activation for one cycle, leading to multiple small spike behavior (test 4).....	133
Figure 67: Orbital Sciences Taurus II and SpaceX Falcon 9 launch vehicles, designed to provide commercial access to space (photo credit: Orbital Sciences Corp., 2010, and SpaceX Corp., 2010)	143
Figure 68: Predicted growth of passenger demand for suborbital space tourism, taken from “Suborbital Space Tourism Revisited” (Futron Corp, 2006).....	144
Figure 69: Dry-heat sterilization of a Viking Lander (photo credit: NASA, 2008).....	151
Figure 70: Schematic of a proposed policy architecture where NASA and the private sector each independently and autonomously oversee their respective Planetary Protection responsibilities.....	158
Figure 71: Schematic of a proposed policy architecture where NASA controls all domestic Planetary Protection efforts.....	161
Figure 72: Schematic of a proposed policy architecture where NASA and the private sector are both subject to external Planetary Protection review.....	164

Table of Tables

Table 1: Relative magnitude of pressure and volume effects as a function of volume compression ratio for a hypothetical isentropic and adiabatic compression	40
Table 2: Articulation rig increments.....	56
Table 3: Assumed Torque Effects Present at Each Test Condition	61
Table 4: Test Matrix for EMU Arm Study	62
Table 5: Statistical analysis of pressure effects in the closed arm volume, with statistically significant values shown in gray.....	74
Table 6: Shift in torque data between 6/08 and 6/09 open volume tests	76
Table 7: Shift in torque data between 6/08 and 6/09 closed volume tests	77
Table 8: Statistical analysis of pressure effects in the closed arm volume based on 6/09 data, with statistically significant values shown in gray.....	79
Table 9: P-values and % change in torque during elbow flexion due to pressure effects in a representative full EMU closed volume	81
Table 10: Summary of pressure, volume, and structural effects as a function of angle for the EMU arm (closed volume, arm-only test condition).....	86
Table 11: Summary of pressure, volume, and structural effects as a function of angle for the EMU arm (closed volume, arm + pipe test condition).....	86
Table 12: Prototype Pressure Regulation System Study Test Matrix.....	122
Table 13: A summary of US policy options regarding NASA-private space Planetary Protection regulatory architectures	168

List of Acronyms / Definitions

DAQ	Data Acquisition
EMU	Extravehicular Mobility Unit
EVA	Extravehicular Activity
HPR	High Pressure Reservoir
ISS	International Space Station
IVA	Intravehicular Activity
LPR	Low Pressure Reservoir
MCP	Mechanical Counter-Pressure
MIT	Massachusetts Institute of Technology
MVL	Man-Vehicle Laboratory
NASA	National Aeronautics and Space Administration
PVC	Polyvinyl Chloride
SSR	Solid State Relay
Pressure Effects	Torque required to compress the internal working gas in the closed operating environment due to volume changes during joint movement
Volume Effects	Torque required to isobarically displace the internal working gas due to volume changes during joint movement
Structural Effects	Torque required to elastically deform the suit fabric wall in its pressurized state
$\tau_{Pressure}$	Torque contribution from Pressure Effects
$\tau_{Structural}$	Torque contribution from Structural Effects
τ_{Volume}	Torque contribution from Volume Effects

Thesis Aims, Format and Structure

This thesis addresses two separate yet equally important challenges associated with current and future space exploration missions. First, an engineering analysis of gas pressurized space mobility is presented, with the specific aim of experimentally isolating and determining the individual contributors to current space suit joint rigidity. Based on the findings of this experimentation, design recommendations are presented to improve and enhance overall suit mobility. Second, a policy analysis of domestic Planetary Protection issues related to private spaceflight is presented, with the specific aim of developing a recommended framework to govern the behavior of new and emerging US private space organizations.

This document is organized into four major sections (3 engineering sections and 1 policy section), outlined below:

Part I – Gas-Pressurized Space Suit Mobility: Background, Previous Work, and Modeling. Part I serves to establish the enhancement of gas-pressurized space suit mobility as a critical engineering challenge as NASA and other agencies prepare for future human planetary exploration missions. Previous work related to the study of space suit mobility, gaps in the current literature, and limitations to current modeling efforts and results are presented.

Part II – Experimental Characterization of Structural, Volume and Pressure Components to Gas-Pressurized Space Suit Joint Rigidity. Part II documents an experiment conducted to specifically isolate and determine the individual components to total gas-pressurized suit rigidity. Motivation, experimental design, results, analysis and discussion of this experiment are presented.

Part III – Active Pressure Regulation as a Method to Improve Gas-Pressurized Space Suit Mobility. Part III presents the design and testing of a proof-of-concept novel active pressure regulation system designed to improve and enhance mobility of current and future gas-pressurized space suits. Recommendations for refinement and further development of this system are also presented.

Part IV – US Planetary Protection Policy Analysis for the Private Spaceflight Industry. Part IV analyzes current Planetary Protection policies in place at both governmental space agencies (like NASA) and the newly emerging private spaceflight sector, and explores the international rules and regulations that dictate these policies. Recommendations for a Planetary Protection policy framework to appropriately govern and regulate new commercial space organizations are presented.

A cumulative summary of research findings and contributions is then presented at the end of this document.



PART I

Gas-Pressurized Space Suit Mobility Background, Previous Work, and Modeling

The sky calls to us. If we do not destroy ourselves, we will one day venture to the stars.

- Carl Sagan

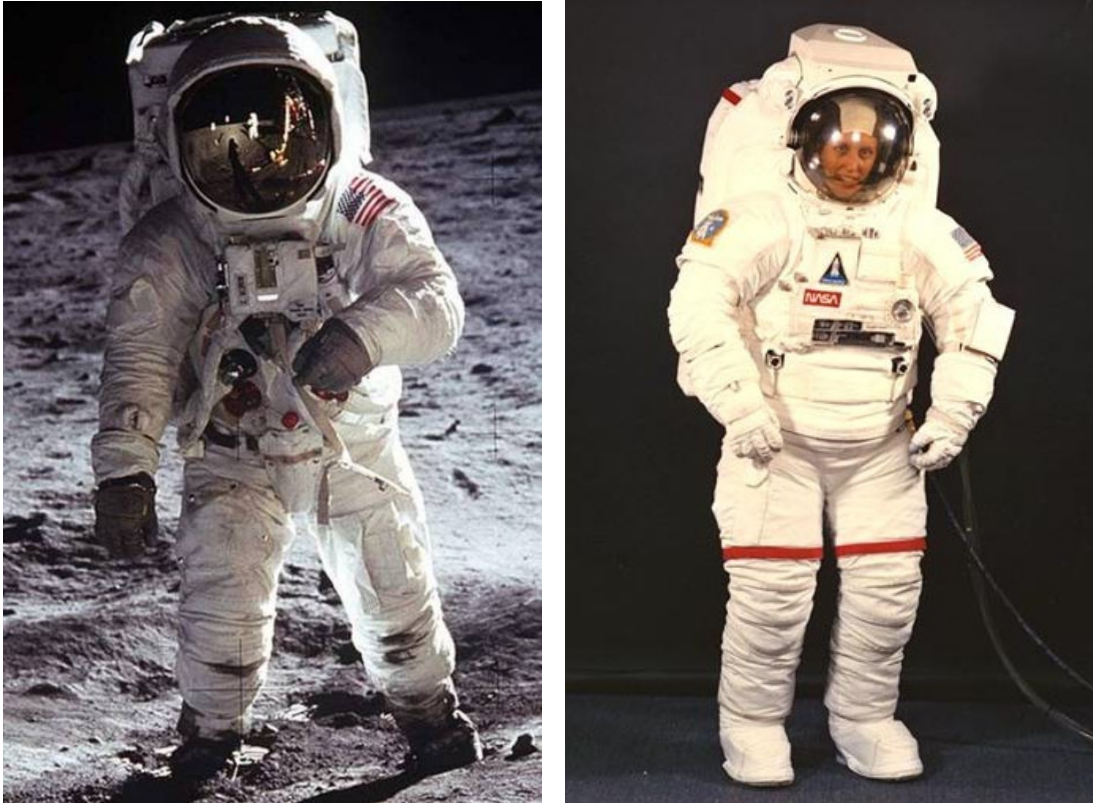
1.1 – INTRODUCTION

1.1.1 – Background

The space environment is a harsh and unforgiving place for humans when compared to the environment on the Earth's surface. Temperatures fluctuate hundreds of degrees between the sun and the shade; dangerous ionizing radiation and micrometeoroids pose a constant threat to astronauts working outside their spacecraft; and the near-perfect vacuum means there is no inherent access to breathable oxygen or counter-pressure against the skin (two physiological necessities for human survival) (Larson, 1999) (Buckey, 2006). Human-rated spacecraft are specifically designed to protect astronauts from these threats, making it possible for astronauts to safely perform tasks within the vehicle (known as Intravehicular Activity, or IVA) without additional protective measures. However, there are several critical tasks that require astronauts to leave the protective shell of the spacecraft and venture into the unforgiving space environment (such as habitat/station construction, repair and maintenance, and in the case of planetary missions, field science and exploration). Because these operations (known as Extravehicular Activity, or EVA) directly expose astronauts to the dangerous vacuum of space, all spacewalkers must don protective space suits if they hope to survive long enough to complete their mission.

Since the first spacewalk performed by Alexi Leonov in 1965, astronauts conducting EVAs have donned suits that rely upon the concept of gas-pressurization to keep the astronaut safe (Skoog et al., 2002). These space suits function by creating an artificial gas environment that surrounds the user, mimicking Earth's atmosphere by providing both a breathable atmosphere and the total pressure normally imparted against the skin by the weight of an atmospheric gas column (i.e. counter-pressure) found on the surface of the Earth. Each space suit is multi-layered to maintain the internal pressure environment and to protect the user from thermal, micrometeoroid and radiation threats posed by the dangerous space environment (Kozloski, 1994). While considerable advances have been made in the field of space suit design since the 1960s (as materials and technologies have matured), the fundamental design concept of gas-pressurization has remained unchanged,

and both the current suit and next-generation suit designed are built around this concept. Two examples of gas-pressurized space suits (from the Apollo and Shuttle eras, respectively) are included as Figures 1a-b.



Figures 1a-b: Gas-pressurized space suits from the Apollo Program (A7L suit) and Shuttle Program (Extravehicular Mobility Unit, or EMU) taken from (NASA, 1969) and (NASA, 2009)

In many ways, the iconic footage of astronaut Neil Armstrong stepping on to the Lunar surface wearing his Apollo A7L suit in 1969 cemented gas-pressurized space suits as a symbol of human space exploration. This association has earned gas-pressurized space suits a special place in popular culture, and their continuing role in current/future space mission architectures suggests this association will continue for the foreseeable future.

1.1.2 – Motivation and Objective

While the primary purpose of the space suit is to keep the astronaut safe, it is also critical that the suit does not prevent the astronaut from physically completing the task at hand. Behind safety, flexibility and mobility are perhaps the most important design considerations for suit engineers (Hodgson, 2008). However, gas-pressurized suits are effectively balloons (they naturally stiffen when pressurized), and as a result tend to oppose any bending motion away from their equilibrium position. To illustrate this concept, imagine bending a long and narrow balloon (like the type used for making balloon animals): the tendency of the balloon is to return to its original position once released from a bent position. This is analogous to the behavior of a gas-pressurized space suit when bent by an astronaut articulating their arms or legs - anytime an astronaut bends his or her joints, the pressurized suit resists this motion (Jordan et al., 2006) (Hoffman, 2008). This is especially critical when considering the fact that astronauts regularly conduct several, multi-hour EVAs on a typical mission: the fatigue resulting from constantly fighting the inflexibility of the suit could potentially affect the astronaut's ability to complete mission/EVA objectives (Newman et al., 1997).

NASA and the newly-emerging private space industry are currently envisioning a return to Lunar/planetary exploration, which will necessarily result in an increase in the number and physicality of astronaut EVAs (Carr, 2001). As a result, the critical need for a highly mobile gas-pressurized space suit increases by an order of magnitude. This problem was expressed in very clear terms by retired Apollo astronauts in a study conducted at NASA Johnson Space Center in September 2007. This study, entitled "The Apollo Medical Operations Project: Recommendations to Improve Crew Health and Performance for Future Exploration Missions and Lunar Surface Operations", interviewed 64% of surviving Apollo astronauts (14 of 22) to identify aspects of the Apollo missions that require improvement before humans attempt to return to the Moon. They recommended, among other things, that general EMU/EVA Suit mobility be increased "by a factor of four". Dr. Richard Scheuring, lead author of the study, noted the sentiment that "the crews often felt they were fighting the resistance in the suit ... this was fatiguing, especially in the thighs" (Scheuring, 2007). An examination of video footage from

Apollo 17, when Dr. Jack Schmitt was upended when trying to pick up a dropped tool because the stiff knee joints in his suit acted like springs when bent, perhaps most perfectly illustrates the mobility issues that plagued the Apollo suits, and still affect the current EMU (NASA, 1972).

The critical need to improve gas-pressurized space suit mobility for future planetary exploration serves as the primary motivation of this thesis. The objective of this work is to build upon previous research on the characterization and enhancement of space suit mobility, with the ultimate goal of providing suit designers with information and design recommendations that might lead to practical improvements in future EVA suit mobility.

1.2 – LITERATURE REVIEW & PREVIOUS WORK

What follows is an examination of the literature surrounding gas-pressurized space suit mobility, including the evolution and tradeoffs of pressure garment design, modeling efforts to characterize and predict the underlying mechanisms that dominate suit rigidity, and recent experimental studies to map the flexibility of current suit designs.

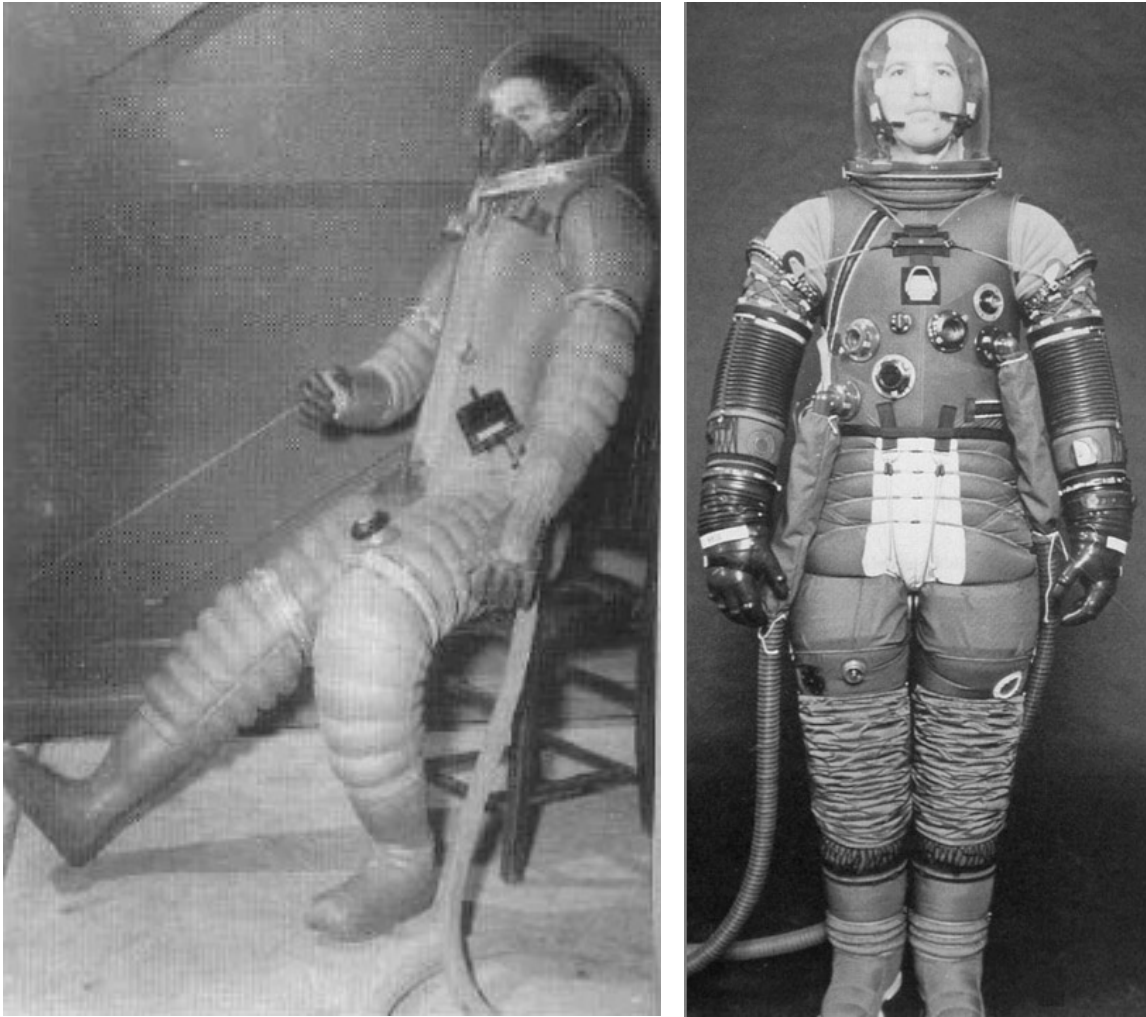
1.2.1 – Gas-Pressurized Space Suit History and Mobility Tradeoffs

The issues related to mobility of gas-pressurized garments have been documented since their inception as high-altitude flight suits in the 1930-40s. It was recognized from the onset on that maintaining constant volume during pressurized joint articulation would be beneficial from a mobility standpoint, based on the fundamental relationship between work (W), pressure (p), and volume (V),

$$W = \int pdV \quad \text{eq. 1}$$

which states that any change in volume necessarily requires that work be done on the surrounding gas (it is for this reason that the EMU is also operated well below atmospheric pressure – space suit joint stiffness has been shown to increase linearly with operating pressure) (Iberall, 1970) (Abramov et al., 1994). One of the earliest practical full-body high-altitude pressure suits constructed for the Army Air Corps, the XH-5 suit developed by B.F. Goodrich Company between 1942-44, was one of the first pressure suits that “allowed the pilot to assume a seated position”, though it was also reported that while in the suit, “movement required extreme effort” (Kozloski, 1994). This suit introduced one of the first significant design breakthroughs in pressurized suit mobility: the convolute joint (a design that is still utilized in suits today). The convolute joint, which resembles an accordion or bellows, includes additional, collapsing material on both the inside and outside of the joint to accommodate the stretching/bunching that takes place when a pressurized soft cylinder is bent. Because these joints more closely maintain constant volume during movement than non-convolute soft-joints, they

theoretically enable suits to be built with soft materials while avoiding many of the mobility issues associated with soft-material pressure suits. Images of the XH-5 suit and the Apollo A7LB suit, both of which incorporated convolute joints, are included as Figures 2a-b. Soft-convolute joints have evolved considerably since their inclusion in these early suits, and are still utilized today: the current EMU incorporates advanced soft-convolute joint designs in both the elbow and the knee.



Figures 2a-b: The XH-5 suit (with convolute elbow hip and knee joints) and Apollo A7LB suit (with convolute knee, elbow and thigh joints) taken from (Kozloski, 1994)

While soft-fabric convolute joints offer a partial solution to gas-pressurized suit mobility issues, other radically different designs have been proposed. If maintaining constant volume is considered highest priority, such behavior can be easily achieved using hard

joint segments connected with rotating bearings (Kozloski, 1994) (Newman et al., 2001). Hard joint designs perfectly maintain constant volume, because joint movement is achieved solely by moving the suit segments relative to one another along the bearing interface (no soft material exists, thus no buckling or crumpling takes place to cause changes in the internal suit volume). Example experimental suits that incorporate this design concept are included as Figures 3a-b.



Figures 3a-b: The AX-2 suit (1968) and AX-5 suit (1988), which utilize hard joint segments separated by bearings to maintain constant volume during movement, taken from (Kozloski, 1994) (NASA, 1988)

While hard suits succeed in maintaining constant volume, they are considerably more massive than soft-suits, which may cause additional mobility issues if used for planetary

exploration. Further, they can be uncomfortable for the wearer, requiring additional padding to prevent injury due to contact with the suit (Newman et al., 2001).

Engineers must then consider the tradeoff that exists between soft and hard joints when creating new suit designs, as this decision affects overall system mass, flexibility, and comfort. And because each human body joint differs in terms of strength, flexibility, and degrees-of-freedom, an optimal suit may include both hard and soft joints strategically designed to accommodate each joint and its respective functions and limitations. The current EMU design uses soft limb segments connected to a rigid upper torso: this torso segment is made from hard fiberglass (known as the Hard Upper Torso, or HUT); the shoulder and waist joints connect to the HUT using rotational bearings; and the knee and elbow joints are soft convolute joints, and connect to the shoulder and hip bearings. These components of the EMU are shown below as Figures 4a-c.



Figures 4a-c (Clockwise from Top Left): The EMU HUT, EMU waist bearing and knee joints, and EMU shoulder and elbow joints, taken from (NASA, 2008)

1.2.2 – Mechanical Counter-Pressure to Improve Astronaut Mobility

As an alternative to gas-pressurized space suits, mechanical counter-pressure (MCP) space suit designs have been proposed as a fundamentally different way of protecting the astronaut in space, and these suits are especially promising from a mobility standpoint. As the name implies, MCP suits create the necessary pressure on the skin mechanically (i.e. with tightly stretched material), rather than through a pressurized gas (Annis et al, 1971). As a result of this fundamental design difference, these skin suits avoid all of the mobility problems associated with gas-pressurized suits – there is no gas against which the astronaut has to work, thus, the “balloon effect” previously described does not exist. Prototypes like the BioSuit™ developed at MIT (shown below as Figures 5a-b), have the potential to revolutionize space suit design (Newman et al., 2001). However, the technologies underlying these suits have not matured to the point where they are operationally feasible (for example, donning and doffing remains a significant challenge). Until these issues are resolved, the less mobile, yet technically- and operationally-proven gas-pressurized suit concept will continue to serve as the standard for space suit design.



Figures 5a-b: MIT BioSuit™ concept and physical mock-up (photo credits: Dava Newman, Guillermo Trotti, Dainese, Donna Coveny)

1.2.3 – Descriptive Assessments of Suit Rigidity

Several studies have been conducted to experimentally assess the rigidity characteristics of gas-pressurized space suits, the majority of which were conducted on the current EMU (Abramov et al., 1994) (Schmidt et al., 2001) (Dionne, 1991) (Menendez et al., 1994) (Morgan et al., 1996). The results of these studies generally agree with each other (similar hysteresis behavior and non-linear torque vs. angle trends were documented in all cases), though discrepancies in torque magnitudes have been documented, and the source of these discrepancies is still unresolved. Typical torque vs. angle data for the EMU elbow and shoulder joints is included as Figure 6.

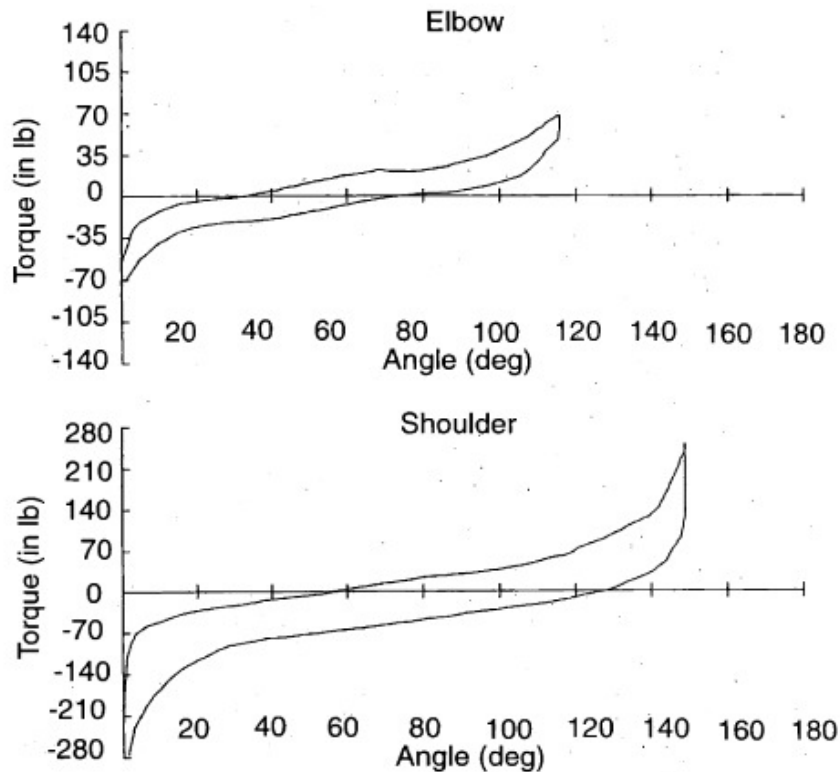


Figure 6: EMU elbow and shoulder torque vs. angle data, taken from (Dionne, 1991)

While these types of study are useful when it comes to characterizing the total rigidity characteristics of the suit, they do not provide much insight into the underlying physical mechanisms that lead to the stereotypical torque vs. angle relationship seen above.

1.2.4 – Physical Modeling of Suit Rigidity Components

Attempts have been made to physically model the underlying mechanisms that contribute to overall gas-pressurized suit rigidity (Corner et al., 1963) (Main, 1993) (Main et al., 1995) (Lukasiewicz et al., 1985) (Fay et al., 1999) (Fay et al., 2000). These models have the potential to greatly improve suit design: if engineers can understand and predict rigidity characteristics of proposed suit designs based solely on the physical characteristics of the prototype and physical processes at work, they could take explicit steps to mitigate these issues during the design phase. Not only would this be significantly less costly than building and testing multiple designs to experimentally determine their mobility characteristics, it would likely lead to more mobile suits due to a better understanding of the actual mechanisms at work (allowing engineers to implement specific mitigating strategies). What follows is a brief discussion of two primary (and competing) models designed to predict space suit joint rigidity: the beam model, and the membrane model (Corner et al., 1963) (Schmidt, 2001). This review will also examine efforts to validate these models against actual EMU joint-torque data.

Beam Model: The space suit beam model, first investigated by Comer and Levy in 1963, treats a gas-pressurized suit joint as a long, slender member, and assumes the only resistance to bending stems from the elastic properties of the material fabrics and the buckling characteristics of these materials (Corner et al., 1963). This model assumes that no changes in internal volume take place (thus no contributions to total rigidity stem from the pressure-volume work effects previously discussed), and assumes that buckling occurs due to wrinkles forming in the fabric stemming from bending under a tip-loading condition. When compared to experimental data, this model was found to over-predict the maximum failure stress of the beams. Corner and Levy's model was refined by Main, Peterson, and Strauss in the early 1990s, to include additional stresses acting in directions beyond the longitudinal direction (a limitation of Corner and Levy's original model). Main, Peterson and Strauss' model was found to agree with a specific subset of experimental data for pressurized beams (beams with a length-to-diameter ratio > 10), but did not agree with data from beams with a smaller L/D ratio (Main et al., 1993) (Main et al., 1995).

Membrane Model: The membrane model serves as a conceptual opposite to the beam model. This model assumes that the fabric wall of the pressurized cylinder is inextensible, meaning that the work required to bend the cylinder stems exclusively from the fact that the internal volume of the cylinder decreases when bent. Fundamentally, this model requires estimates of the volume deformation of a pressurized cylinder as it is bent through its complete range of motion. Such calculations were originally attempted by Lukasiewicz and Glockner in 1985, when they modeled the buckling geometry of “air-supported cylindrical membranes” assuming midway isometric deformation (Lukasiewicz et al., 1985). This model was further refined and generalized by Fay and Steele in 1999 and 2000, and resulted in an assumed volume vs. bending angle relationship that could be used to calculate the bending moment as a function of bending angle (based on the work required to decrease the internal volume for a given, and fixed, constant pressure) (Fay et al., 1999) (Fay et al., 2000).

Experimental Assessment of Beam/Membrane Models: Because the beam and membrane models represent two fundamentally different philosophies regarding the source and nature of gas-pressurized suit rigidity, to assess the true dominating source it was necessary to compare each model’s predictions to real space suit data. Such a study was conducted by Schmidt and Newman at the MIT Man-Vehicle Laboratory (MVL) in 2001 (Schmidt et al., 2001). A complete, pressurized EMU was outfitted on a Robotic Space Suit Tester (RSST), enabling researchers to articulate each joint independently to mimic human motion while accurately recording joint angles and torques. Using the RSST, EMU joints were articulated through their full ranges of motion, and the resultant torque vs. angle relationships were determined. The torques measured for the elbow and knee joints were then compared to the output of both the beam and membrane models to determine which model best described the torque-angle behavior of the EMU joints (and thus, to determine which physical mechanism most affects suit rigidity). Elbow data from Schmidt et al.’s study, compared against each model, is presented as Figures 7 and 8. Note only the elbow data is presented (knee data followed identical trends), and that the elbow data presented in both plots is identical (though the differences in scale are misleading).

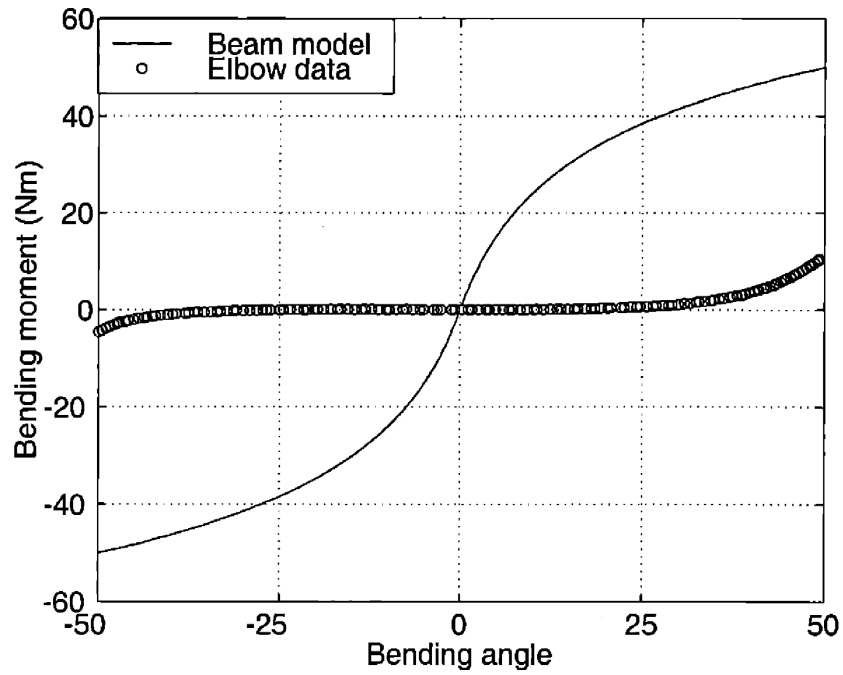


Figure 7: EMU elbow torque vs. angle data, compared to the Beam Model, taken from (Schmidt, 2001)

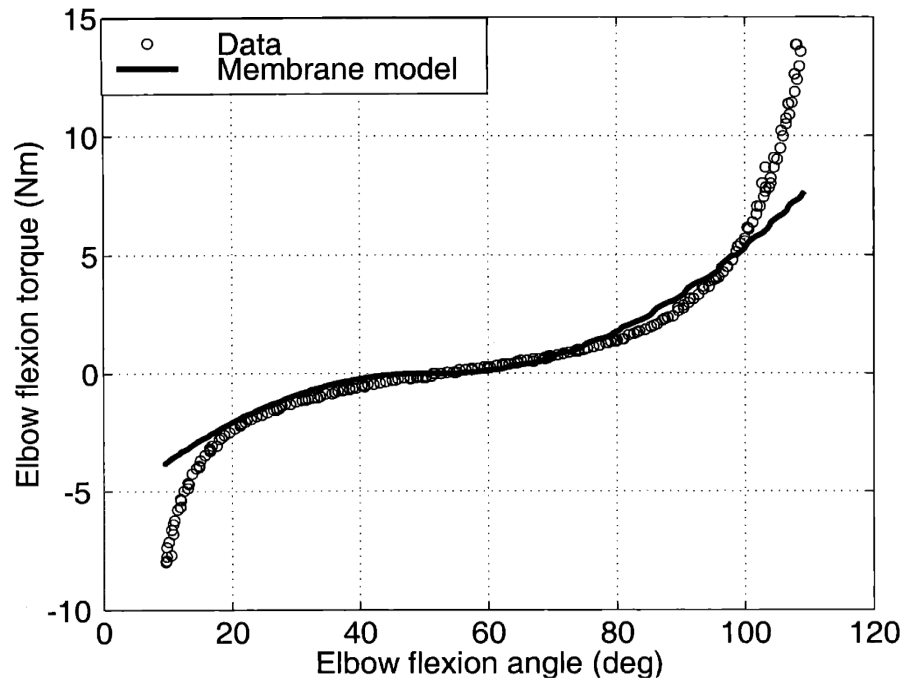


Figure 8: EMU elbow torque vs. angle data, compared to the Membrane Model, taken from (Schmidt, 2001)

As is evident from Figures 7 and 8, the actual EMU elbow data closely matches the torques predicted by the membrane model and is not well matched to the torques predicted by the beam model. However, at large flexion angles, the membrane model under-predicts total torque. Based on this comparison, Schmidt et al. concluded that “elastic deformation of the suit fabric [does] not contribute significantly to the torque needed to bend the elbow joint near the equilibrium angle”, though it may play a role at larger flexion angles where the membrane model breaks down (Frazer et al., 2002). Their findings, that changes in internal volume dominate total suit rigidity, are consistent with the long-standing design philosophy that constant-volume joints will lead to increased suit mobility.

1.2.5 – Summary

Long-recognized mobility issues with gas-pressurized space suits have caused space suit designers to seek both conventional and radical approaches to joint and suit design in an attempt to maximize suit mobility. Fundamental gas dynamics dictate that constant-volume joints should be a design goal, and both soft suit designs (specifically, convolute joints) and hard suit concepts (rigid sections separated by rotational bearings) have been proposed as potential methods for improving overall suit mobility by maintaining constant volume during joint articulation. Paradigm-shifting suit concepts (like MCP suits that abandon gas-pressurization entirely) could lead to drastic improvements in EVA mobility once certain technical and operational challenges are resolved.

The current EVA suit (the EMU – a traditional gas-pressurized suit) uses a hard torso section connected to soft limbs. The mobility characteristics of this suit have been mapped using a variety of experimental methods, and the torque vs. angle relationships of this suit are well documented. Modeling efforts to determine whether volume changes (as opposed to the suit fabric’s elastic properties) define overall suit rigidity suggest that the former, rather than the latter, are the dominant source of suit stiffness. Experimental data more closely matches the output of the membrane model, which assumes only volume change contributes to joint torque, though this model breaks down at high flexion angles.

1.3 – LIMITATIONS OF PREVIOUS WORK & OPEN QUESTIONS

Given the current state of gas-pressurized space suit modeling efforts, several gaps in the present body of knowledge have been identified:

1. While Schmidt et al. concluded that the membrane model better matched EMU torque data and thus volume changes are the dominating source of suit rigidity, they suggest that the real effect is likely a combination of both elastic properties and volume changes (i.e. a combination of both the beam and membrane models). They suggest that a combination of these sources is conceptually believable, and such a model might solve the discrepancy documented between the membrane model and the EMU data at high flexion angles. However, since the study only compared the disparate models to experimental data, it was not possible to experimentally determine whether the EMU torque values measured actually represented a combination of these two potential sources of suit rigidity (Schmidt et al., 2001) (Frazer, 2002).
2. The membrane model relies upon theoretical geometric relationships between bending angle and internal volume. At the time of this writing, no experimental assessments of the volume change behavior of a gas-pressurized space suit joint as a function of angle had been conducted or documented.
3. The membrane model assumes that suit pressure remains locally constant despite changes in internal volume, and that torque stems from the isobaric work required to reduce the internal volume (Schmidt et al., 2001). Given the fact that the suit is a closed operating environment, changes in volume necessarily cause changes in pressure (unless mitigated by a regulator). At the time of this writing, no experimental assessment of the effect of volume change on internal pressure, or of the effect of pressure changes on total suit stiffness, had been conducted.

These apparent gaps in the current body of research surrounding gas-pressurized space suit mobility represent the impetus for the experimental sections of this research effort.

Specifically, the following research questions were used to guide the experiments that are presented in Parts II and III of this document:

1. Is it possible to experimentally isolate and measure the elastic buckling and volume change contributions to total suit rigidity to assess Schmidt et al.'s conclusions?
2. What is the magnitude of volume change during EMU joint movement?
3. What effect does this volume change have on EMU suit pressure?
4. Do these changes in pressure affect overall suit stiffness?

Of specific interest is the role that **pressure spikes stemming from volume changes** during movement play in overall suit stiffness. These effects represent a previously ignored effect, therefore their detection/characterization could lead to potentially new methods for understanding and improving suit mobility.

1.3.1 – Pressure, Volume, and Structural Effects Nomenclature

For the remainder of this document, three potential sources of gas-pressurized space suit rigidity will be discussed and analyzed in detail. To simplify the discussion of these effects, the following terms will be used when referring to each effect:

Structural Effects The torque required to elastically deform the suit fabric wall in its pressurized state (i.e. the torque predicted by the beam model)

Volume Effects The torque required to isobarically displace the internal working gas due to volume changes during joint movement (i.e. the torque predicted by the membrane model)

Pressure Effects The torque required to *compress* the internal working gas in the closed operating environment due to volume changes during joint movement (a source of rigidity not considered by either the beam or membrane models)

1.3.2 – Volume vs. Pressure Effects

At first glance, volume effects and pressure effects may appear to be the same thing. While it is true that they both stem from the same problem (changes in internal volume), they are separable effects. When a hypothetical volume of gas undergoes an isobaric compression, work is done on the system and pressure remains constant; if the same volume of gas undergoes a similar, but non-isobaric, compression (for example an isentropic compression), work is done on the system *and* pressure increases. As a result, this total isentropic work will be greater than that of the isobaric process. This concept is easily demonstrated by examining a hypothetical pressure-volume (P-V) diagram. The work done during a given compression is represented by the area under the P-V curve. In Figure 9, an isobaric compression is represented by the movement from state A to B (with the work required, $P\Delta V$, represented by the solid region). This region represents volume effects. An isentropic compression is represented by the movement from state A to C (with the work required represented by the sum of the solid and striped regions). The difference in these work values (the striped region), represents the additional work required to compress a gas in a non-isobaric process (pressure effects). From the perspective of space suit design, it is this additional work (pressure effects caused by volume changes associated with astronaut movement) that could be potentially mitigated by maintaining strict control of internal pressure, even if the space suit joints themselves cannot be improved (i.e. even if internal volume change is unavoidable).

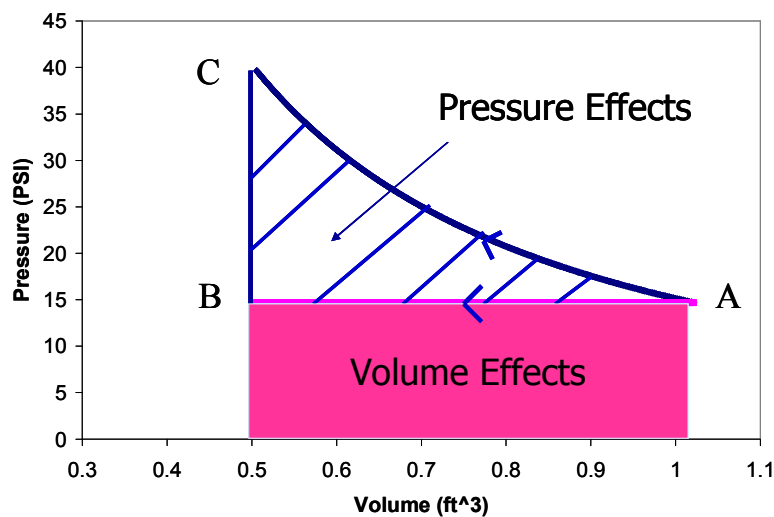


Figure 9: Pressure and Volume Effects in a hypothetical compression

1.4 – MODELING EFFORTS

To understand the relative influence of pressure and volume effects during space suit joint articulation, a simple model was developed to quantify the contributions of each effect for a hypothetical compression. The details of this model are given in this section.

1.4.1 – Isentropic Compression Model

For simplicity, an isentropic, reversible adiabatic process was chosen to model the compression. An equation for the total work required to complete such a compression was derived, starting with a general equation for work (equation 1 from section 1.2.1):

$$W = \int_{V_1}^{V_2} PdV \quad \text{eq.1}$$

By definition, during an isentropic compression (for an ideal gas):

$$PV^\gamma = \text{constant} \quad \text{eq.2}$$

where P is pressure, V is volume, and γ is the ratio of specific heats of the gas being used. Rearranging equation 2 provides the following relationship for pressure and volume between two isentropic states:

$$P_2 = P_1 \left(\frac{V_1}{V_2} \right)^\gamma \quad \text{eq. 3}$$

Substituting this into equation 1 gives:

$$W = \int_{V_1}^{V_2} P_1 \left(\frac{V_1}{V} \right)^\gamma dV \quad \text{eq. 4}$$

Integrating equation 4 provides the following relationship:

$$W_{TOTAL} = P_1 V_1^\gamma \frac{V_2^{1-\gamma} - V_1^{1-\gamma}}{1-\gamma} = \frac{P_1 V_1}{1-\gamma} \left(\left(\frac{V_2}{V_1} \right)^{1-\gamma} - 1 \right) \quad \text{eq.5}$$

Thus by knowing the initial state of the gas (pressure and volume), the size of the compression (i.e. the final volume), and the characteristics of the working gas (gamma), it is possible to calculate the total work required to complete the compression isentropically and adiabatically. Alternatively, if the final volume is unknown and the total work is known, the change in volume can be calculated. Knowing these quantities, it is then possible to analytically determine the specific contributions of pressure effects and volume effects to total work based on the definition of volume effects (work stemming from isobaric compression):

$$W_{VOLUME} = P_1(V_2 - V_1) \quad \text{eq.6}$$

$$W_{TOTAL} = W_{PRESSURE} + W_{VOLUME} \quad \text{eq.7}$$

$$W_{PRESSURE} = \left[\frac{P_1 V_1}{1-\gamma} \left(\left(\frac{V_2}{V_1} \right)^{1-\gamma} - 1 \right) \right] - [P_1(V_2 - V_1)] \quad \text{eq.8}$$

Consider a hypothetical 1 m³ volume of air at standard atmospheric conditions (P₁ = 101.3 kPa, γ = 1.4). If this volume of air was compressed isentropically and adiabatically, the total work would be comprised of both pressure effects and volume effects, and the relative magnitude of these effects would be dependent on the size of the volume change. Table 1 shows how the relative magnitudes of these effects change as the magnitude of the isentropic compression increases.

Table 1: Relative magnitude of pressure and volume effects as a function of volume compression ratio for a hypothetical isentropic and adiabatic compression

% Volume Change	Total Work (J)	Volume Effects (J)	Pressure effects (J)	Volume Effects (%)	Pressure Effects (%)
1.00	-1020	-1013	-7	99.30	0.70
2.00	-2055	-2027	-29	98.60	1.40
3.00	-3105	-3040	-65	97.89	2.11
4.00	-4170	-4053	-117	97.19	2.81
5.00	-5251	-5066	-185	96.48	3.52
6.00	-6348	-6080	-268	95.77	4.23
7.00	-7461	-7093	-368	95.06	4.94
8.00	-8591	-8106	-485	94.35	5.65
9.00	-9739	-9119	-619	93.64	6.36
10.00	-10904	-10133	-771	92.93	7.07

As can be seen in this table, the magnitude of both pressure effects and volume effects increase as the size of the compression increases. However, as the size of the compression increases, the *relative* magnitude of pressure effects increases when compared to volume effects (i.e. a greater percentage of total work is comprised of pressure effects). For a 1% change in total volume, pressure effects only contribute 0.7% of total work. However for a 10% change in total volume, pressure effects contribute 7.07% of total work. And if even greater volume changes take place, the relative contribution of pressure effects will also increase.

The implications of this phenomenon related to space suit design are clear: pressure effects will be of greatest concern for space suit joints that fail to maintain constant volume (upwards of 7% of total work will stem from pressure effects for joints that undergo 10% volume changes during movement, assuming pressure and volume effects are the only contributors to total suit rigidity). If these effects can be mitigated in such a joint (through active pressure regulation) then overall joint rigidity could be reduced by 7% without changing the design of the joint whatsoever.

1.5 – EXPERIMENTAL ASSESSMENT OF THEORY

Based on the gaps in the current literature and the outcome of the previous modeling efforts, two experiments were designed and conducted to further investigate and mitigate the individual components to space suit rigidity. Brief descriptions of these experiments are included below, and complete discussions are included in Parts II and III of this document.

1.5.1 - Characterization of the Components to Gas-Pressurized Space Suit Joint Rigidity

The goal of this study was to empirically isolate and determine the exact contributions of pressure, volume, and structural effects to total EMU joint rigidity. An EMU arm section was pressurized to 30 kPa (4.3 psid), which is representative of the exact state the suit is in when donned by an astronaut for EVA. The arm was flexed from its natural resting position to its maximum flexion angle, and torque vs. angle measurements were taken throughout its range of motion. These tests were repeated for two volume conditions: an unconstrained, open volume; and a capped (constrained), closed volume. The difference in these torque measurements was used to determine the specific contribution of pressure effects to total joint torque. Additionally, internal volume was measured as a function of angle. These measurements were used to calculate the contribution of volume effects to total joint torque (using the known relationship between volume change and torque stemming from isobaric work). Finally, the magnitude of structural effects was then calculated based on the difference between the open-volume torque measurements and the calculated volume effects. The background, methods, experimental design, results and discussion of this work can be found in Part II.

1.5.2 – Active Pressure Regulation as a Method to Improve Gas-Pressurized Space Suit Mobility

The goal of this study was to develop and test a proof-of-concept active pressure regulation system designed to enhance gas-pressurized suit mobility by reducing pressure

effects. A design proposed by engineers at the MIT MVL was developed into a functional prototype using commercially available products for approximately \$500. This system was then tested for a variety of volume changes, and its ability to actively sense and mitigate changes in pressure stemming from these volume changes was assessed. The background, methods, experimental design, results and discussion of this work can be found in Part III.



PART II

Experimental Characterization of Structural, Volume and Pressure Components to Gas-Pressurized Space Suit Joint Rigidity

The truth may be puzzling. It may take some work to grapple with. It may be counterintuitive. It may contradict deeply held prejudices. It may not be consonant with what we desperately want to be true. But our preferences do not determine what's true. We have a method, and that method helps us to reach not absolute truth, only asymptotic approaches to the truth -- never there, just closer and closer, always finding vast new oceans of undiscovered possibilities. Cleverly designed experiments are the key.

- Carl Sagan

2.1 - INTRODUCTION

As discussed in Part I, a limited number of experimentally-focused torque vs. angle studies of the EMU and other space suit models have already been conducted. These earlier studies characterized the total rigidity of pressurized suits as their joints were articulated through their operational range of motion. Such studies are useful, because understanding the total torque behavior of suit joints helps suit designers establish and validate mobility requirements relative to the known torque values achievable by the human body.

While descriptive investigations of this nature are interesting and necessary, such studies make little attempt to experimentally characterize joint rigidity by directly examining the individual factors that comprise total joint torque. The study outlined in this section aimed to fill this gap by experimentally characterizing the individual contributions to suit rigidity (beyond a generalized statement that the membrane model is a “better fit” than the beam model) in order to better understand the well-established descriptive suit torque vs. angle relationships. Knowledge gained from this study helps to determine which effects dominate total rigidity (and also whether this domination is consistent throughout the full range of joint motion), enabling suit designers to approach future designs with an emphasis on correcting the underlying mechanisms that limit suit flexibility and mobility.

This study focused on the relative roles of structural, volume, and pressure effects, providing an independent assessment of the existing predictive beam and membrane suit joint torque models. As previously stated, these models predict that volume effects are the primary contributor to total suit rigidity with structural effects playing at best a minor role (and do not consider pressure effects whatsoever). This study assessed whether the previously-ignored pressure effects are a significant contributor to total suit rigidity, the outcome of which could lead to an evolution of existing joint torque theory.

2.1.1 - Conceptual Overview of Joint Torque Experiment

A study designed to experimentally characterize not only the total torque vs. angle behavior of a Class III EMU elbow joint but also the constituent effects that lead to total torque behavior was conducted in the MIT MVL from June 2008–June 2009. A Class III EMU arm specimen was pressurized and driven through its complete elbow flexion/extension envelope using a custom designed external articulation rig. Torque vs. angle measurements were collected using a digital torque wrench for each angle in the flexion envelope for both open and closed internal volume conditions. This data characterized the total torque required to articulate the arm, and served as a check against previous elbow flexion torque tests. Additionally, the difference between the open and closed internal volume torque measurements was calculated to determine the pressure effects contribution to total joint rigidity. Internal volume vs. angle measurements were also collected for each angle in the flexion envelope using water level measurements. These measurements were used to calculate the contribution of volume effects to total suit rigidity. With this data, structural effects were calculated by taking the open internal volume torque measurements and subtracting the volume effects contribution.

This joint-torque study and its results are presented in the following sections.

2.1.2 - Hypotheses

This study sought to assess the following two hypotheses:

1. In addition to **Volume Effects**¹ and **Structural Effects**², a third (and not well studied) contributor to gas-pressurized suit rigidity exists: **Pressure Effects**. These effects are defined as the work required to compress the internal working gas of the suit in the closed operating environment due to volume changes during joint movement.
2. **Pressure Effects** are a statistically significant torque contributor to the EMU elbow joint.

2.1.3 - Objectives

In order to assess these hypotheses, the following experimental objectives were established:

1. Obtain a Class III EMU arm section.
2. Develop a test rig that allows the elbow joint to be isolated and articulated through its range of motion in its pressurized state in a repeatable manner.
3. Determine torque vs. angle behavior for the elbow joint in its pressurized state through its complete range of motion in both open- and closed-volume configurations, with gravity effects removed.
4. Determine volume vs. angle behavior for the elbow joint in its pressurized state.
5. Determine directly (or indirectly through calculation) the individual contributions of each rigidity effect to total joint rigidity.

The following sections will discuss in detail the efforts taken to meet these objectives.

¹ Volume Effects are defined as the torque required to isobarically displace the internal gas of the suit due to volume changes during joint movement (considered a primary contributor in the membrane model)

² Structural Effects are defined as the torque required to elastically deform the suit fabric wall in its pressurized state (considered a primary contributor in the beam model)

2.2 - EXPERIMENTAL HARDWARE AND SETUP

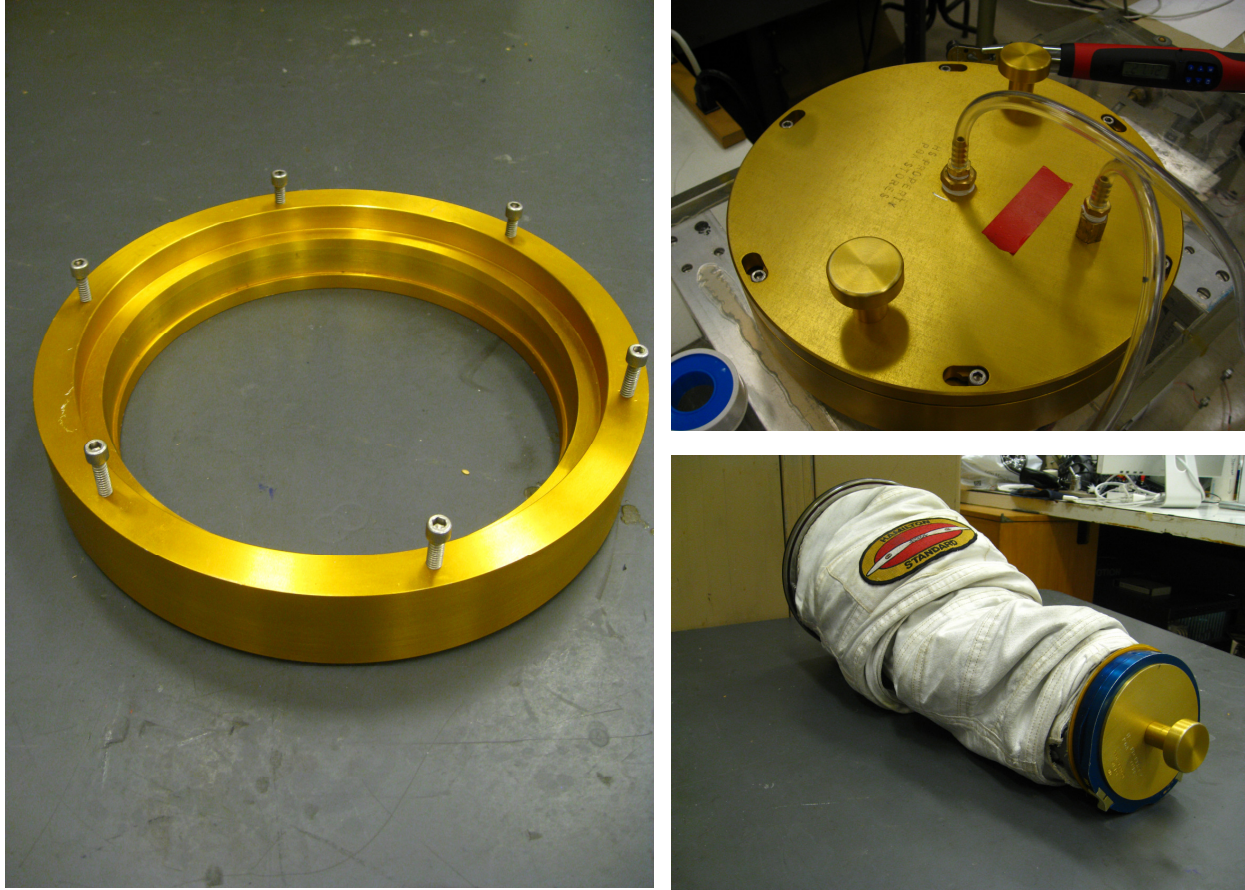
2.2.1 - Class III EMU Space Suit Arm Specimen and Hardware

Two arm sections from a Class-III EMU suit were loaned to the MIT MVL from engineers at Hamilton Sundstrand in Windsor Locks, CT. Based on the general condition of the two specimens, one was selected and used for every torque and volume test conducted in this study. An example of one arm received is pictured below in Figure 10.



Figure 10: One of two Class III EMU arm section provided by Hamilton Sundstrand (pictured with glove attached)

Included with the arm specimens were three additional pieces of hardware: a shoulder housing unit, enabling the arm to be mounted to a vacuum chamber at the shoulder bearing; a shoulder housing unit cap, enabling the arm to be capped at the shoulder bearing interface, thereby sealing the internal volume of the arm from the open test environment; and a wrist bearing plug, enabling the glove specimen to be removed while maintaining the capability to pressurize the arm. These three pieces of hardware are pictured in Figures 11a-c, respectively.



Figures 11a-c (clockwise from left): EMU shoulder housing unit, shoulder housing unit cap, and EMU arm with wrist bearing plug (all pieces shown in gold)

Using this equipment, the EMU arm was mounted in a low pressure chamber, which is described in detail in the next section.

2.2.2 - MVL Vacuum Chamber

A pre-existing 1.07 m x 0.30 m x 0.30 m (3.5 ft x 1 ft x 1 ft) low pressure chamber located in the MVL, shown in Figure 12, was outfitted with this EMU hardware. This chamber was previously used for mechanical counter pressure (MCP) leg garment testing, and as such included a 23 cm (9 in) diameter leg access point on the top surface (this was the only chamber access point) (Judnick, 2007). The EMU arm was placed in the shoulder housing unit such that it was held in place at the shoulder bearing. The glove was removed and the wrist bearing plug was inserted, and the housing unit was

placed over the leg access point. Common weather stripping was attached to the top of the chamber in a circle around the outer diameter of the leg access point, which formed an air-tight seal between the chamber and the bottom surface of the housing. See Figure 13 for a side-view schematic of this sealing configuration.

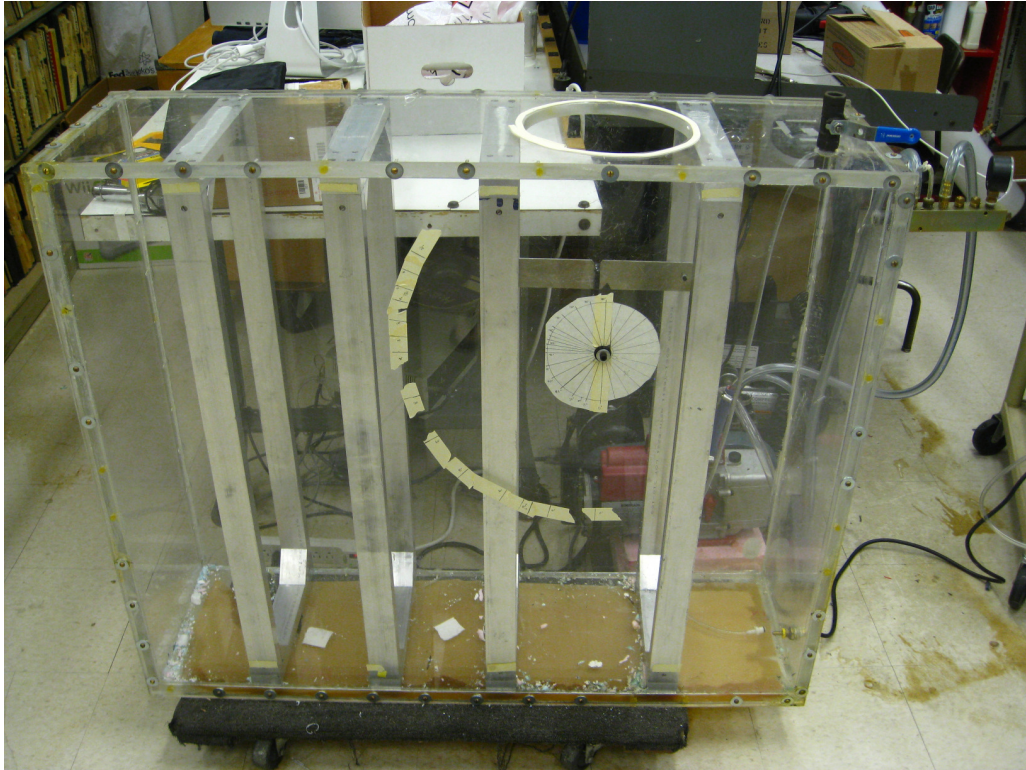


Figure 12: MIT MVL vacuum chamber

The pressure chamber was equipped with two vacuum pumps of different power levels ($\frac{1}{2}$ horsepower and $\frac{1}{4}$ horsepower respectively). A pressure gage was installed in the chamber to monitor the internal pressure, and a release valve was installed to allow the chamber to vent to ambient conditions if desired. For all EMU arm tests, the chamber pressure was maintained at 71.7 kPa absolute pressure (10.4 psia), and the room was open to atmospheric conditions which were assumed to be 101.3 kPa (14.7 psia). This created a pressure differential across the suit of 29.6 kPa (4.3 psi), which is representative of its pressurized condition in space. Because the chamber had small leaks in various places, it would not hold a constant pressure differential without intervention. A method was devised to obtain a constant pressure differential despite chamber leakage – this method is included as Appendix A.

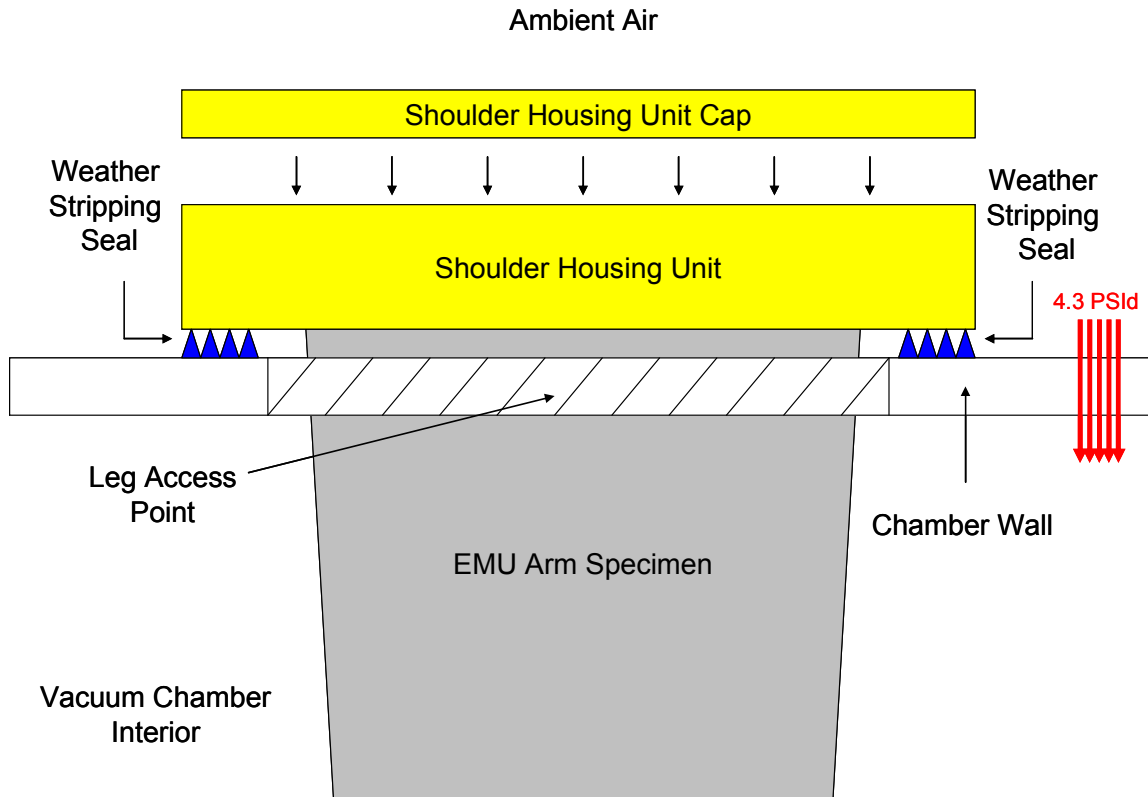


Figure 13: Side-view schematic of the shoulder housing unit/vacuum chamber seal configuration (not to scale)

2.2.3 - EMU Space Suit Arm Articulation Rig

In order to characterize the torque vs. angle behavior of the arm specimen, it was necessary to develop a method for articulating the arm through its range of motion in its pressurized state while measuring the required torque in a repeatable fashion. This could be accomplished in a number of ways, including (but not limited to): articulating the arm internally using a robotic testing device, as was done in previous torque tests conducted in the MVL using NASA's Robotic Space Suit Tester (RSST) (Schmidt et al., 2001); articulating the arm externally using a modified spring-scale system, which is the method currently being considered by NASA engineers for testing future suit designs (Matty et al., 2009); or developing custom hardware in-house that would enable external articulation of the arm using a brace-type structure and a simple wrench.

Internal articulation of the arm was discarded as an option, because such a testing architecture prevented the arm from being sealed using the shoulder housing unit cap previously described. This was unacceptable, because testing the arm with a sealed internal environment was the only method by which pressure effects could be assessed.

External articulation of the arm using a modified fish-scale (spring scale) system was also discarded as an option. Such a testing architecture required the arm to be manually pulled through its range of motion using a simple spring-scale inside the pressure chamber, with the forces being read manually off the scale. This approach was impractical, because it required another large access point to be installed in the chamber. Only then was it possible for the arm to be mounted to the chamber *and* manually and externally pulled through its range of motion. This method was also deemed to be unsatisfactorily imprecise, as it required measurements to be read by hand from an unsteady scale inside the chamber, and was impossible to guarantee that the arm was articulated only through the elbow joint and in a repeatable manner.

External articulation of the arm using a custom brace-type structure was thus selected as the best testing architecture for this study. This setup allowed the arm to be moved through its range of motion, in its pressurized state, without precluding the use of the shoulder housing cap to seal the arm when desired. Additionally, a clever design of this system guaranteed that the arm was articulated only at the elbow joint, and the torque was measured and recorded precisely using an electronic torque wrench.

Three pieces of hardware were developed in accordance with this architecture:

1. A custom-designed brace that provided a framework to articulate the forearm section about the elbow joint when mounted to the arm within the vacuum chamber environment.
2. A wrist plate that attached to the wrist bearing plug and then mounted to guide rails of the forearm brace.
3. A wrench adapter that extended from outside the vacuum chamber through a hole drilled in the chamber wall and mated with the forearm brace inside the chamber,

enabling the brace (and thus the EMU forearm itself) to be articulated about the elbow joint externally.

Three-dimensional models of these pieces of hardware, created using Pro/ENGINEER design software, are included below as Figure 14 (scale: 1 cm = 4.4 cm).

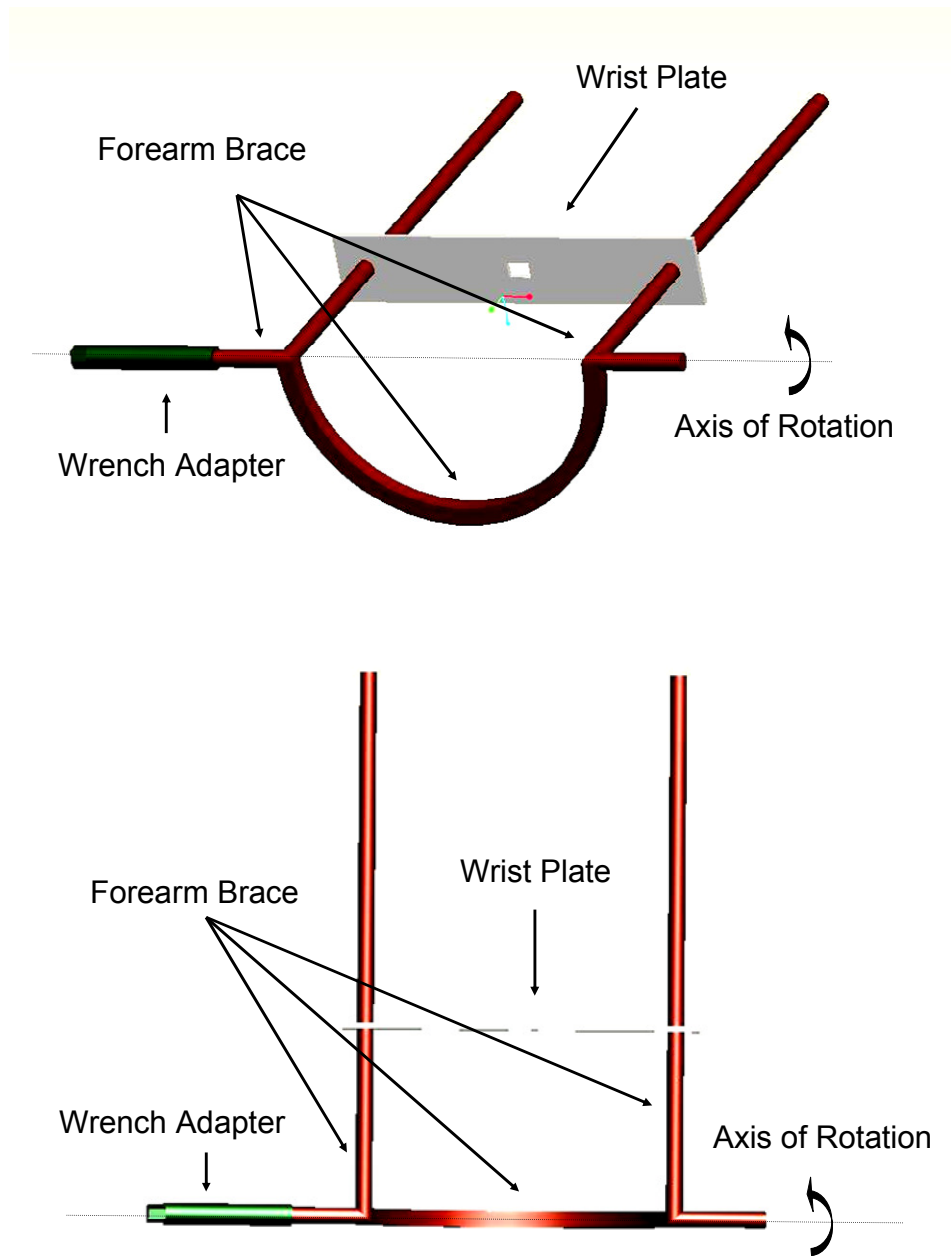


Figure 14: Isometric- and top-view model of the EMU elbow articulation rig

A top-view schematic of this architecture, assembled within the vacuum chamber (without the arm) is shown in Figure 15.

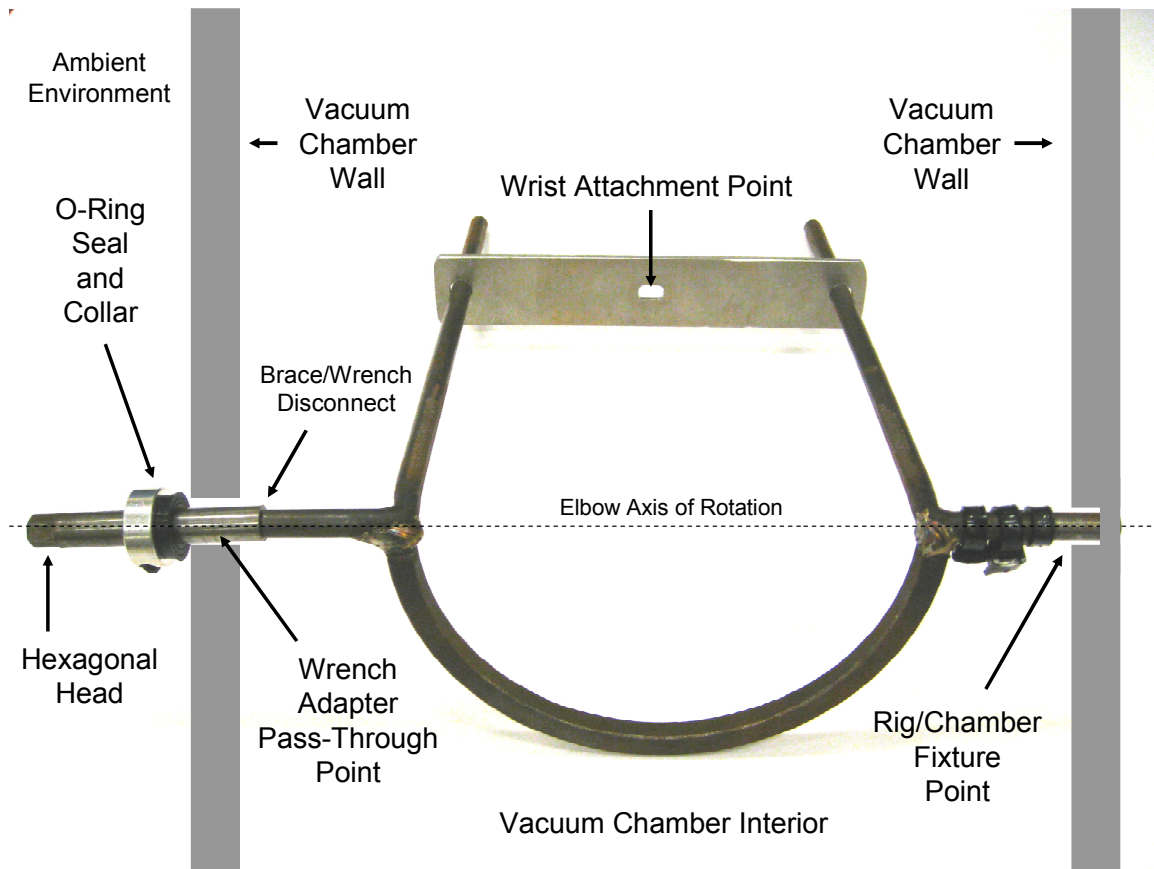


Figure 15: Top-view schematic of the EMU Elbow Articulation Rig inside the MVL vacuum chamber (not to scale)

The forearm brace was constructed from two steel L-shape rods, which were then welded to a steel loop designed to match the outer diameter of the EMU elbow in its pressurized state. The wrist plate was constructed from 6061 aluminum alloy, and included three holes (one in the center to attach to the wrist plug, and one on each edge to mount to the rails of the brace). The wrench adapter was constructed from stainless steel, and was milled to include a square socket that mated with the forearm brace inside the chamber. This was intended to be easily deconstructed because the forearm brace and wrench did not fit through the access point of the chamber as one unit. The wrench adapter included a rubber O-ring and an aluminum collar that maintained a pressure seal around the hole drilled for the adapter. The external end of the wrench adapter was milled into an 11 mm

(7/16 in) hexagonal head that enabled the entire rig to be articulated using a standard wrench. Engineering drawings of this rig are included in Appendix B. Examples of the hardware rigged to the EMU arm in its unpressurized state are presented in Figure 16.

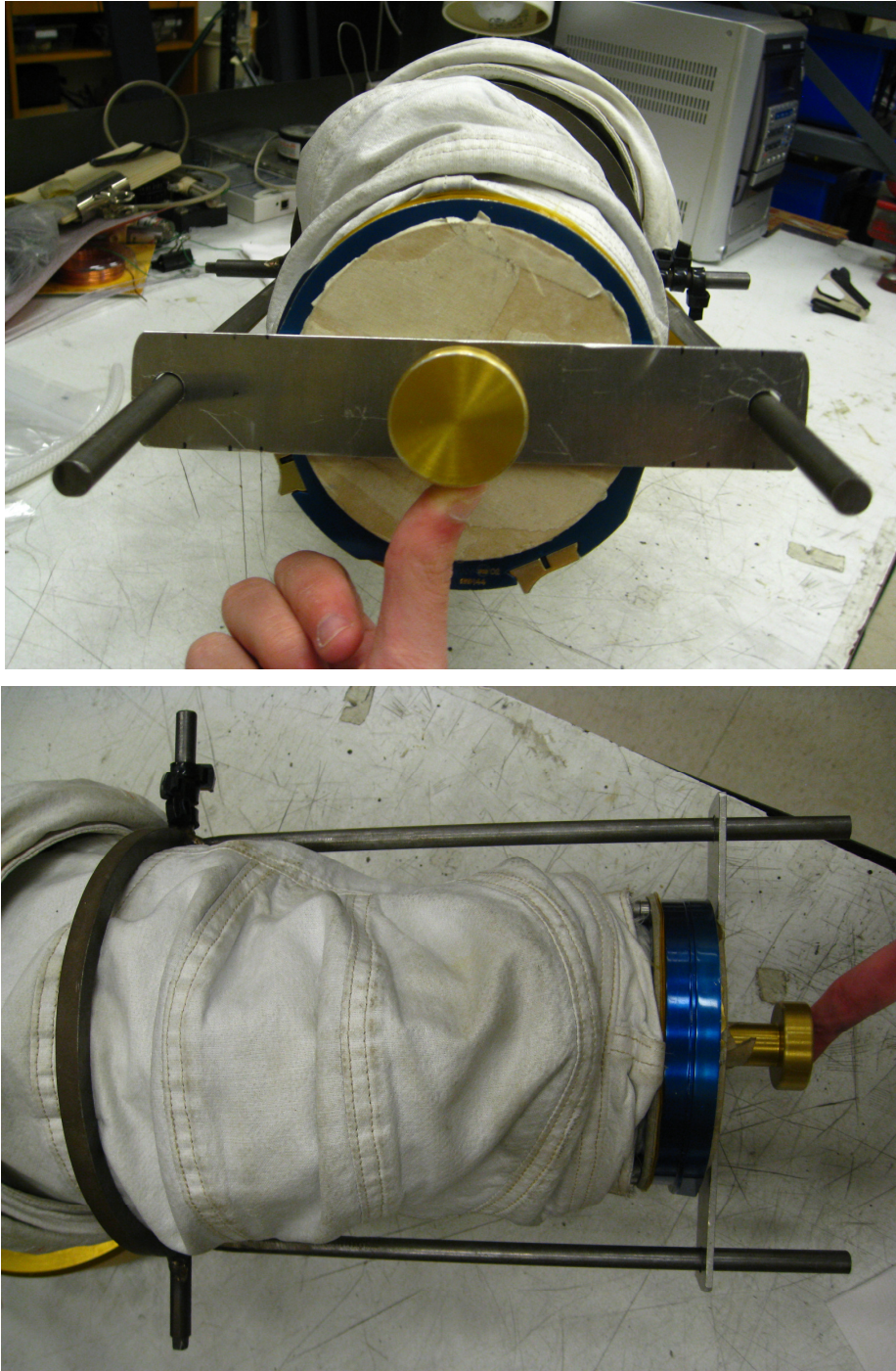


Figure 16: Front and top view of the wrist plate attached to the wrist bearing plug and mounted on the brace rails on an EMU arm, respectively

2.2.4 – Space Suit Angle Measurement

With this rig installed in the vacuum chamber, the EMU arm was movable through its complete flexion/extension cycle using any tool capable of mating to an 11 mm (7/16 in) hexagonal head. In order to collect torque vs. angle measurements, a method was developed to measure the specific angle to which the arm was being driven. This method was designed to be repeatable (i.e. as free from sources of human error as possible), because multiple tests were necessary to treat the data in a statistically-meaningful way.

To measure the angle of the arm when flexed, a protractor-like angular scale with increments between 0-115° was sketched to the exterior of the vacuum chamber using masking tape (with 0° defined as the arm being perfectly straight, 90° being bent perpendicularly at the elbow, etc.). The operator flexed the arm such that the rails on the forearm brace matched the angular increment of interest. The exact angle measurements marked on the chamber are included in Table 2.

Table 2: Articulation rig increments

Angle Increments (degrees)												
0	15	25	30	45	60	75	90	95	100	105	110	115

These angles served as the independent variable for all tests. The angle values were selected with an intentionally higher resolution near the extreme end of the flexion envelope (increments of 5° at angles $\geq 90^\circ$ vs. increments of 15° at angles $< 90^\circ$). This was done because it was believed that pressure effects and volume change were most significant at these higher angles, and as such a higher resolution was desired to more fully understand these phenomena. Also, an increment was added at 25° - this identified the neutral position of the arm when pressurized (which, as will be discussed in future sections, was treated as the starting zero-torque angle for each of the pressurized tests).

Originally, a short-radius angular scale was implemented (with a radius of demarcation approximately 7.62 cm [3 in] from the axis of rotation). Upon preliminary testing, it was

determined that this short-radius scale was not precise enough to guarantee repeatable tests because it was near impossible to resolve 5° angular differences only 7.62 cm (3 in) from the axis of rotation (especially given the relative thickness of the forearm brace rails). To correct this problem, a large-radius (30.5 cm, or 12 in) angular scale was implemented. This increased the actual distance between increments by a factor of 4, which was a sufficiently large increase to allow operators to measure all angle conditions consistently and without ambiguity. These two angular scales are shown in Figure 17.

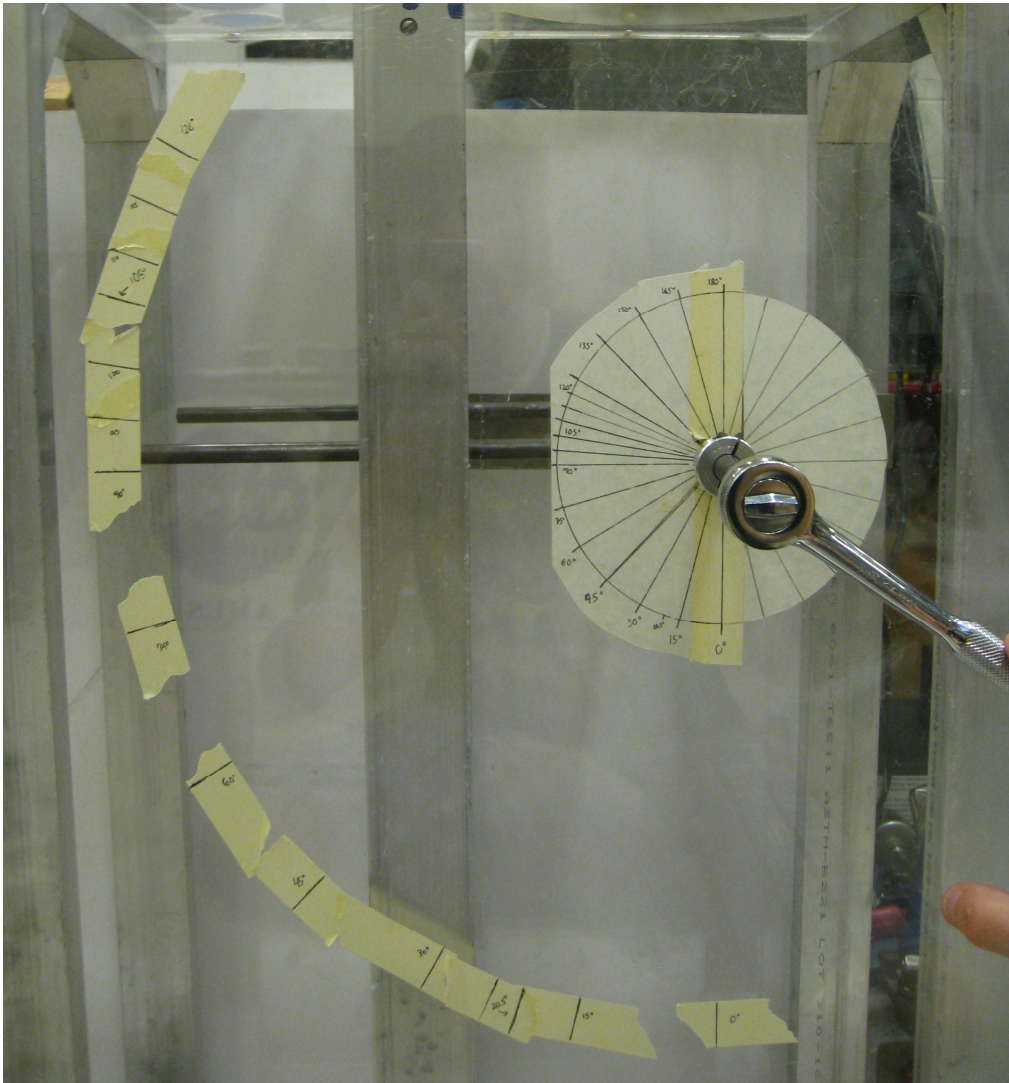


Figure 17: Short and long radius angular scales on the MVL vacuum chamber (with forearm brace flexed to 90° visible in the background)

2.2.5 - Torque Measurement

To measure the torque required to articulate the arm to a specific angle using the elbow rig, a 6.35 mm (1/4 in) drive TECHMEMORY™ electronic torque wrench was purchased from SnapOn Inc. and outfitted with an 11 mm (7/16 in) socket adapter. The torque wrench (model number TECH1FRM240) arrived pre-calibrated and certified by SnapOn, and had an operating range of 2.7-27.12 Nm, a resolution of 0.01 Nm, and an accuracy of 1%. It also included both a real-time digital display and the capacity to store up to 1000 data points in internal memory, which could be offloaded to a PC running Microsoft Excel using the included TORQLOG™ software and serial cable (Snap-On, 2008).

This wrench was selected because its accuracy and resolution were the highest obtainable for all wrenches surveyed that met both the budget constraints (\leq \$500 after academic discounts) and the torque range that was needed for the study (approximately 0-30 Nm).

For the exact data collection and retrieval methods used with this wrench, and a list of its detailed specifications (including the certificate of calibration), refer to Appendices C-D, respectively. This wrench, configured to the elbow rig, is depicted in Figure 18.



Figure 18: Electronic torque wrench configured to the EMU articulation rig

2.2.6 - Hardware Integration

The complete configuration required integration and use of all hardware described in previous sections (EMU arm, shoulder housing unit, shoulder housing unit cap, wrist bearing plug, vacuum chamber, articulation rig, angle measurement scale and digital torque wrench). This final hardware integration is depicted in Figure 19, and demonstrates a preliminary test with the arm pressurized and flexed between 75-90°.

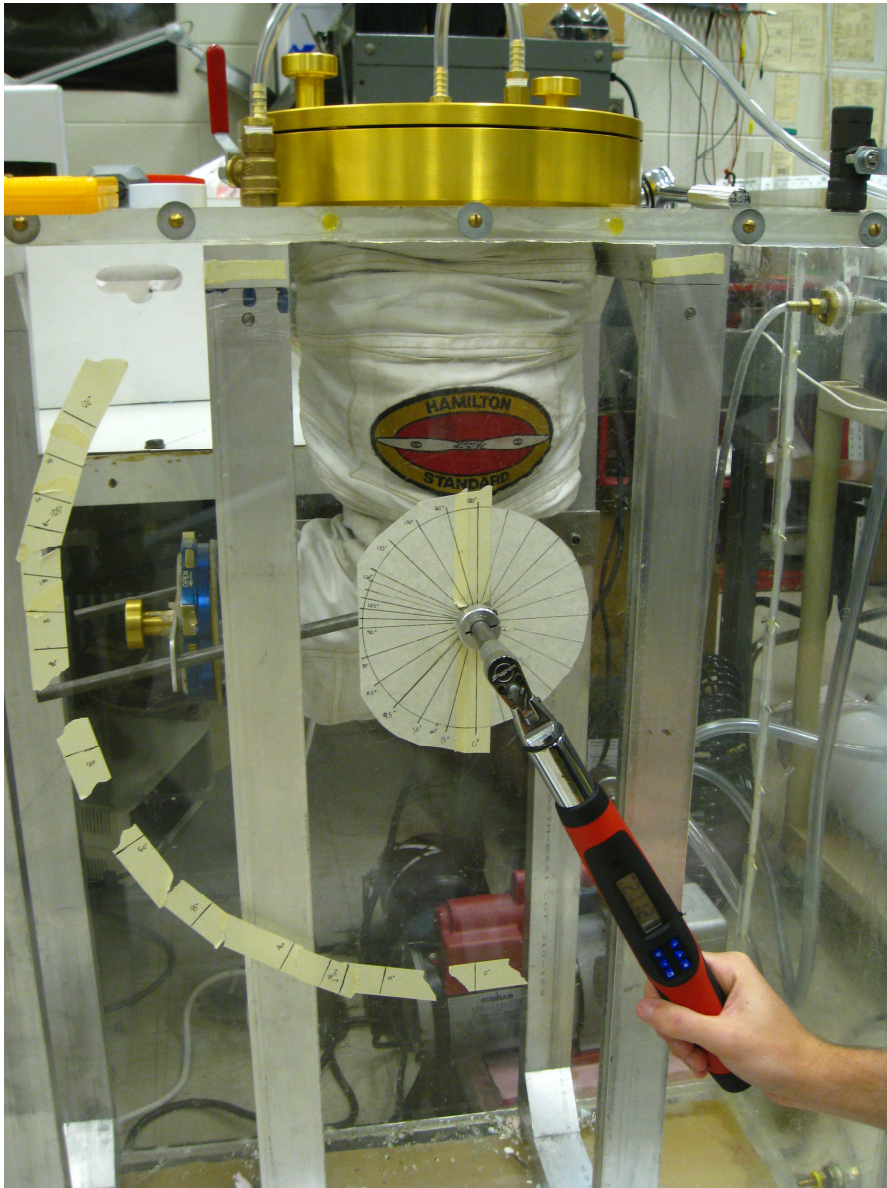


Figure 19: Example of final hardware integration, with arm shown flexed between 75-90°

2.3 - EXPERIMENTAL TEST PLAN AND METHODS

2.3.1 - Test Plan Overview

Using the equipment previously described, a test plan was devised to characterize both the total torque vs. angle relationship of the EMU arm specimen, and the individual contributions of structural, volume, and pressure effects to total joint torque. Five test conditions were defined to accomplish these goals. Each test condition isolated a specific subset of the torque effects of interest in the EMU elbow joint (pressure, volume, and structural effects), such that comparisons of data between different test conditions led to an isolation and characterization of each of the three effects.

Before measuring the torque required to articulate the rig in different pressurized configurations, the effect of gravity on the arm/test rig had to be removed from the data. This was necessary because the arm was housed vertically in the chamber, meaning each articulation of the arm/rig system worked against the force of gravity in addition to the torque effects of interest (these gravity effects represented an additional torque component that *only* existed because of the configuration of the test setup, and are not a true contributor to suit rigidity in microgravity). Additionally, in order to quantify the contribution of volume effects to total torque, the internal volume of the pressurized arm as a function of angle was directly measured.

The five test conditions were defined as follows:

1. Baseline torque vs. angle test with the arm unpressurized and in an open-volume configuration (the shoulder housing unit cap was removed, leaving the arm volume open to the ambient air), which characterized the role of gravity effects
2. Total torque vs. angle test with the arm pressurized and in an open-volume configuration (the shoulder housing unit cap again was removed)
3. Total torque vs. angle test with the arm pressurized and in a closed-volume configuration (which was accomplished by capping the arm using the shoulder housing unit cap, with the internal volume only that of the unoccupied arm), which characterized the role of pressure effects in the volume of the arm

4. Total torque vs. angle test with the arm pressurized and in a closed-volume configuration (which was accomplished by capping the arm using the shoulder housing unit cap, with the internal volume including both the unoccupied arm and a 0.028 m³ dummy volume designed to represent a full, occupied and pressurized EMU), which characterized the role of pressure effects in a realistic volume
5. Internal volume vs. angle test using water as an indicator of changes in internal volume, with the arm pressurized and uncapped

Included in Table 3 is a breakdown of the torque effects (gravity, volume, structural, and pressure) that were assumed to be present in each test condition:

Table 3: Assumed Torque Effects Present at Each Test Condition

Test Condition	Torque Effects Present
1. Unpressurized Arm	Gravity
2. Pressurized, Uncapped Arm	Gravity, Volume, Structural
3. Pressurized, Capped Arm	Gravity, Volume, Structural, Pressure ³
4. Pressurized, Capped Arm + Dummy Volume	Gravity, Volume, Structural, Pressure
5. Pressurized, Uncapped Arm Volume Test	N/A (torque not measured)

Thus, the torque (τ) measured in each test condition was broken down into its constituent effects mathematically as follows:

$$\tau_{UNPRESSURIZED} = \tau_{GRAVITY} \quad \text{eq. 9}$$

$$\tau_{PRESSURIZED-UNCAPPED} = \tau_{GRAVITY} + \tau_{VOLUME} + \tau_{STRUCTURAL} \quad \text{eq. 10}$$

$$\tau_{PRESSURIZED-CAPPED} = \tau_{GRAVITY} + \tau_{PRESSURE} + \tau_{VOLUME} + \tau_{STRUCTURAL} \quad \text{eq. 11}$$

By definition, volume effects (torque due to isobaric work) were found using:

$$\tau_{VOLUME} = \frac{(P_i * \Delta V)}{\phi} \quad \text{eq. 12}$$

³ Pressure effects in this condition were not representative of the real effects of the suit, as the closed operating volume used was only that of the arm, not that of the full suit.

where $P_i = 1 \text{ atm} = 101.3 \text{ kPa}$ (because the arm's internal environment was initially open to standard atmospheric conditions), ϕ was the angle of the arm in radians, and ΔV was measured directly in Test 5. Thus, by substitution and manipulation of equations 9-12, it was possible to solve for the remaining effects (pressure and structural effects) explicitly:

$$\tau_{PRESSURE} = \tau_{PRESSURIZED-CAPPED} - \tau_{PRESSURIZED-UNCAPPED} \quad \text{eq. 13}$$

$$\tau_{STRUCTURAL} = \tau_{PRESSURIZED-UNCAPPED} - \tau_{UNPRESSURIZED} - \frac{P_i * \Delta V}{\phi} \quad \text{eq. 14}$$

With these relationships assumed and test conditions defined, the following test matrix (Table 4) was developed to structure the testing procedure:

Table 4: Test Matrix for EMU Arm Study

Elbow Angle (Degrees)	Unpressurized Torque (Nm)	Pressurized [Open Volume] Torque (Nm)	Pressurized [Closed Volume Arm Only] Torque (Nm)	Pressurized [Closed Volume Arm + Dummy] Torque (Nm)	Δ Volume (cm3)
0					
15					
25					
30					
45					
60					
75					
90					
95					
100					
105					
110					
115					

EMU elbow angle served as the independent variable for each of the five test conditions, with the increments chosen intentionally to focus on high flexion angles. Torque served as the dependent variable for tests 1-4, and Δ Volume served as the dependent variable for test 5. The pressure of the vacuum chamber pressure was controlled as a test parameter, and was maintained at -29.6 kPag (-4.3 psig) for all pressurized tests. The ambient air in the test environment was assumed to be constant at atmospheric room temperature conditions. The specific test methods used for each test condition are described in the next section.

2.3.2 - Test Method 1: Unpressurized Arm Torque Tests

The following protocol was implemented for the unpressurized arm torque tests:

1. Mount the EMU arm to the chamber using the shoulder housing unit, and attach it to the elbow articulation rig
2. Rotate the shoulder joint 90° off axis from the elbow (this is to ensure that the arm only bends at the elbow joint, and not at the shoulder)
3. Note the neutral resting position of the arm (this position is 0° in the unpressurized condition)
4. Flex the elbow to the first angle of interest using the torque wrench
5. Record the angle manually, and save the torque value to the wrench's internal memory using the method described in Appendix C
6. Return the arm to its original neutral position using a standard wrench (this is to ensure the arm begins at the same resting position to avoid hysteresis effects)
7. Repeat steps 4-6 for each angle of interest

See Figure 20 for a depiction of this test configuration:

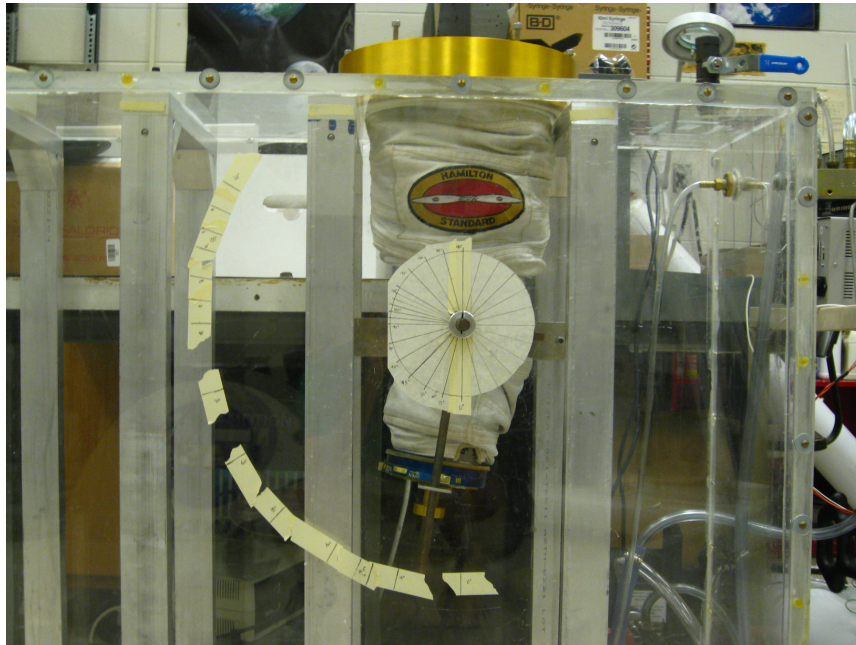


Figure 20: Unpressurized Arm Torque Test

2.3.3 - Test Method 2: Pressurized, Open Volume Torque Tests

The following protocol was implemented for the pressurized, open volume arm torque tests (see Figure 21 for a depiction of this test configuration):

1. Mount the EMU arm to the chamber using the shoulder housing unit, and attach it to the elbow articulation rig
2. Rotate the shoulder joint 90° off axis from the elbow
3. Pressurize the chamber to -29.6 kPag (-4.3 psig) using the method described in Appendix A
4. Note the neutral resting position of the arm (this position is approximately 25° in the pressurized condition)
5. Flex the elbow to the first angle of interest using the torque wrench
6. Record the angle manually, and save the torque value to the wrench's internal memory using the method described in Appendix C
7. Return the arm to its original neutral position using a standard wrench
8. Repeat steps 5-7 for each angle of interest

2.3.4 - Test Method 3: Pressurized, Closed Volume (Arm Only) Torque Tests

Note that for all closed volume tests, it was necessary to install a relief valve in the shoulder housing unit cap. This was used to “recharge” the internal volume of the arm to atmospheric conditions before each flexion to ensure that any leakage of air from inside the arm to the vacuum environment (which was found to occur) did not compromise the test. The following protocol was implemented for the pressurized, closed volume (arm only) torque tests (see Figure 22 for a depiction of this test condition):

1. Mount the EMU arm to the chamber using the shoulder housing unit, and attach it to the elbow articulation rig
2. Rotate the shoulder joint 90° off axis from the elbow
3. Attach the shoulder housing unit cap to the arm, thereby closing the internal volume
4. Open the relief valve

5. Pressurize the chamber to -29.6 kPag (-4.3 psig) using the method described in Appendix A
6. Note the neutral resting position of the arm (this position is approximately 25° in the pressurized condition)
7. Close the relief valve
8. Immediately flex the elbow to the first angle of interest using the torque wrench
9. Record the angle manually, and save the torque value to the wrench's internal memory using the method described in Appendix C
10. Open the relief valve
11. Return the arm to its original neutral position using a standard wrench
12. Repeat steps 7-11 for each angle of interest

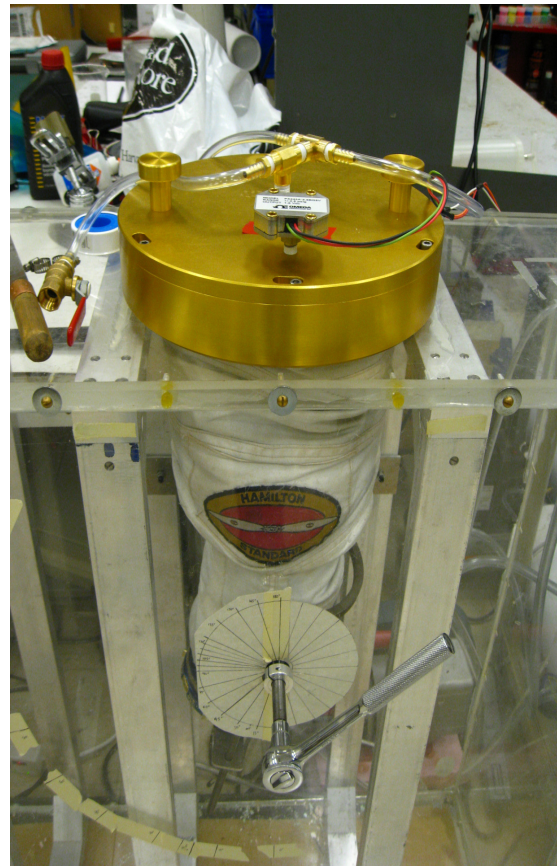
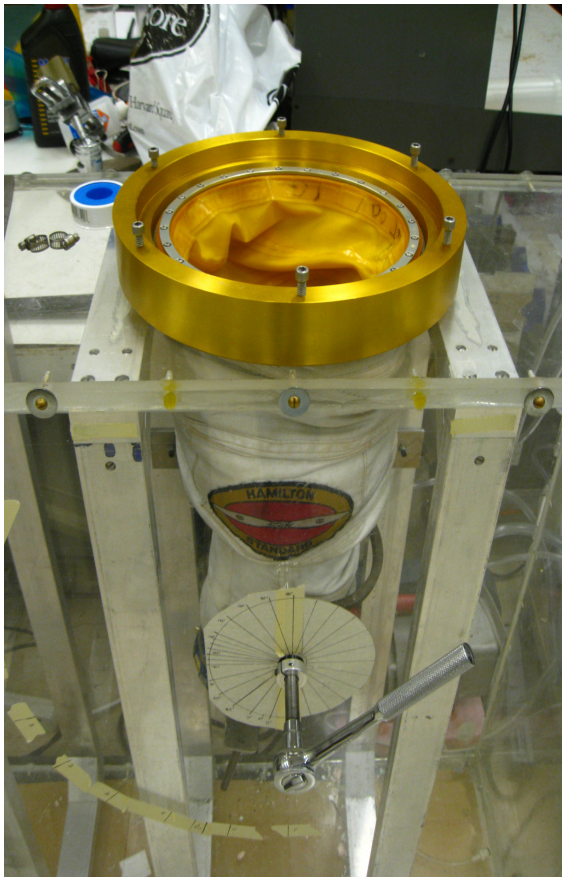


Figure 21: Pressurized, open volume torque test (left)
Figure 22: Pressurized, closed volume torque test (right)

2.3.5 - Test Method 4: Pressurized, Closed Volume (Arm + Dummy Volume) Torque Tests

Note that for all closed volume tests, it was necessary to install a relief valve in the shoulder housing unit cap. This was used to “recharge” the internal volume of the arm to atmospheric conditions before each flexion to ensure that any leakage of air from inside the arm to the vacuum environment (which was found to occur) did not compromise the test. The following protocol was implemented for the pressurized, closed volume (arm + dummy volume) torque tests (see Figure 23 for a depiction of this test condition):

1. Mount the EMU arm to the chamber using the shoulder housing unit, and attach it to the elbow articulation rig
2. Rotate the shoulder joint 90° off axis from the elbow
3. Attach the shoulder housing unit cap to the arm, thereby closing the internal volume
4. Connect the shoulder cap to a dummy volume representative of the free volume of an occupied, pressurized EMU using common 9.5 mm (3/8 in) plastic tubing (for these tests, a 0.028 m³ [1 ft³] PVC pipe was used as the dummy volume based on estimates of the EMU free volume (Hamilton-Sundstrand, 2003))
5. Follow steps 4-12 of the Test Method 3 protocol

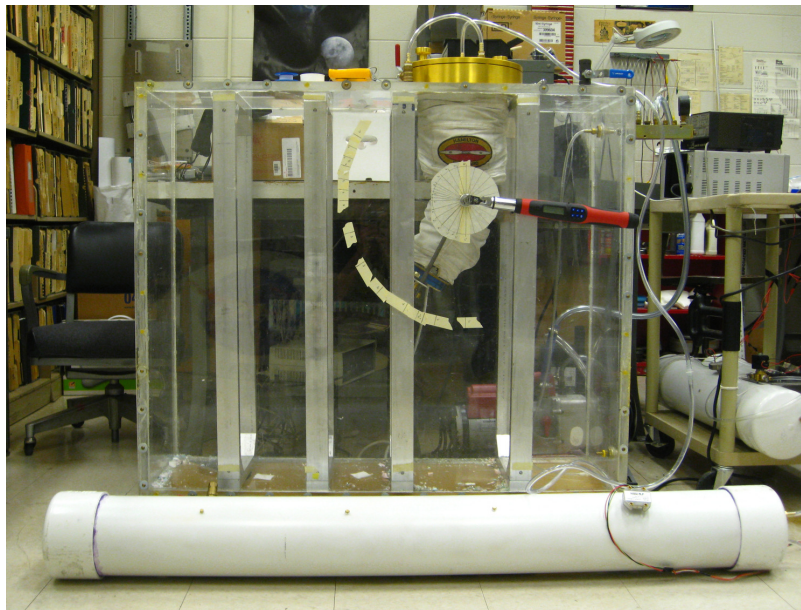
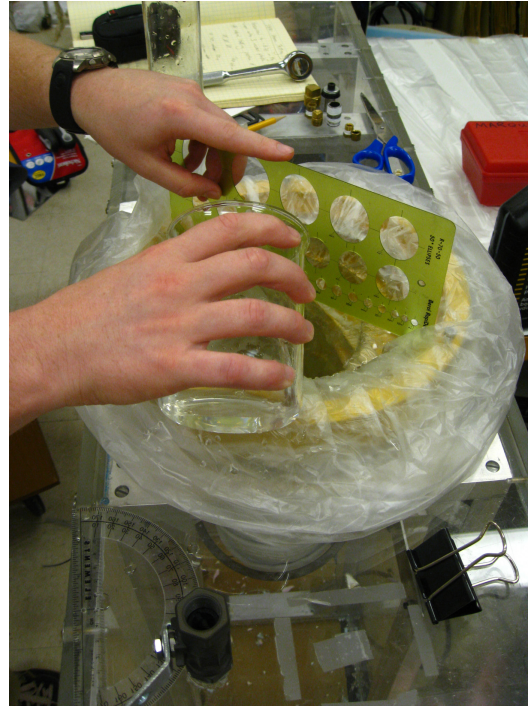


Figure 23: Pressurized, closed volume (arm + dummy volume) torque test

2.3.6 - Test Method 5: Pressurized, Uncapped Δ Volume Water Tests

The following protocol was implemented for the pressurized, uncapped Δ Volume arm tests (see Figures 24a-c for a depiction of this test configuration):

1. Mount the EMU arm to the chamber using the shoulder housing unit, and attach it to the elbow articulation rig
2. Rotate the shoulder joint 90° off axis from the elbow
3. Line the interior of the arm with at least two layers of protective material akin to garbage bags (to ensure that no water leaks into the arm layers)
4. Fill the arm approximately 80% full with water (using a graduated cylinder or some other type of liquid measuring device), keeping track of the total amount of water used
5. Pressurize the chamber to -29.6 kPag (-4.3 psig) using the method described in Appendix A
6. Wiggle the arm back and forth 2-3 times to ensure that the liners have settled as completely as possible into the newly-expanded pressurized volume of the arm
7. Flex the arm to its maximum angle and hold it in this position (for the tests described herein, the arm was flexed to 105° rather than its true maximum at 115° because it was deemed too risky to push the arm to maximum flexion given the relative strength of the protective liners used)
8. Fill the remaining volume of the arm with water (keeping track of how much is used) such that the water level exactly matches the top of the shoulder bearing – the method used to determine the exact water level involved the use of a leveling tool (the green plastic stencil depicted in Figures 24a-c), which was placed across the shoulder bearing and water was added until it first came into contact with the bottom edge of the stencil
9. Sum the water totals from steps 4 and 8 – this represents the total volume of the arm at its maximum flexion angle
10. Relax the arm to the next largest angle increment
11. Repeat steps 8-10 to determine the total volume at each angle of interest



Figures 24a-c (clockwise from top left): Engineer measuring the total water required to fill the arm at 25° flexion; close-up views of the protective lining and leveling tool used to determine exact water levels at each angle

2.4 - RESULTS

2.4.1 - Test 1: Unpressurized Elbow Flexion Torque vs. Angle Test

The first test, torque vs. angle of the arm in its unpressurized state, aimed to characterize the baseline torque of the system (gravity effects). The results of this test are included below as Figure 25 (the flexion image, which appears in all subsequent torque vs. angle figures, was modified from (Schmidt, 2001)).

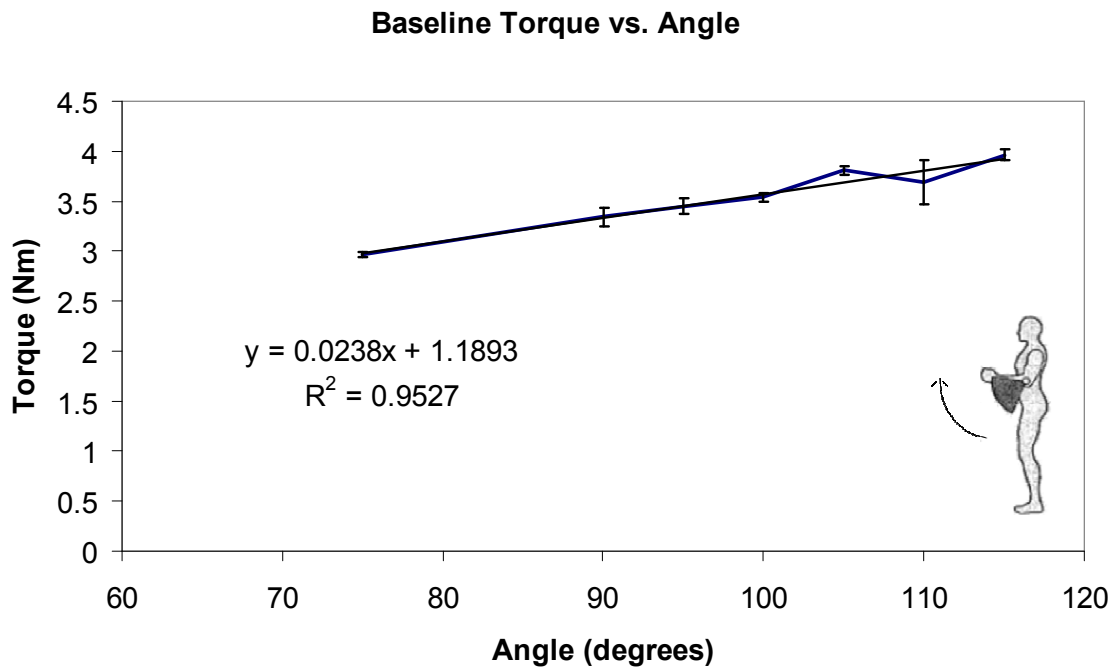


Figure 25: Baseline torque vs. angle of the arm/rig in its unpressurized state

This test was repeated 5 times: the data points shown represent the average torque value for each angle, and the error bars shown represent 95% confidence intervals based on the repeat tests. Data for angles lower than 75° was not collected, because the torque values in that regime were too small to be detected by the torque wrench used (< 2.7 Nm).

Because it was necessary to characterize the role of gravity effects for the entire test spectrum, including the angles below the measurement threshold of the torque wrench, a best-fit approximation was used to estimate the magnitude of gravity effects at low angles. This best-fit approximation, based on a linear model, is displayed on the data.

All subsequent torque vs. angle plots appearing in this work have been calibrated to remove this torque contribution from gravity effects (best fit approximation values were used for angles $< 75^\circ$, and measured values were used for angles $\geq 75^\circ$). Thus, all subsequent torque data is attributable to only the three effects of interest: structural, volume, and pressure effects.

2.4.2 - Test 2: Pressurized, Open Volume Torque vs. Angle Test

The second test, torque vs. angle of the arm in its pressurized and open volume state, aimed to characterize the total torque of the system based on only volume and structural effects. The results of this test are included below as Figure 26.

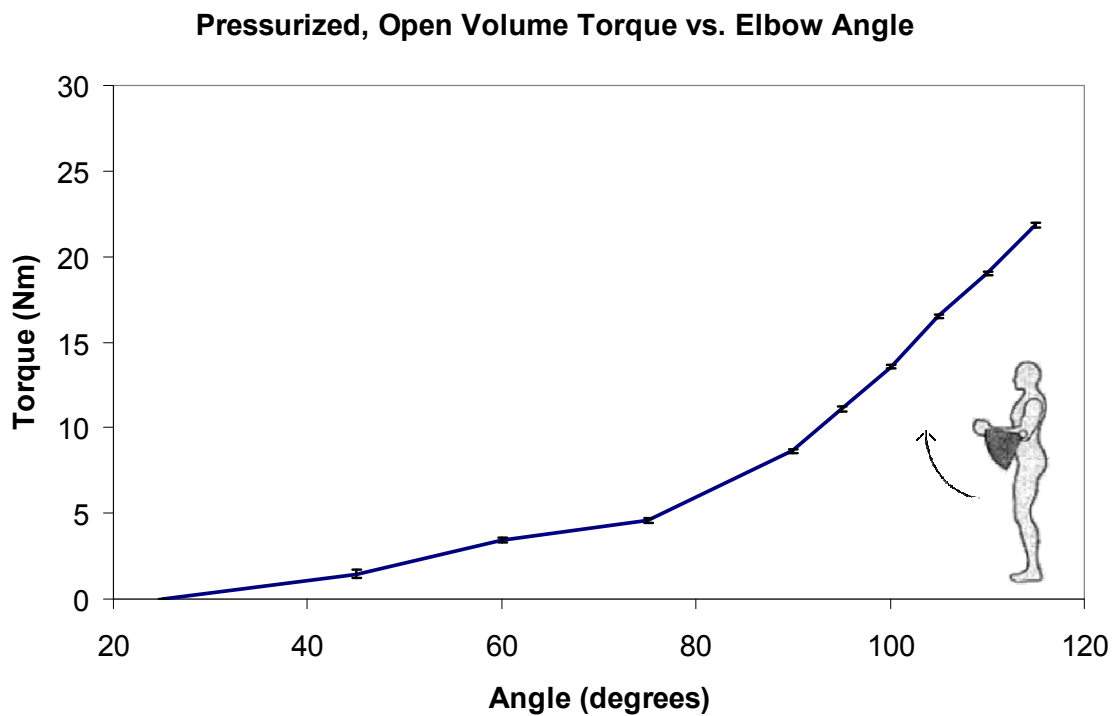


Figure 26: Total torque vs. angle of the arm in its pressurized and open volume state, with gravity effects removed

This test was repeated 8 times: the data points shown represent the average torque value for each angle, and the error bars shown represent 95% confidence intervals based on these repeat tests. The neutral resting position of the arm when pressurized was found to

be approximately 25° - this represents the starting point of the test, and the point where torque was considered to be zero. Additionally, these torque values only represent the torque required to flex the arm from its starting neutral position to the angle of interest. Hysteresis effects were not considered.

Torque was found to increase as flexion angle increases, which is consistent with expectations and previous work. Furthermore, the relative shape of the curve (with relatively low torque values reported at low flexion angles and a non-linear increase in torque as flexion angle increases) is also consistent with expectations and previous work. As a reference, a previous torque vs. angle test conducted on the EMU elbow in its pressurized state by researchers in the MVL is included below as Figure 27.

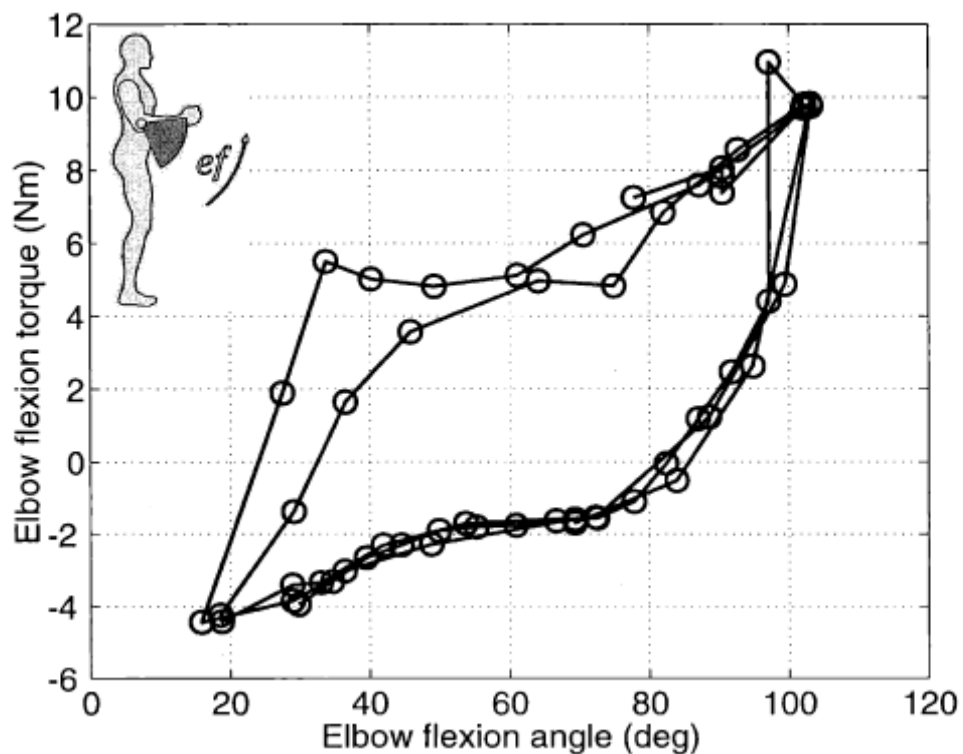


Figure 27: Previous total torque vs. angle test of the EMU elbow in its pressurized state, conducted by MVL researchers, taken from (Schmidt, 2001)

The data presented in this figure, which characterizes the total torque vs. angle behavior of the elbow joint through its flexion envelope (including its hysteresis behavior, which

again is not of interest of this study), is consistent with the findings from this study presented in Figure 26: in the previous test, torque was found to generally increase non-linearly as flexion angle increases, especially at high angles of flexion; the neutral position of the elbow (position where torque is zero) was found to be approximately 25°; and the magnitudes of torque values measured were consistent with the current study.

2.4.3 - Test 3: Pressurized, Closed Volume (Arm only) Torque vs. Angle Test

The third test, torque vs. angle of the arm in its pressurized and closed volume state (with the closed volume only that of the capped and unoccupied arm), aimed to characterize the total torque of the system based on volume, structural and pressure effects in the closed volume of the EMU arm. The results of this test are included below as Figure 28.

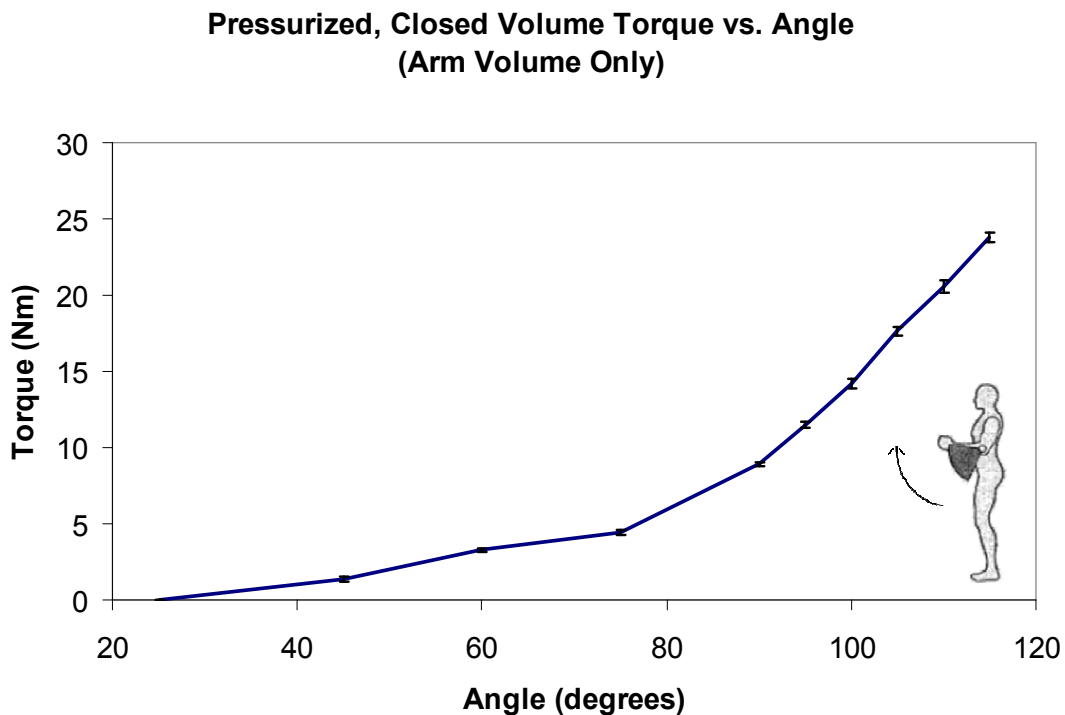


Figure 28: Total torque vs. angle of the arm in its pressurized and closed volume state, with gravity effects removed

This test was repeated 7 times: the data points shown represent the average torque value for each angle, and the error bars shown represent 95% confidence intervals based on these repeat tests. Again, the neutral resting position of the arm when pressurized was found to be approximately 25° - this represents the starting point of the test, and the point where torque was considered to be zero. And again, these torque values only represent the torque required to flex the arm from its starting neutral position to the angle of interest. Hysteresis effects were not considered.

Comparing the data from Figures 26 and 28 provides a direct assessment of the magnitude of pressure effects acting in the closed volume of the EMU arm. This comparison is presented in Figure 29.

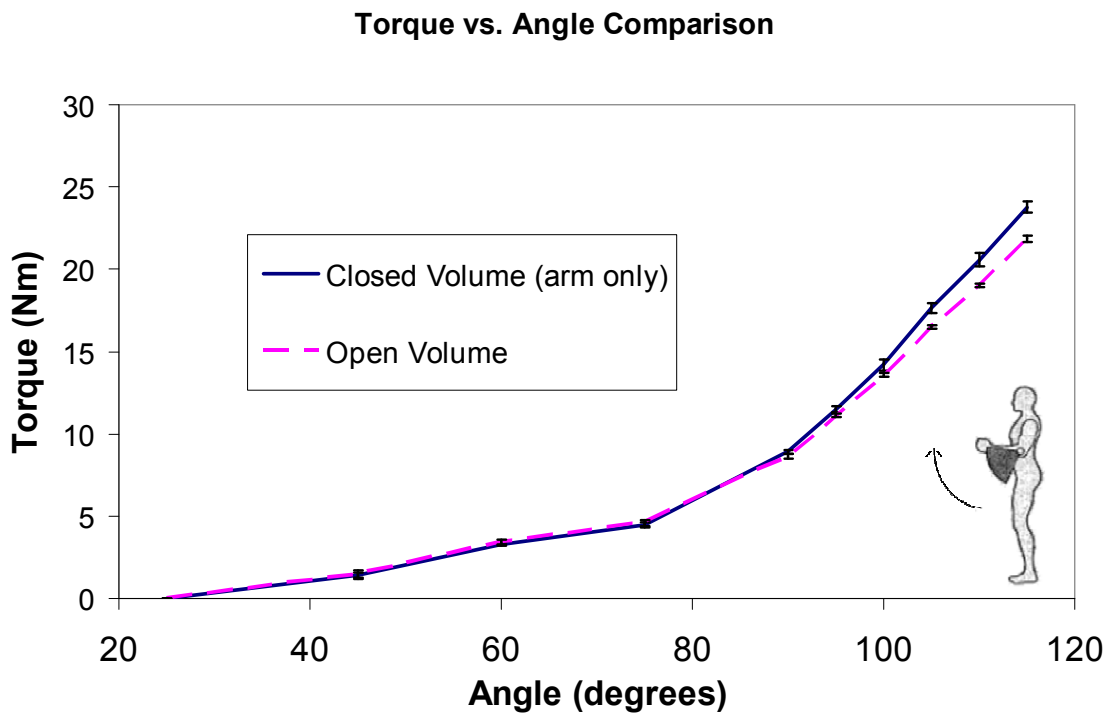


Figure 29: Comparison of total torque vs. angle of the arm in its pressurized and open/closed volume states, with gravity effects removed

The magnitude of pressure effects contributions to total torque, determined by subtracting the closed volume torque from the open volume torque values, was found to increase as the arm was flexed from 25°-115°, with the largest contribution occurring at the

maximum flexion angle (115°). Using a two-sample t-test for equal means, statistically significant ($p < 0.05$) torque increases due to pressure effects were detected at angles of 90° and greater. At its maximum point (corresponding to maximum flexion), we see an 8.8% increase in torque over the open volume condition attributable to pressure effects. A magnified view of the significant pressure effects regime is presented in Figure 30, and the results of the two-sample t-test are presented in Table 5.

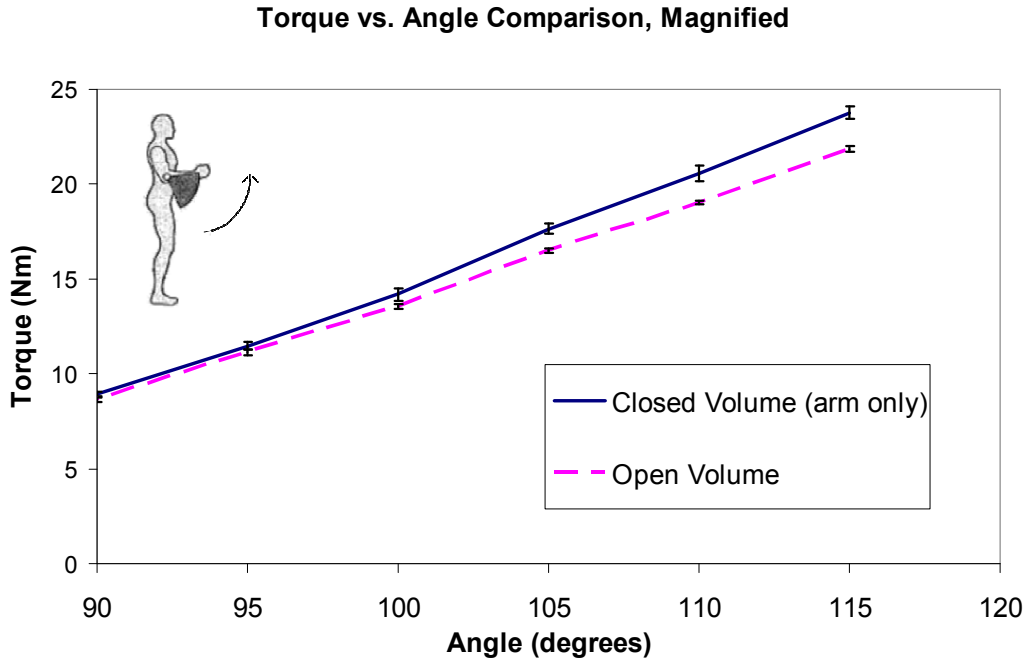


Figure 30: Magnification of the regime where pressure effects become significant in the pressurized, closed volume (arm only) EMU elbow

Table 5: Statistical analysis of pressure effects in the closed arm volume, with statistically significant values shown in gray

2 Sample T-test data						
Angle (deg)	Open Volume Torque (Nm)	Closed Volume Torque (Nm)	% Torque Increase	p-value		
25	0.0	0.0	0.0	N/A		
45	1.5	1.4	-4.3	0.683		
60	3.4	3.3	-4.2	0.167		
75	4.6	4.5	-2.8	0.281		
90	8.6	8.9	3.2	0.007		
95	11.1	11.5	3.2	0.012		
100	13.6	14.2	4.6	0.002		
105	16.5	17.6	6.9	0.000		
110	19.0	20.6	8.1	0.000		
115	21.8	23.8	8.8	0.000		

2.4.4 - Test 4: Pressurized, Closed Volume (Arm + Dummy Volume) Torque vs. Angle Test

The fourth test, torque vs. angle of the arm in its pressurized and closed volume state (with the closed volume that of the capped arm and a 0.028 m³ [1 ft³] PVC pipe acting as a dummy volume), aimed to characterize the total torque of the system using an internal volume truly representative of a full, pressurized and occupied EMU. Due to logistics and test operator availabilities, this test was conducted nearly one year after tests 1-3 (6/2009 as opposed to 6/2008). Because of the long lag between tests, and the fact that the data collected in this test needed to be compared to data from test 2 (the pressurized, open volume torque vs. angle test) to characterize the pressure effects acting on the system, it was determined that a repeat of test 2 was first necessary to ensure that nothing had changed in the test setup during the extended layoff. This was deemed necessary before test 4 could be properly administered. Test 2 was therefore repeated, and a comparison of the test 2 data taken in 6/09 and the test 2 data taken in 6/08, both calibrated for gravity effects, is included below as Figure 31.

Torque vs. Angle Data Drift

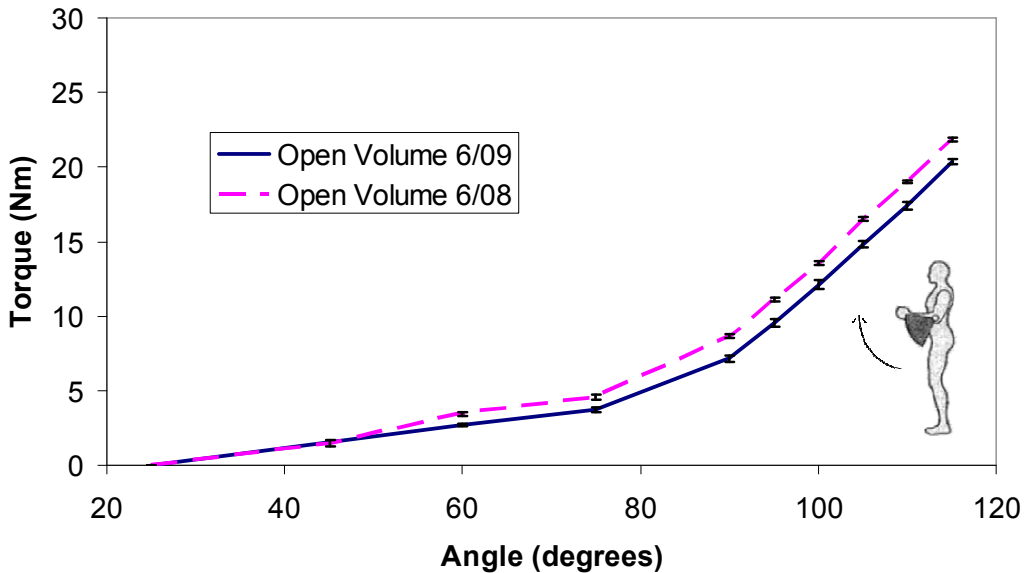


Figure 31: Test 2 data comparison between 6/08 and 6/09 tests, with gravity effects removed

The 6/09 test was repeated 8 times: the data points represent the average torque value for each angle, and the error bars represent 95% confidence intervals. Note that a significant shift is evident. For nearly every data point, the torque recorded decreased by 1-1.5 Nm. A quantitative treatment of data drift is shown in Table 6.

Table 6: Shift in torque data between 6/08 and 6/09 open volume tests

Data Drift				
Angle (deg)	Open Volume Torque 6/08 (Nm)	Open Volume Torque 6/09 (Nm)	Difference (Nm)	
25	0.0	0.0	0.0	
60	3.4	2.7	-0.7	
75	4.6	3.7	-0.9	
90	8.6	7.2	-1.5	
95	11.1	9.5	-1.6	
100	13.6	12.1	-1.4	
105	16.5	14.8	-1.7	
110	19.0	17.4	-1.6	
115	21.8	20.4	-1.5	

Two possible sources were identified for this drift: either the arm had become “worn in”, having undergone countless flexion/extension demonstrations throughout the year, thus making it easier to bend (a reduction in structural effects); or the pressure/volume behavior of the arm had somehow changed, reducing the role of pressure/volume effects. Other potential sources (the torque wrench calibration had changed, or the baseline torque of the arm/rig system had changed) were deemed unlikely due to the fact that the torque wrench went unused between 6/08 and 6/09 (it was not used as part of the demonstrations), and the rigid arm/rig system was not likely to be affected by repeated use. It became necessary to resolve the source of this drift before continuing with test 4, because any changes in pressure/volume behavior of the arm between 6/08 and 6/09 would confound the analysis of the test 4 data (again the purpose of which was to characterize the pressure effects in an EMU-representative enclosed volume).

To determine the cause of the data drift, test 3 was also repeated (a pressurized closed volume torque vs. angle test, with a closed volume of just the unoccupied arm). This served to assess whether the magnitude of pressure effects had changed from the previous tests. If these effects had in fact changed, it would suggest that changes in the pressure/volume behavior, rather than structural behavior, were the cause of the data

shift. Comparing the test 3 data from 6/09 and 6/08, an identical shift in the data was evident. This shift, calibrated for gravity effects, is represented in Figure 32.

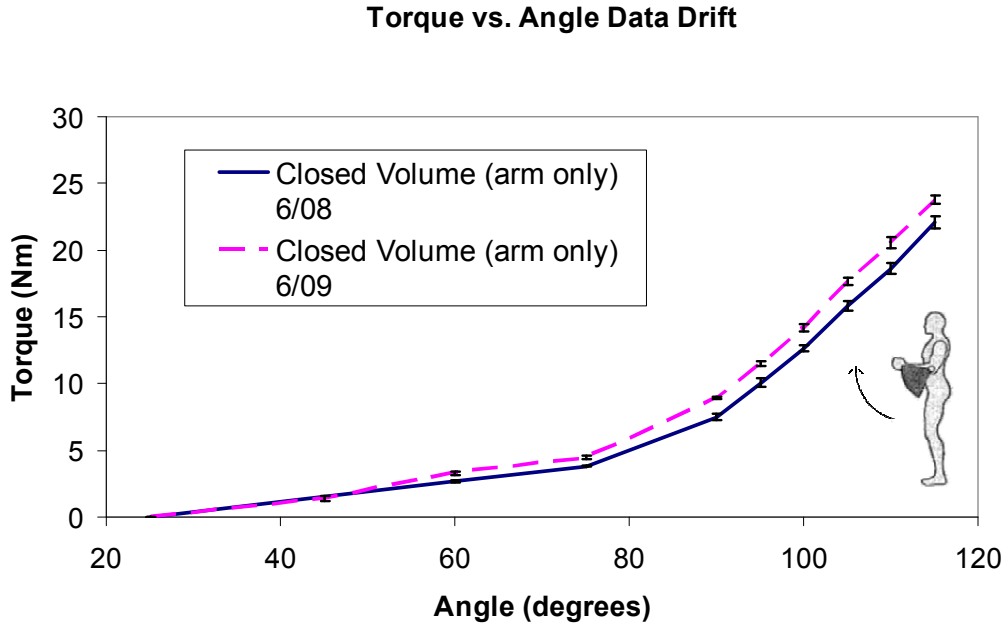


Figure 32: Test 3 data comparison between 6/08 and 6/09 tests, with gravity effects removed

Again, the 6/09 test was repeated 8 times: the data points represent the average torque value for each angle, and the error bars represent 95% confidence intervals. The magnitude of the data shift was very similar to that from the open torque case (the torque values had decreased by 1-1.5 Nm). And again, a quantitative treatment of the data drift is shown in Table 7.

Table 7: Shift in torque data between 6/08 and 6/09 closed volume tests

Data Drift				
Angle (deg)	Closed Volume Torque 6/08 (Nm)	Closed Volume Torque 6/09 (Nm)	Difference (Nm)	
25	0.0	0.0	0.0	
60	3.3	2.7	-0.6	
75	4.5	3.8	-0.6	
90	8.9	7.5	-1.4	
95	11.5	10.0	-1.4	
100	14.2	12.7	-1.5	
105	17.6	15.8	-1.8	
110	20.6	18.6	-2.0	
115	23.8	22.1	-1.7	

Because both the 6/09 open and 6/09 closed volume data demonstrated the same data shift, it was decided that a direct comparison between the two (like was previously done in Figure 29 to determine the magnitude of pressure effects acting in the elbow) could be conducted without unduly confounding the assessment (i.e. it would still be an apples-to-apples comparison). Such a comparison is included as Figure 33.

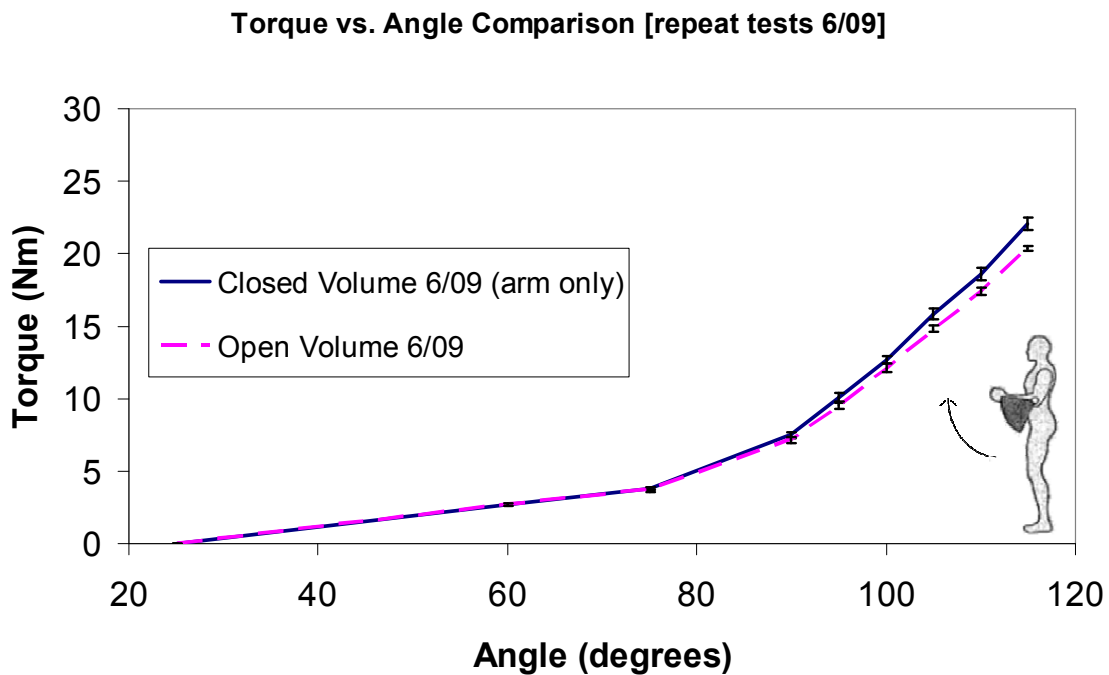


Figure 33: Repeat comparison of total torque vs. angle of the arm in its open and closed volume states, using 6/09 data, with gravity effects removed

Identical pressure effects behavior was demonstrated in the 6/09 open and closed volume tests when compared to the 6/08 tests: pressure effects only become significant at angles $\geq 90^\circ$, with the maximum flexion angle corresponding to the maximum pressure effects. And again, using a two-sample t-test for equal means, statistically significant ($p < 0.05$) torque increases due to pressure effects were detected at angles of 90° and greater. At its maximum point (corresponding to maximum flexion), we see an 8.3% increase in torque over the open volume condition attributable to pressure effects. This is nearly identical to the 6/08 tests, where an 8.8% increase in torque was detected at maximum flexion. The results of this t-test are presented as Table 8.

Table 8: Statistical analysis of pressure effects in the closed arm volume based on 6/09 data, with statistically significant values shown in gray

2 Sample T-test data					
Angle (deg)	Open Volume Torque (Nm)	Closed Volume (Arm Only) Torque (Nm)	% Torque Increase	p-value	
25	0.0	0.0	0.0	N/A	
60	2.7	2.7	0.0	0.984	
75	3.7	3.8	3.2	0.191	
90	7.2	7.5	4.6	0.046	
95	9.5	10.0	5.6	0.025	
100	12.1	12.7	4.4	0.018	
105	14.8	15.8	6.8	0.000	
110	17.4	18.6	7.1	0.000	
115	20.4	22.1	8.3	0.000	

Based on the finding that both the nature and magnitude of pressure effects were nearly identical in the 6/08 and 6/09 tests despite the documented data shift, it was determined that the pressure/volume behavior of the arm had not changed between 6/08 and 6/09. Consequently, the data drift was attributed to the arm becoming “worn in” due to repeated demonstration between 6/08 and 6/09, meaning that structural effects (rather than pressure/volume effects) had decreased in magnitude.

Having identified the source of the data drift, test 4 was then conducted with confidence that the pressure/volume behavior of the arm was still in tact. As a reminder, test 4 aimed to characterize the total torque of the system based on volume, structural, and pressure effects using an internal volume truly representative of a full, pressurized and occupied EMU (the internal arm volume plus 1 ft³ dummy volume). The results of this test are included as Figure 34.

This test was repeated 8 times: the data points represent the average torque value for each angle, and the error bars represent 95% confidence intervals. Again, hysteresis effects were not considered. Comparing the data from the 6/09 open volume test (shown in Figure 31) with the data presented in Figure 34, a direct assessment of the magnitude of pressure effects acting in the closed volume fully representative of an occupied, pressurized EMU is possible. This comparison is presented in Figure 35.

Pressurized, Closed Volume Torque vs. Angle (arm + pipe)

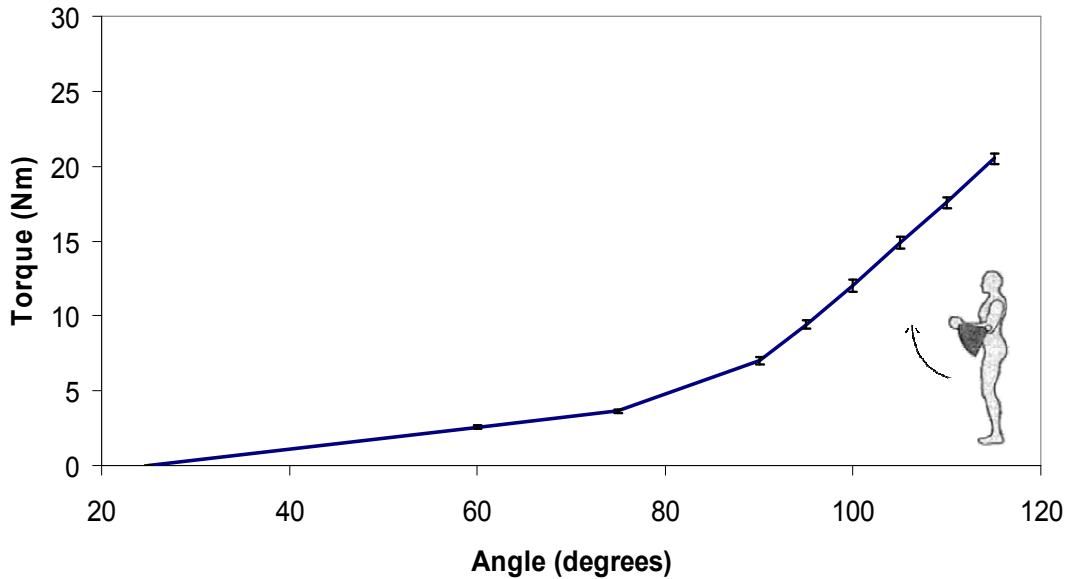


Figure 34: Total torque vs. angle of the arm in its pressurized and closed volume state representative of a full EMU, with gravity effects removed

Torque vs. Angle Comparison [based on 6/09 data]

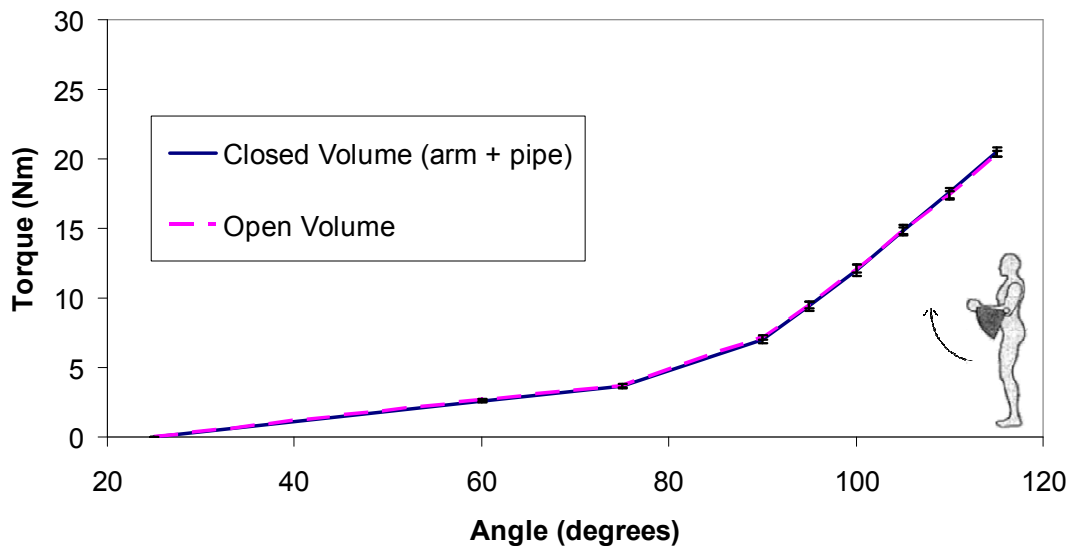


Figure 35: Comparison of total torque vs. angle of the arm in its pressurized and open/closed volume states, based on data from 6/09 tests with a representative EMU volume, with gravity effects removed

The magnitude of pressure effects contributions to total torque, determined by subtracting the closed volume torque from the open volume torque values, was found to be insignificant for all flexion angles. Using a two-sample t-test for equal means, statistically significant ($p < 0.05$) torque increases due to pressure effects were not detected anywhere in the flexion envelope. The results of the two-sample t-test are presented in Table 9.

Table 9: P-values and % change in torque during elbow flexion due to pressure effects in a representative full EMU closed volume

2 Sample T-test data				
Angle (deg)	Open Volume Torque (Nm)	Closed Volume (Arm + Pipe) Torque (Nm)	% Torque Increase	p-value
25	0.0	0.0	0.0	N/A
60	2.7	2.6	-4.8	0.065
75	3.7	3.6	-1.4	0.621
90	7.2	7.0	-2.1	0.377
95	9.5	9.4	-1.0	0.655
100	12.1	12.0	-0.8	0.724
105	14.8	14.9	0.3	0.856
110	17.4	17.6	0.9	0.504
115	20.4	20.5	0.7	0.479

2.4.5 - Test 5: Pressurized, Uncapped Δ Volume Water Tests

The fifth test, volume vs. angle of the arm in its pressurized and open volume state, aimed to characterize the volume change of the elbow as it is articulated through its full flexion envelope. First, total internal volume at maximum flexion (which was considered to be 105° for these tests, not the standard 115° , to prevent undue risk to the arm specimen) was measured, and this baseline was determined to be $7788 \text{ cm}^3 \pm 118 \text{ cm}^3$ ($0.275 \text{ ft}^3 \pm 0.004 \text{ ft}^3$). This was based on four repeat tests, and the uncertainty represents 95% confidence intervals based on these repeat tests.

Changes in internal volume relative to 105° were then measured, and these values were added to the baseline value to establish total volume estimates for the entire flexion envelope. It was assumed that hysteresis effects were insignificant (i.e. that data taken

during flexion would be identical to data taken during extension). The results of this test, after being added to the baseline 105° volume, are included below as Figure 36.

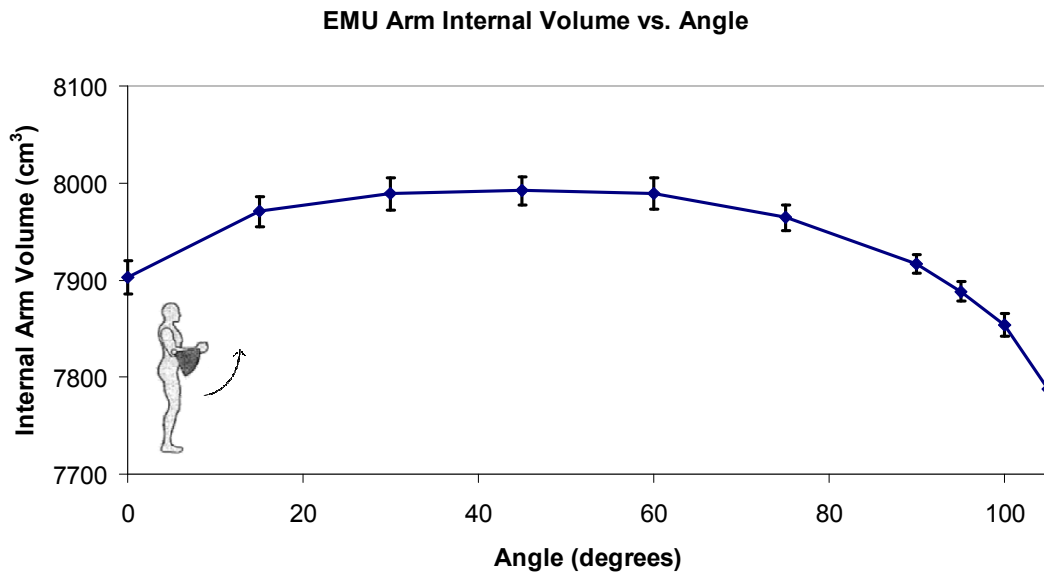


Figure 36: Pressurized EMU arm internal volume as a function of angle

This test was repeated 4 times: the data points represent the average volume for each angle, and the error bars represent 95% confidence intervals of the volume change data only (not the uncertainty in the baseline volume measurement itself).

This data demonstrates that the arm exhibits nearly constant volume behavior between approximately 20-60°, a regime which includes the natural pressurized resting position of the arm (25-30°). This also demonstrates that the maximum internal volume state of the arm corresponds to its natural pressurized resting position (its lowest energy state). Deviations from this resting position (either flexion or extension) result in a decrease in total internal volume, and thus an increase in torque required (due to volume effects and in some cases pressure effects). Additionally, and as expected based on earlier data presented, the EMU arm experiences significant volume change at the extremes of its flexion envelope. This finding is consistent with the statistically significant pressure effects previously demonstrated at high flexion angles (for the arm-only closed volume), because pressure effects by definition stem from changes in pressure due to changes in volume. Finally, at its maximum volume state of ~30°, the total EMU arm volume was

measured to be 7990 cm³ (0.282 ft³) representing a 2.6% increase in volume over the minimum volume state at 105°.

2.4.6 - Structural, Volume, and Pressure Components to total Rigidity

With the information collected from tests 1-5, the contributions of pressure, volume, and structural effects to total suit rigidity were calculated using equations 12-14. Because volume change data is unavailable for angles greater than 105°, volume and structural effects were not calculated at these angles. The individual contributions to total rigidity for the EMU elbow were calculated separately for each closed-volume condition (test 3 and test 4 configurations respectively), both because they represent two fundamentally different suit configurations and because of the data drift problem previously mentioned.

What follows are four graphics: Figure 37 shows a graphical representation of the individual contributions to suit rigidity, as functions of angle, for the arm-only test condition; Figure 38 shows identical information for the arm + dummy-volume test condition; and Tables 10 and 11 show the same data explicitly in quantitative form.

Note that in both cases, at high flexion angles the calculated volume effects exceed that of the measured open volume torque (this phenomenon takes place sooner for the arm + pipe test condition). This results in negative structural effects values calculated at those high angle conditions, based on equation 14. This negative structural effect value, then, is represented graphically by the area of the plot below the x-axis (the zero torque level), resulting in a downward shift of the entire stack plot. Careful examination of these plots, though, will reveal that the top-most level of the stack plot (the value representing the summation of all three effects at each angle) matches the exact closed-volume torque vs. angle data previously presented for each condition.

A detailed discussion of these results, including a discussion of this seemingly strange structural effects behavior, is presented in the next section.

Individual Components to Total Joint Torque (arm only)

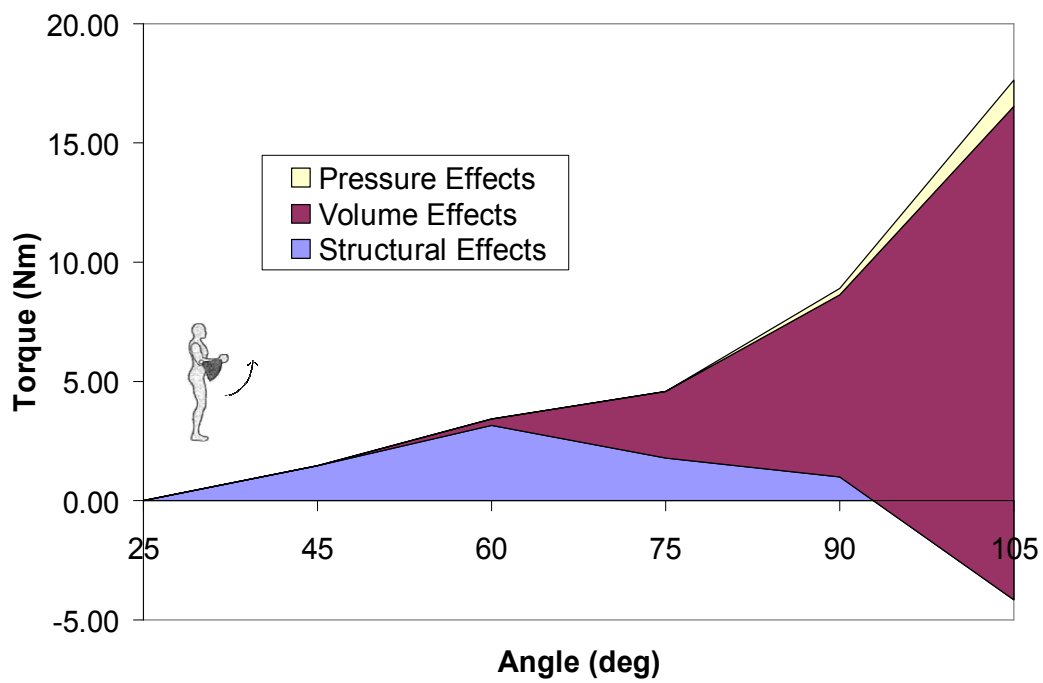


Figure 37: Individual torque components vs. angle (closed volume, arm only), with gravity effects removed

Individual Components to Total Joint Torque (arm + pipe)

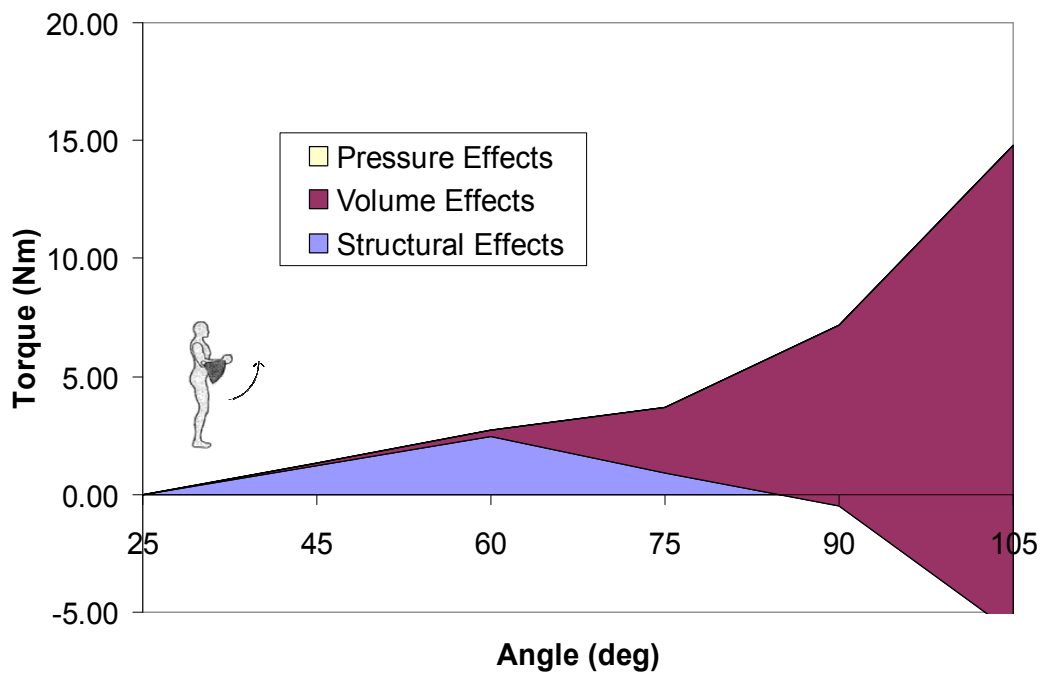


Figure 38: Individual torque components vs. angle (closed volume, arm + pipe), with gravity effects removed

Table 10: Summary of pressure, volume, and structural effects as a function of angle for the EMU arm (closed volume, arm-only test condition)

Angle (deg)	Pressure Effects (Nm)	Volume Effects (Nm)	Structural Effects (Nm)
25	Statistically Insignificant	0.00	0.00
45	Statistically Insignificant	0.00	1.46
60	Statistically Insignificant	0.25	3.18
75	Statistically Insignificant	2.81	1.77
90	0.28	7.62	1.02
95	0.36	10.51	0.61
100	0.62	14.01	-0.44
105	1.14	20.67	-4.16
110	1.55	N/A	N/A
115	1.92	N/A	N/A

Table 11: Summary of pressure, volume, and structural effects as a function of angle for the EMU arm (closed volume, arm + pipe test condition)

Angle (deg)	Pressure Effects (Nm)	Volume Effects (Nm)	Structural Effects (Nm)
25	Statistically Insignificant	0.00	0.00
45	Statistically Insignificant	0.13	1.23
60	Statistically Insignificant	0.25	2.45
75	Statistically Insignificant	2.81	0.89
90	Statistically Insignificant	7.62	-0.47
95	Statistically Insignificant	10.51	-1.00
100	Statistically Insignificant	14.01	-1.89
105	Statistically Insignificant	20.67	-5.86
110	Statistically Insignificant	N/A	N/A
115	Statistically Insignificant	N/A	N/A

2.5 – DISCUSSION

As shown in the previous figures, when the EMU arm was initially flexed from its natural resting position of approximately 30°, suit resistance was primarily caused by structural effects. This was consistent with the volume change data, which showed the elbow maintains approximately constant volume in this regime (rendering volume and pressure effects insignificant). As the arm was flexed further, it began to deform such that the internal volume decreased, and we saw a subsequent increase in the influence of volume effects. At extreme flexion angles, we saw that suit rigidity was dominated by volume effects, which corresponds to the regime where significant volume change takes place.

In the case where the closed internal volume was that of only the unoccupied arm, pressure effects were also found to be statistically significant at flexion angles $\geq 90^\circ$. This finding was consistent with the volume change data presented – because pressure effects stem from changes in volume, it was expected that such effects would act most significantly in regimes where large volume changes exist. Such pressure effects were not present in the larger volume (arm + pipe) test case. This suggests that pressure effects are not significant in the EMU elbow joint when it is pressurized and connected to the closed EMU. The EMU elbow joint, however, is considered to be one of the most simple joints in the suit (1-degree-of-freedom with a relatively small diameter), and as a result has been relatively well optimized for mobility (Hodgson, 2008). While pressure effects were not at all detected in the elbow when connected to a volume representative of the full suit, the fact that they were measured in the smaller volume condition suggests that larger, more complicated and poorly optimized joints (such as the hip or waist) may be especially prone to these effects.

We also saw that structural effects, which dominate at low flexion angles, decreased (and even became negative) as the arm moved into the extreme flexion angles. Based on conversations with Mr. Gary Harris, an expert on space suit design and construction, it is believed that this phenomenon was related to changes in the center of pressure C_p (which is defined as the point on the body where the total sum of the local pressure field acts)

relative to the restraint layer of the garment (the stitching designed to prevent the arm from extending length-wise due to pressurization) during joint movement (Harris, 2009).

To understand this phenomenon, consider a standard convolute elbow joint resting in its pressurized state, depicted in cartoon form in Figure 39 (the space suit arm graphic, which appears in Figures 39-43, was modified from (Kozloski, 1994)). When pressurized and in its neutral state (i.e. its zero-torque condition), the center of pressure aligns with the midline of the joint, which also aligns with the stitched restraint layer of the garment. As a result of this equilibrium, no net torque acts on the arm because these forces are in alignment, and the arm remains in this position unless acted upon by an external force. This steady-state orientation is displayed in Figure 40 (for one section of the convolute joint).

As the elbow is initially flexed, the convolute joint changes shape: the outside edge straightens, and the inside edge bunches together and extends inward. This deformation causes the C_p to shift inward. The restraint layer (which is fixed in place on the arm), however, remains in the same position. The resultant forces, which no longer align, impart a net torque on the arm, thereby breaking the steady state equilibrium established in the neutral resting position. This torque acts against the direction of flexion, and explains the positive structural effect torque seen at low flexion angles (from approximately 25-60°). See Figure 41 for an exaggerated depiction of this effect (for one section of the convolute joint).

Structural effects will reach a maximum at the point that the C_p migrates furthest towards the inside edge of the arm (based on the data collected, this is estimated to take place near 60°). Eventually, the elbow is flexed far enough to induce buckling of the inside-edge fabric, which causes a collapse of the interior volume of the arm near the inside-edge of the elbow. This causes the C_p to migrate backwards, towards its starting position near the midline of the arm. As the C_p and restraint layer move closer to alignment, the net torque acting on the arm decreases in magnitude (but still acts opposite the direction of flexion). This behavior explains the decreasing (but still positive) structural effect torque seen at

mid-range flexion angles (approximately 60-90°). See Figure 42 for an exaggerated depiction of this effect (for one section of the convolute joint).

At extreme flexion angles ($> 90^\circ$), the buckling of the inside-edge fabric becomes so significant that it induces the C_p to migrate backwards such that at one point it again perfectly aligns with the restraint layer. As this threshold is crossed, the arm experiences zero structural effects-related torque. This zero-torque condition is seen in the structural effects data for both test conditions. At flexion angles beyond this zero-torque condition, the extreme buckling near the inner-edge causes the C_p to actually migrate backwards beyond the restraint layer (towards the outside of the elbow), again misaligning the forces, but in the opposite direction as before. This imparts a net torque on the system acting in the *same* direction as the elbow flexion, meaning it actually assists the operator in flexing the joint. This negative structural effects behavior, while conceptually counter-intuitive, is also seen in the data. Furthermore, this buckling theory is consistent with the volume change data previously presented. See Figure 43 for an exaggerated depiction of this effect (for one section of the convolute joint).

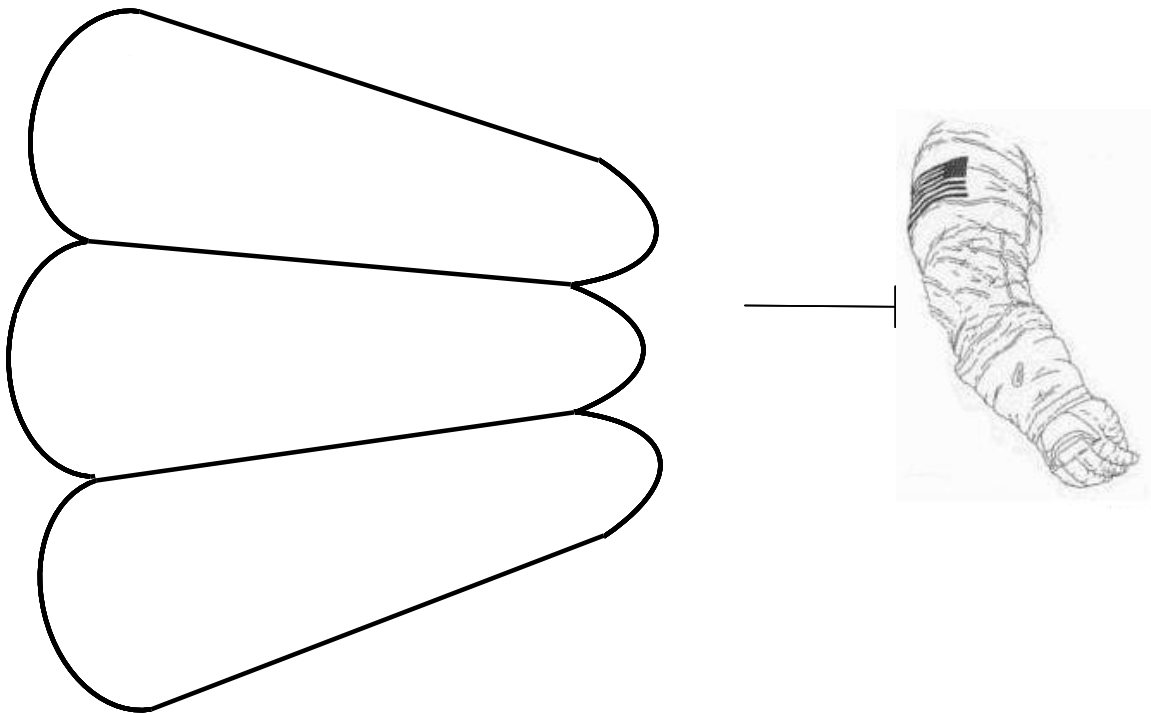


Figure 39: Hypothetical convolute joint in pressurized form (side view)

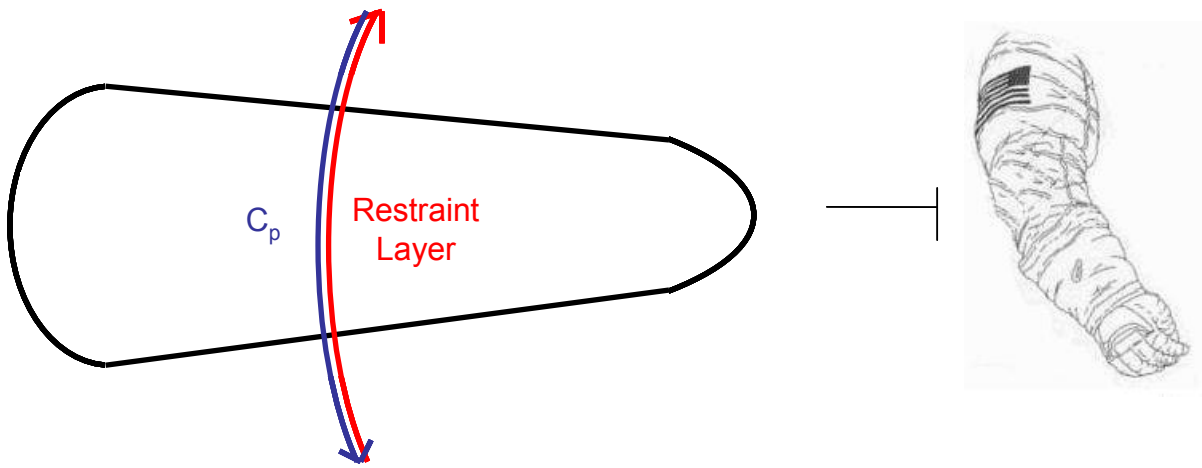


Figure 40: C_p and restraint layer equilibrium in steady-state, pressurized form

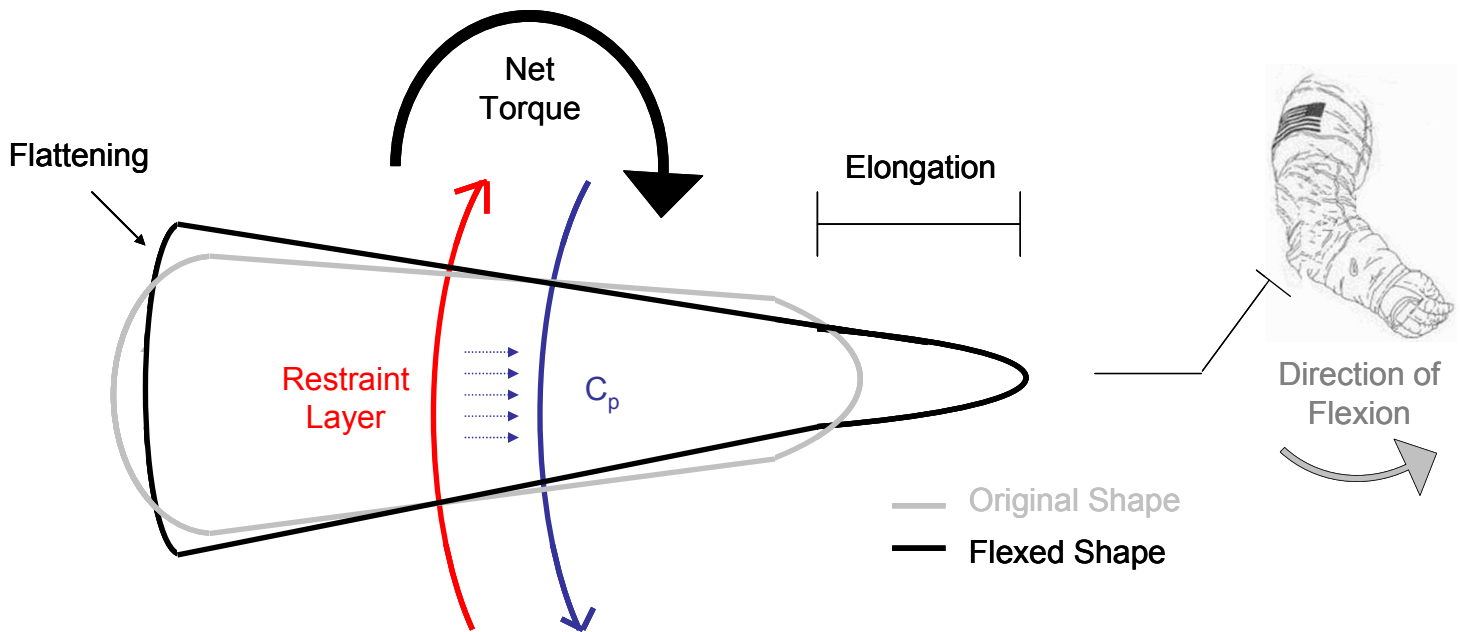


Figure 41: Initial convolute deformation during small flexion, resulting in net torque acting in the opposite direction of flexion

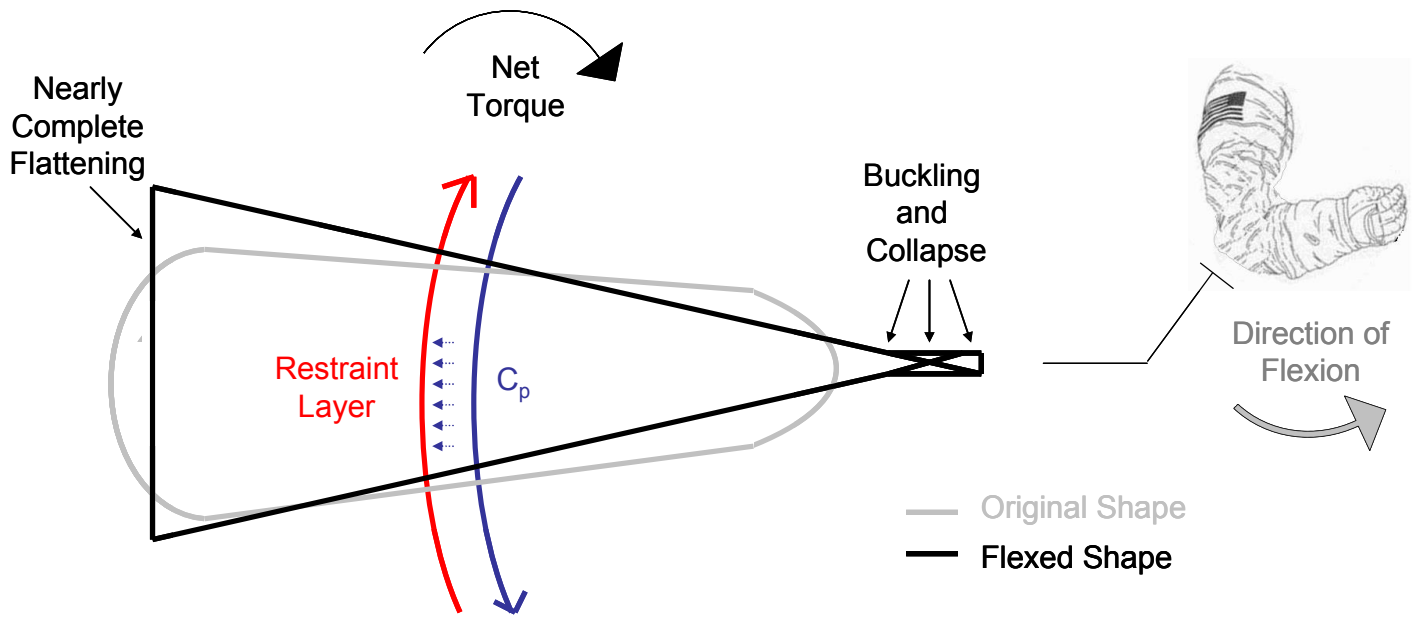


Figure 42: Continued convolute deformation during moderate flexion, resulting in diminished net torque acting in the opposite direction of flexion

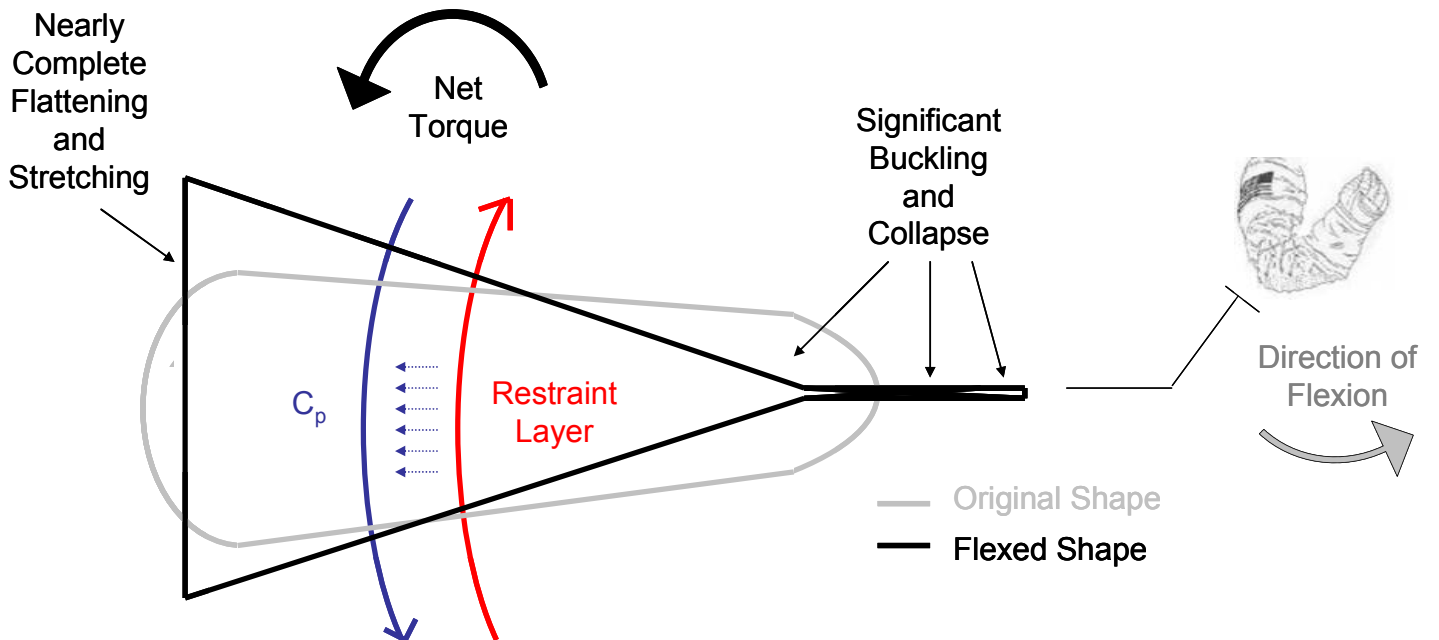


Figure 43: Significant convolute deformation during extreme flexion, resulting in net torque acting in the same direction of flexion as the C_p crosses the restraint layer threshold

While it is believed that the structural effects behavior presented in this report is due to this phenomenon, it is important to note that structural effects dynamics were not the focus of this investigation. It is recommended that further research be conducted to explicitly study these effects to assess this theory.

Finally, we saw different structural effects behavior in the arm + pipe closed volume condition when compared with the arm only volume condition. In the arm + pipe condition, structural effects peak at a lower value, decrease more quickly into the negative regime, and reach larger negative torque values at extreme flexion angles. This difference is not believed to be due to the change in test condition (larger internal volume). Instead, as previously mentioned, this difference is attributable to the data drift presented in Figures 31 and 32. Mathematically speaking, because the open-volume torque values had drifted lower, the calculated structural effects necessarily drifted lower (and more negative) for a given volume change. Physically speaking, because this drift is suspected to stem from the arm being “worn in” due to months of demonstrations, the arm likely experienced both quicker onset of buckling at lower flexion angles and greater magnitudes of buckling at higher flexion angles, leading to an accelerated and greater migration of the C_p past the restraint layer towards the rear of the elbow (resulting in larger negative torque values).

2.5.1 - Hypothesis Assessment and Conclusions

The first hypothesis proposed in this study, that in addition to volume and structural effects a third and not well studied contributor (pressure effects) exists, was supported by the data collected. Pressure effects were documented in the closed volume (arm only) test condition, and contributed upwards of 8% of additional torque at high flexion angles.

The second hypothesis proposed in this study, that pressure effects are a statistically significant contributor to total suit rigidity, was not supported by the data collected. While it is true that capped and uncapped tests of the EMU arm (arm volume only) produced statistically significant results for angles equal to or greater than 90° (or

approximately 60° degrees from neutral position), these findings were not replicated in the tests conducted with a representative EMU volume. No statistically significant increases in torque were measured for any angle for this test condition.

These findings help identify the relative influence of each of the three contributing factors to total space suit rigidity for the well-optimized elbow joint, and also help to map specific rigidity mechanisms to different operating regimes. They confirm prior modeling that identified volume effects as the dominant contributor to joint rigidity. They also shed new light on the non-zero contribution of structural effects to total joint torque, and in doing so expose a seemingly counter-intuitive negative torque contribution at high flexion angles. And as a result, these findings demonstrate that rigidity modeling based solely on volume effects contributions do not fully represent the real life condition.

Perhaps most importantly, though, these findings speak to a potentially unrecognized source to suit rigidity that to this point had not been given serious consideration: pressure effects. While pressure effects were found to be statistically insignificant for the elbow joint when attached to the full EMU, their presence in tests conducted with smaller operating volumes has implications for other joints in the suit. Since the EMU elbow joint does a relatively good job maintaining constant volume, and is a relatively small and simple joint when compared to others in the EMU, it is likely that less-optimized and larger diameter joints will be prone to significant torque increases due to pressure effects stemming from volume changes during movement. Thus, these effects must be considered when modeling joint mobility, designing future suit joint prototypes, and also when crafting suit operating pressure requirements and designing internal pressure regulation systems. And, if pressure effects can be successfully mitigated, suit mobility could be increased in spite of volume changes caused by joint movement.

Incidentally, these findings also demonstrate that any hypobaric chamber joint testing conducted with an open internal volume will not be fully representative of the true suit condition, as these tests would necessarily ignore the contribution of pressure effects.

In summary, these findings expose both the strengths and shortcomings of current joint torque modeling efforts, and provide new information relevant to suit mobility and design. Ultimately, these contributions may lead to more mobile gas-pressurized suit concepts.

2.5.2 - Limitations

A small leak was detected early on between the EMU arm housing and the hypobaric chamber, causing the “closed-volume” gas contained inside the arm when capped to slowly leak into the vacuum environment over time. While several attempts were made to eliminate this leak, we were unable to completely mitigate the problem throughout the testing process. The consequences of this leak are not fully understood, though it stands to reason that it may have artificially weakened the pressure effects seen in this study since the arm was not perfectly capable of sustaining pressure spikes stemming from changes in volume (meaning the pressure effects values presented here may have actually underestimated the true effect). Proper countermeasures were put in place in the test method to prevent this leak from affecting the data (such as installing a valve in the arm cap which allowed the internal arm environment to be “reset” before each test). However, the full effect of this leak on the pressure effects measured cannot be fully characterized (it should be noted that the significance of detecting pressure effects in the smaller volume elbow joint tests necessarily increases given the existence of this leak).

Hysteresis effects related to joint movement, which have been well documented in space suit mobility studies (Schmidt et al., 2001), were largely ignored in this study. With the exception of the volume change tests, all tests were conducted in the flexion direction only, and the arm was reset to its original neutral position between each flexion. It was assumed that the volume change tests, which were conducted starting at maximum flexion and moving through extension to the neutral resting position of the arm, were not affected by hysteresis effects. The tests were done in this manner for practicality purposes, because extension of the arm induced increases in volume (thus causing the water level to drop), making it possible for testers to add water to characterize the change

in volume. Conducting these tests in the flexion direction (which would have raised the water level at each increment due to progressively decreasing volume and required testers to remove water to measure the changes), would have vastly increased the difficulty of accurately measuring the change in volume.

As previously discussed, the measurements taken towards the end of this study were affected by a data drift issue. It is believed the effects of this drift were minimized by repeating earlier tests at the end of the study, enabling “apples-to-apples” comparisons. However, because the source of this data drift was not identified with complete certainty, it is possible that it stemmed from physical changes in the test specimen over time, which may confound the analysis presented herein.

Finally, the PVC pipe used as a dummy volume for the EMU may not have been a perfect substitution for attaching the arm to a complete suit. While the pipe was sized to match the free volume of a pressurized, occupied suit, it was relatively independent of the arm volume (it was connected using rubber tubing) and was considerably different in shape than the free volume inside a suit (the pipe was cylindrical with no internal objects or corners to disrupt gas movement). This may have introduced errors into the transient response of the working gas during flexion.

2.5.3 - Future Work

While gaps in the current literature may be filled as a result of this study, there are several new (and many old, yet still unanswered) questions regarding space suit mobility and pressure effects that warrant further investigation. There is a deficiency in the literature regarding both the changes in internal volume that take place during complex joint movement, and the pressure effects that stem these changes. A first attempt at collecting this data was conducted in this study with the EMU arm, but many other joints are in need of similar characterization. Carrying such research to its logical conclusion (calculating pressure, structural, and volume effects contributions to total torque for each complex joint movement) could lead to an even more thorough understanding of the

forces at work against total suit mobility. Such studies would be best applied to new planetary space suit designs, so that practical improvements could be made to the next generation of space suit hardware. Other future work prospects include: assessing the individual contributions to suit rigidity with hysteresis effects considered; specific investigation of the dynamic structural effects behavior documented in this study; and repeating the tests of this study with the arm attached to the full pressurized and occupied EMU (rather than a dummy volume).



PART III

Active Pressure Regulation as a Method to Improve Gas- Pressurized Space Suit Mobility

Since, in the long run, every planetary society will be endangered by impacts from space, every surviving civilization is obliged to become spacefaring — not because of exploratory or romantic zeal, but for the most practical reason imaginable: staying alive.

- Carl Sagan

3.1 - INTRODUCTION

Based on the results of the suit torque study detailed in Part II, it is clear that space suit designers need to be cognizant of pressure effects (in addition to volume and structural effects) when designing highly mobile gas pressurized suits. To eliminate pressure effects (and thereby increase overall suit mobility), suit designers have two options: either create soft joints that maintain constant volume throughout their entire range of motion, or find ways to deal with the changes in internal pressure given imperfect (non-constant volume) joints. The first option presented is clearly the ideal choice – constant volume soft joints would by definition eliminate both volume and pressure effects contributions to overall joint rigidity, leading to considerable increases in suit mobility. As evidenced by the volume studies previously presented, however, such an idealization is likely impossible in even the most simple joints given the current state of the art. This reality leaves suit designers with no choice but to deal with internal pressure changes induced by volume changes stemming from astronaut movement if they hope to mitigate pressure effects in future designs.

Active pressure regulation, in theory, would be capable of eliminating transient pressure changes stemming from joint movement, thereby eliminating pressure effects despite imperfect joint design. Because pressure effects represent a previously undetected contributor to joint rigidity, though, no studies exist that specifically quantify the ability of active pressure regulation to mitigate pressure effects (and increase suit mobility). To do such a study, first a concept for an active pressure regulation system capable of implementation in the current suit architecture was developed, and then the system was tested against real time changes in pressure in an analogous environment to determine its effectiveness. It is believed that such development and testing could lead to a new and proven mobility-enhancing pressure regulation system concept, which would be highly valuable for suit designers as they move forward with the next generation of space suit development.

3.1.1 - Conceptual Overview of Active Pressure System Experiment

A novel active pressure regulation system concept was first developed, and a prototype of this system was created and assembled in the MIT MVL in fall of 2008. A study designed to experimentally characterize the effectiveness of this regulation system at mitigating (in real time) pressure spikes caused by volume changes driven in a representative EMU dummy volume was then conducted in the MIT MVL in December 2008.

The regulator prototype was mounted to a dummy volume (a sealed PVC pipe) representing the pressurized, occupied volume of the current EMU. Adiabatic volume changes were driven in the dummy volume at a variety of rates and repetitions using an oversized veterinary syringe, and pressure vs. time measurements of the dummy volume were collected using real time pressure transducers both with and without active pressure regulation. This data characterized the effectiveness of the regulator system at mitigating in real time pressure spikes induced by changes in internal volume, and provided an estimate of the behavior of the regulation system if it were to be implemented in an actual EMU and used during joint movement. This provided an indirect assessment of regulator's effectiveness at reducing pressure effects during joint movement, and therefore also its effectiveness at increasing overall suit mobility.

This regulator concept, as well as the aforementioned study and its results, are presented in the following sections.

3.1.2 - Hypothesis

This study sought to assess the following hypothesis:

1. Active pressure regulation can mitigate pressure effects within a space suit despite changes in internal volume.

3.1.3 - Objectives

In order to sufficiently assess this hypothesis, the following experimental objectives were established:

1. Develop a viable active pressure regulation system concept.
2. Build a functional prototype of this regulation system.
3. Develop a test rig that allows precise volume changes to be driven within a closed, pressurized, occupied EMU volume in a repeatable manner.
4. Determine the pressure vs. time behavior of the EMU volume for a variety of changes in internal volume, both with and without active pressure regulation.
5. Determine directly the ability of the active pressure regulation system to mitigate pressure spikes due to volume change, and infer from this determination its ability to mitigate pressure effects and increase suit mobility.

The following sections will discuss in detail the efforts taken to meet these objectives.

3.2 – PRESSURE REGULATION ARCHITECTURE

3.2.1 – Pressure Regulation System Design Requirements

To develop an active pressure regulation system concept capable of mitigating pressure effects in the closed environment of the suit, a set of requirements was first developed to frame the system design (with benchmarks relative to the current EMU pressure regulation system). These requirements were as follows:

1. In real time, the system must: sense the ambient pressure environment, process this sensing information, and be capable of actively responding to changes in state.
2. The system must be sustainable (i.e. consumable gases removed from the ambient environment must be containable and reusable).
3. The system must perform at least as effectively as the current suit regulation system⁴ (i.e. maintain ambient pressure within 0.7 kPa [0.1 psi] of its starting value) (Hamilton-Sundstrand, 2003).

3.2.2 – Active Pressure Regulation Prototype Concept

Given these requirements, an active pressure regulation system concept was developed with MVL researcher Dr. James Waldie (Waldie, 2008). A schematic of this system is included as Figure 44. The system consists of two reservoirs: a high pressure reservoir (HPR) and low pressure reservoir (LPR)⁵, both of which are connected to the volume of interest via electronically controlled solenoid valves. In the schematics presented, the volume of interest is a chamber representing the unoccupied volume of a pressurized EMU when donned by an astronaut (labeled “primary chamber”); in the idealized final application, the volume of interest would be the actual suit volume (and the reservoirs would be directly connected to the suit). The primary chamber and pressure reservoirs are equipped with real-time pressure sensors to monitor their respective pressure states.

⁴ For a schematic of the current suit pressure regulator, refer to Appendix I.

⁵ “High” and “Low” pressure are relative to the pressure of the chamber to be regulated. In this concept, the chamber of interest was set to 1 atm, meaning that the reservoirs would be set above and below 1 atm.

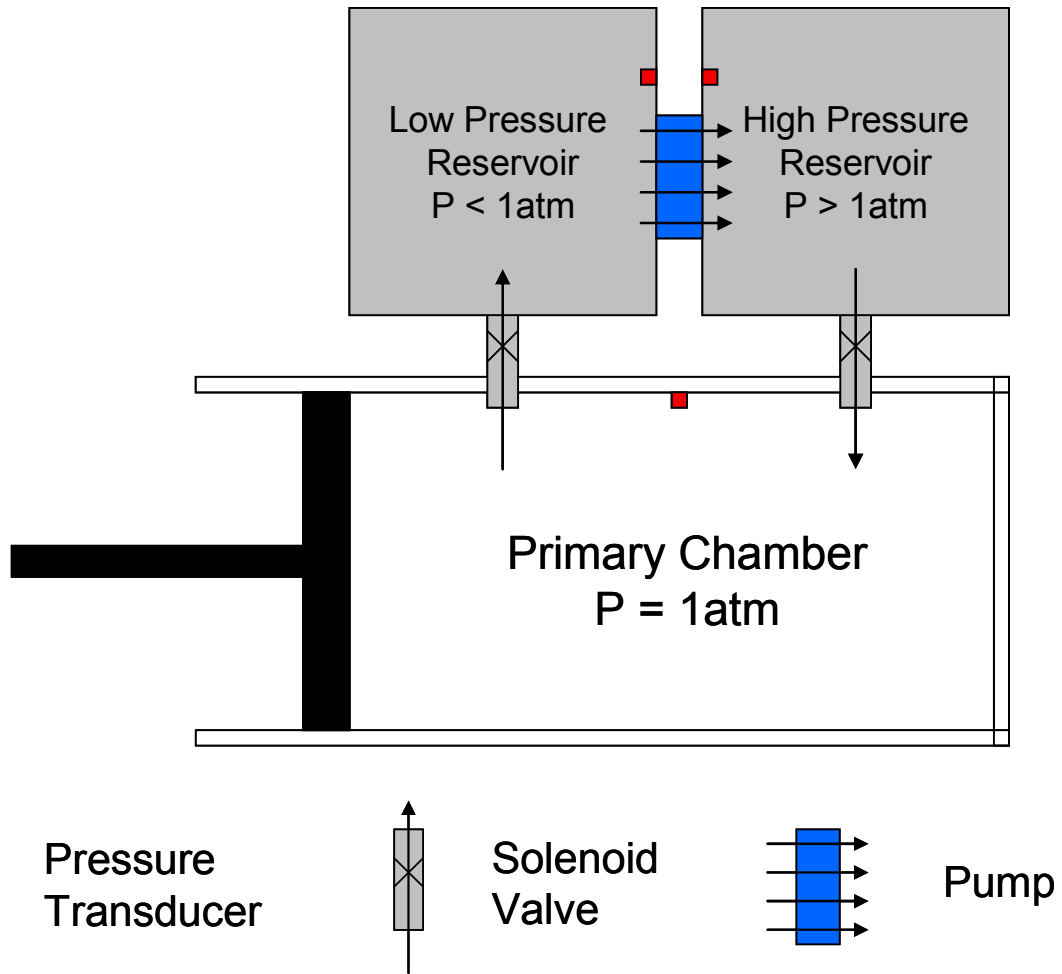


Figure 44: Active pressure regulation system concept

When changes in primary chamber pressure are detected (stemming from volume changes caused by joint movement), the system responds in one of two ways. If the system detects an increase in pressure (indicating a decrease in volume), the solenoid valve connecting the primary chamber to the LPR is opened (see Figure 45). This will evacuate gas from the primary chamber to the reservoir, which in turn will cause the primary chamber pressure to decrease. Once the primary chamber has stabilized to its initial pressure, the solenoid valve is closed. Similarly, if the system detects a decrease in primary chamber pressure (indicating an increase in volume), the valve connecting the primary chamber to the HPR is opened (see Figure 46). This will cause high pressure gas to enter the primary chamber, which will cause its pressure to increase. Once the primary chamber has stabilized to its initial pressure, the valve is closed.

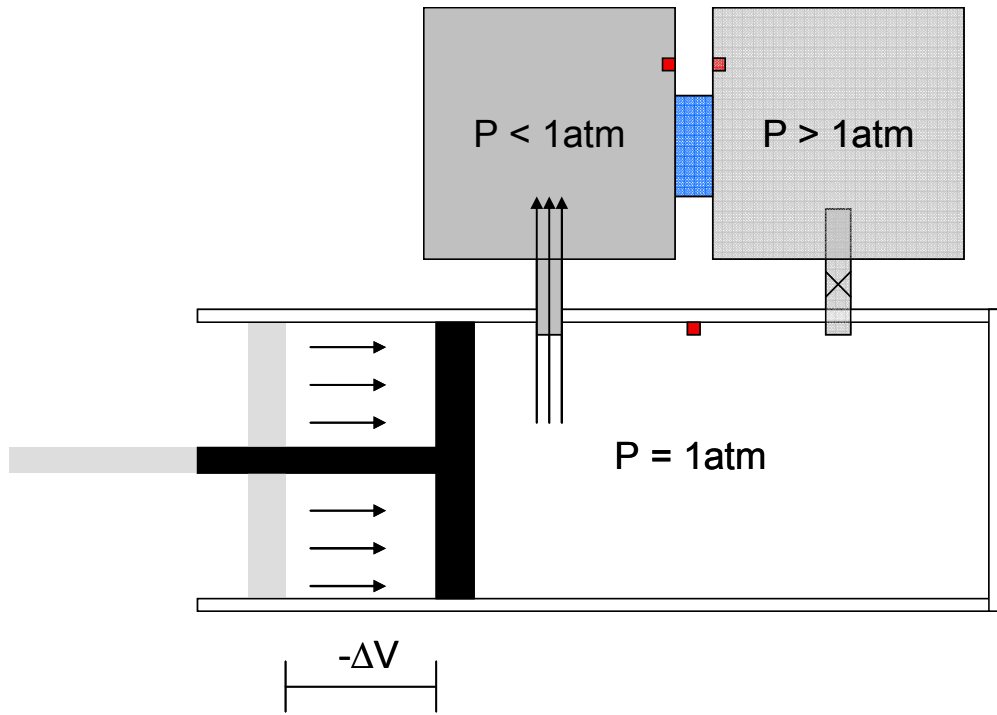


Figure 45: System response to pressure increases due to volume reduction

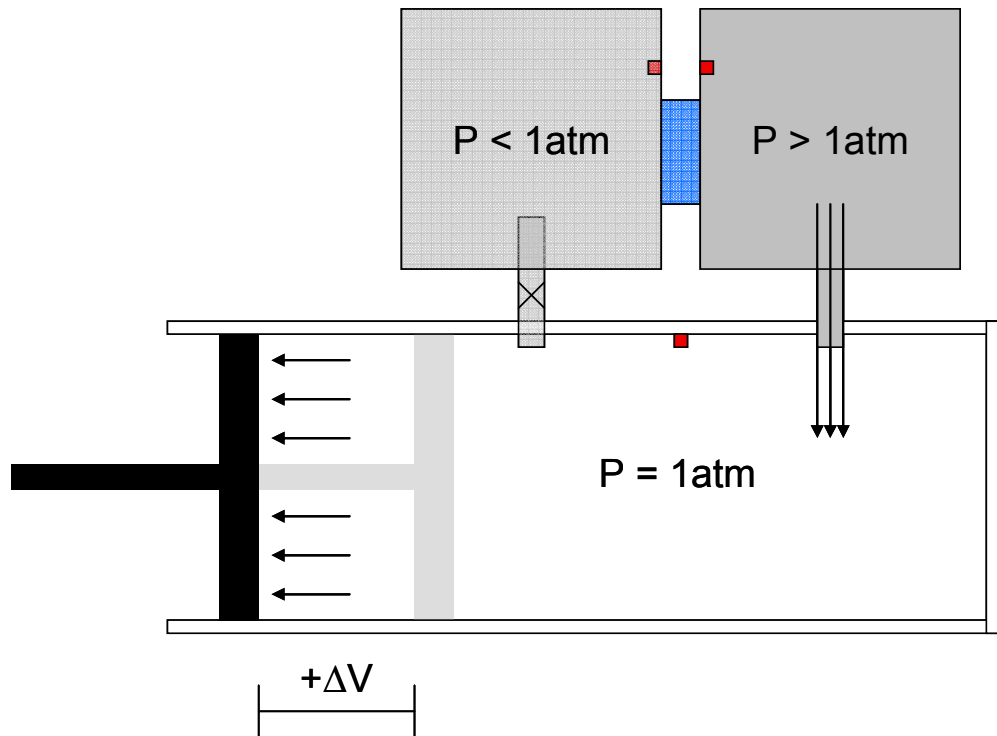


Figure 46: System response to pressure decreases due to volume increase

Thus, for either increases or decreases in pressure, the system has at its disposal a reservoir charged and ready to intervene by intelligently moving gas throughout the three-chamber system. Because the HPR and LPR are of finite volume, though, without intervention the system performance will degrade over time as the reservoirs lose their initial pressure charge relative to the primary chamber. To maintain the pressure differential between the reservoirs and the primary chamber over multiple tests, a pressure pump exists between the reservoirs to pump the working gas from the LPR to the HPR (see Figure 47). This will allow the system to operate indefinitely, assuming electrical power for the sensing/control system is available.

Given adequately capable sensing and control equipment, then, this regulator concept theoretically meets all design requirements. To fully validate this system concept, though, a physical prototype was created and tested. This creation and validation phase is detailed in the following section.

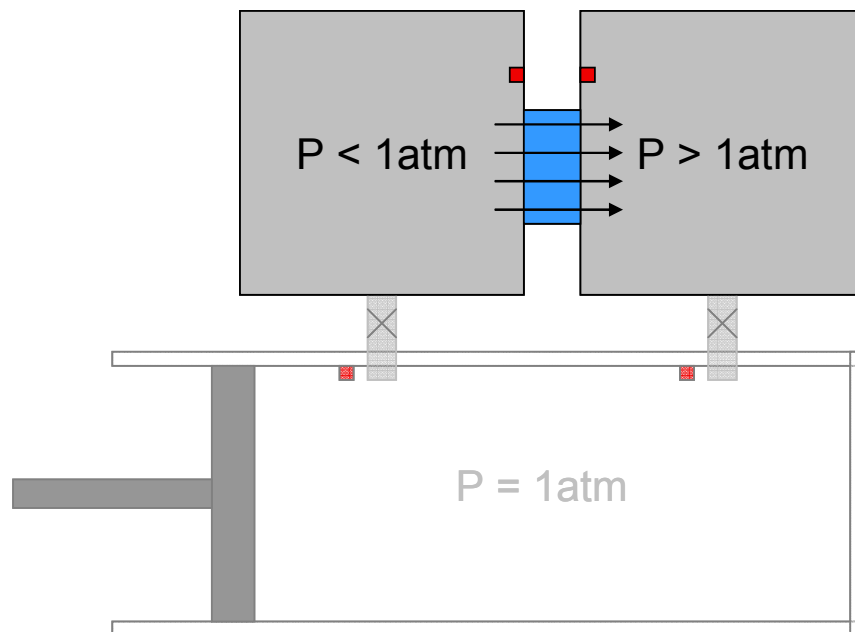


Figure 47: System reservoir sustainability using an in-line pressure pump

3.3 – PROTOTYPE DEVELOPMENT

A prototype of this regulator was developed to demonstrate proof of concept. As such, it was designed using readily available and inexpensive materials, and without traditional space system engineering considerations (mass/power minimization, space hardening, etc.). Similarly, for the sake of experimental simplicity, the system used air (rather than O₂) and was configured to a primary chamber set to atmospheric pressure (rather than EMU suit pressure of 29.6 kPa, or 4.3 psi).

3.3.1 – Primary Chamber, HPR, and LPR Construction

The HPR, LPR, and primary chamber were all constructed from 15.2 cm (6 in) diameter, Schedule 40 polyvinyl chloride (PVC) pipe. PVC was chosen for its price, ease of machining, and strength given the pressure regimes of interest (Schedule 40 pipe is rated to greater than 690 kPa [100 psi] maximum operating pressure, far beyond the pressures needed for this study (Engineering Toolbox, 2005)). The primary chamber was designed to approximately mimic the free volume of a pressurized, occupied EMU (0.028 m³, or 1 ft³), and was therefore set to 1.52 m (5 ft) in length (Hamilton-Sundstrand, 2003). It was capped on each end using standard PVC pipe caps and PVC pipe cement. The HPR and LPR were each set to 0.76 m (2.5 ft) in length (containing approximately 0.014 m³, or 0.49 ft³, of internal volume), and were similarly capped and cemented. This reservoir sizing represented a compromise between performance (larger reservoirs take longer to deplete and thus increase system sustainability) and practicality (smaller tanks are easier to manipulate). The primary chamber is pictured below in Figure 48, and the HPR and LPR are pictured in Figure 49.



Figure 48: Primary chamber, constructed from Schedule 40 PVC pipe

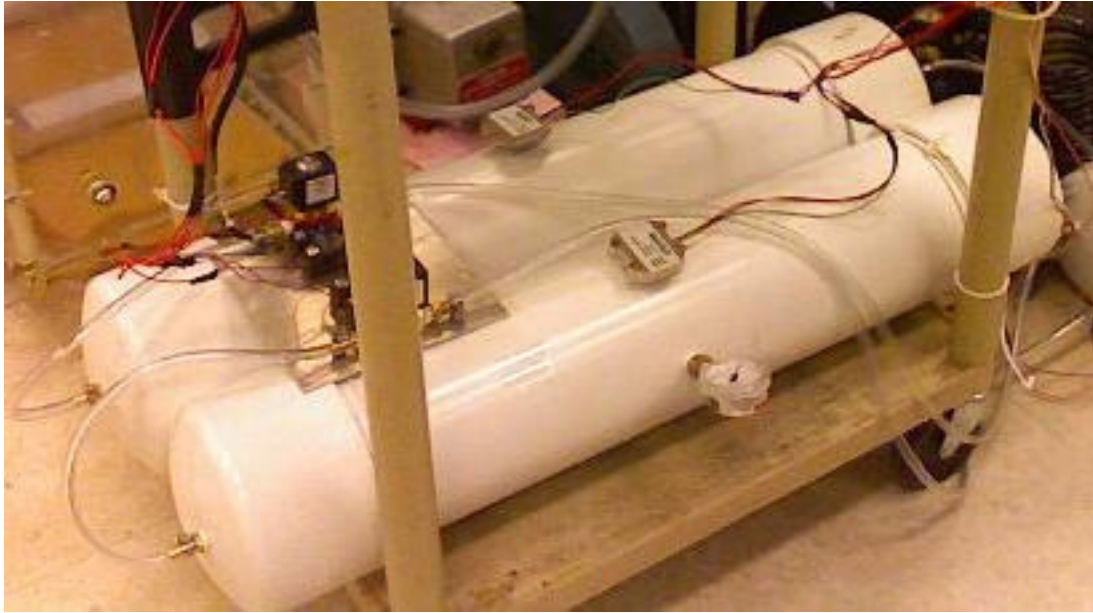


Figure 49: HPR and LPR, constructed from Schedule 40 PVC pipe

3.3.2 – Plumbing

The reservoirs and primary chamber were outfitted with 6.35 mm ($\frac{1}{4}$ in) pipe barbs, and were linked to each other and to the solenoid valves using 6.35 mm ($\frac{1}{4}$ in) clear vinyl tubing.

3.3.3 – HPR-LPR Pump

Due to time and cost considerations, the pump prescribed by the system concept was not implemented in the prototype system. While the prototype was incomplete without this component, its absence did not preclude development and testing of its basic capability.

3.3.4 – Sensing and Control Architecture

The backbone of the regulation system, quite obviously, was the sensing and control architecture. Without precise and accurate sensing, real time data acquisition and processing, and responsive and lag-free control actuation, high performance active pressure regulation would not be possible.

Because size, power, and complexity were not considerations in the prototype design, it was decided that the data processing and control was best achieved using a standard laptop computer physically separated from the regulator hardware (rather than onboard using embedded processing). This laptop served as the nervous system of the prototype, both receiving inputs from independently powered analog pressure sensors and issuing commands to independently powered, digitally activated solenoid valves (SVs), all in real time. This two-way communication was accomplished using a standard USB-powered data-acquisition board (DAQ). However, because a standard USB DAQ was not powerful enough on its own to actuate a solenoid valve (such DAQs provide orders-of-magnitude lower voltage than necessary), solid-state relays (SSRs) were required between the DAQ and valves. These relays served as power switches for each valve: external power sources with sufficient voltage to actuate the valves were connected to each relay, and the relay switched the power based on signals from the USB DAQ (the activation threshold of each SSR was low enough to be triggered by the DAQ). This architecture, presented as a block-diagram, is shown in Figure 50.

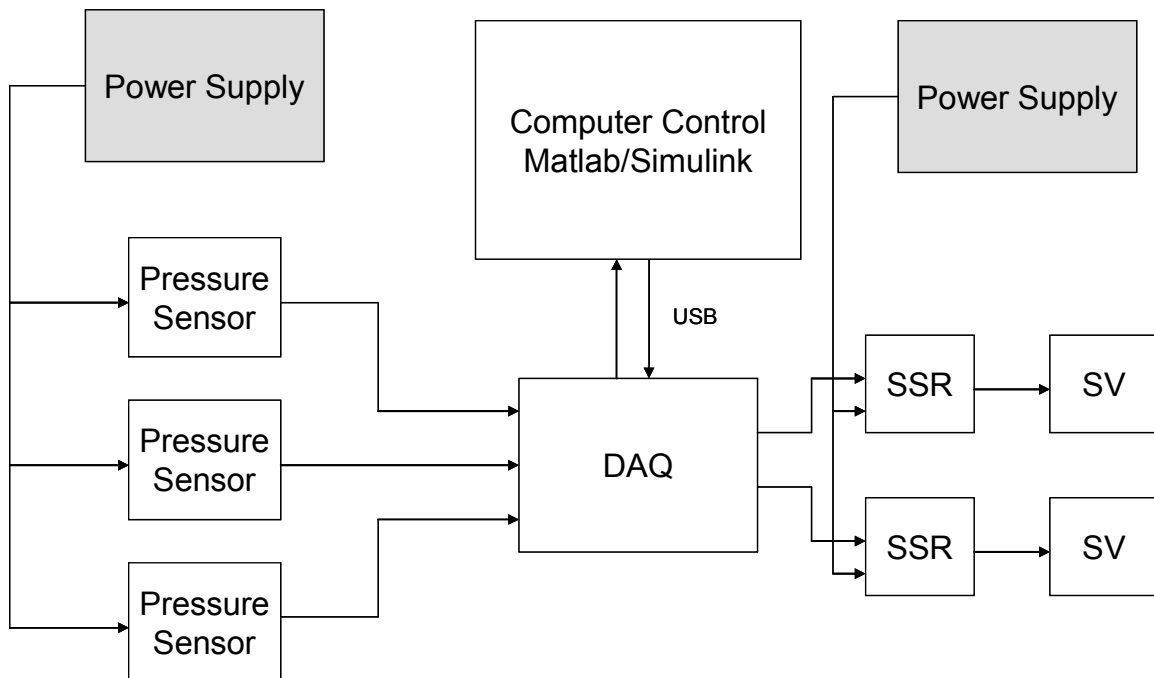


Figure 50: Sensing and control architecture block diagram

Due to the high sensitivity of total system performance to the capabilities of these components (i.e. bad sensors/valves would mean a bad regulator) implementation of this architecture required specific attention to the technical specifications of each component. However, the financial constraints imposed upon the project (total hardware costs could not exceed \$500) meant that simply buying the best sensors/valves available was not a realistic option. Therefore each component was selected based on a combination of its technical capability and its price. These components (sensors, valves, relays, DAQ, and control software) are described in the following sections.

3.3.5 – Pressure Sensors

Three pressure sensors were needed for this prototype: one to monitor the primary chamber pressure, and one each to monitor the HPR and LPR pressures. Each of the three chambers housed vastly different pressure regimes:

- HPR: 0-690 kPa gauge (0-100 psig)
- LPR: -101.3-0 kPa gauge (-14.7-0 psig)
- Primary Chamber: ± 6.9 kPa gauge (± 1 psig)

Each sensor was individually tailored to match the operating range necessary for its particular chamber. Furthermore, not all chambers required the same level of accuracy and precision in their pressure measurements: the minimum capability requirements of the primary chamber pressure sensor were far greater than the minimum capability requirements of the HPR and LPR sensors. This was because the primary chamber pressure sensor was responsible for the most critical piece of sensing of the entire system: monitoring and reporting the state of the chamber whose pressure was being actively regulated. This meant that the dead-band of the entire regulator system was explicitly determined by the precision and resolution of this sensor (and a large dead-band would likely render this system useless at mitigating small pressure changes caused by astronaut movement in a space suit – its ultimate purpose). Less precise measurements were necessary for the HRP and LPR, as the information reported by these sensors was not

actively used in the regulation process (these sensors were simply available to monitor the states of the reservoirs for the sake of system sustainability). The selection of the primary chamber pressure sensor was further complicated by the requirement that the sensor must be able to operate in both positive and negative pressure regimes, which is a non-standard capability of most pressure sensors on the market (and certainly a non-standard capability of inexpensive pressure sensors). After surveying the available pressure sensors that met both the design and budget requirements, the following three sensors (from the same sensor family) were selected from Omega.com:

- Primary Chamber: PX243A-2.5BG5V (range ± 17.3 kPag, or ± 2.5 psig)
- HPR: PX242A-060G5V (range 0-413 kPag, or 0-60 psig)
- LPR: PX241A-15NG5V (range -101.3-0 kPag, or -14.7-0 psig)

These sensors were each housed in a stainless steel case and could be attached to any chamber via its 1/8-27 NPT male port (such ports were easily installed in the PVC chambers). An example of these sensors is included in Figure 51.



Figure 51: PX240A series pressure sensor, taken from (Omega.com, 2008)

The sensors required 8 Vdc regulated input, and produced an analog output voltage between 1-6 Vdc depending on the detected pressure. The output voltage varied linearly with pressure, with 1 Vdc and 6 Vdc corresponding to the minimum and maximum pressure readings based on the range of the specific sensor. The output voltage

represented a linear interpolation between these minimum and maximum pressure limits. The accuracy of each sensor was certified to 0.25% of its maximum range, and each sensor had a response time certified to 1 ms (Omega.com, 2008). This specification was most important for the PX243A sensor (to be used in the primary chamber) – with a total range of only 34 kPag (5 psig), this sensor’s resolution was certified to 0.09 kPag (0.0125 psig), creating a system-level sensing dead-band 8 times smaller than the current EMU pressure regulation capability (0.09 kPag vs. 0.7 kPag, or 0.0125 psig vs. 0.1 psig) (Hamilton-Sundstrand, 2003). A more detailed specification chart for these sensors can be found in Appendix E.

3.3.6 – Solenoid Valves

The specifications of primary concern for this application in terms of solenoid valve performance were the valve opening/closing time, maximum/minimum operating pressure, DC activation voltage, and flow factor (C_v). Several inexpensive solenoid valves were available that met the requirements of this system. After surveying the available valves that met both the design and budget requirements, nominally closed SV3307 valves (2-way, direct acting) with optional 12 Vdc coils (SV8COIL-12DC) were selected from Omega.com for both the HPR/primary chamber and LPR/primary chamber interfaces. An example of these valves is included in Figure 52.



Figure 52: SV3300 series solenoid valve, taken from (Omega.com, 2008)

These valves were capable of handling both positive and negative pressure differentials, and required 12 Vdc (8 W) to activate (Omega.com, 2008). These valves were also selected for their relatively small C_v value (0.14), a seemingly counter-intuitive decision. C_v , which is a coefficient that measures relative flow rate capacity through a valve (Emerson Industrial, 2009), should ordinarily be maximized in this pressure control system design because a higher flow rate leads to a faster response time (and thus a tighter control of primary chamber pressure). However, because the data processing and control algorithm computation rates were largely unknown at the time of component selection, a reduced C_v was selected to minimize the likelihood of uncontrollability (i.e. if the reservoir gases mixed with primary chamber gases faster than the sensing/control system could accommodate, the system would likely enter unstable and uncontrollable oscillation). This was a significant threat that could have potentially rendered the system inoperable. Conversely, the only threat posed by selecting valves with a reduced (non-optimal) C_v was a potential weakening of system performance (meaning poorer pressure control bandwidth - pressure spikes might decay more slowly than they would with higher performing valves). Because this was a proof-of-concept prototype, though, it was determined that this inherent weakness could be easily improved in later designs by either adding additional valves or by increasing the C_v of the current architecture.

A more detailed specification chart for these sensors can be found in Appendix F.

3.3.7 – Solid State Relays

Standard solid state relays were selected from Digikey.com based on the activation voltage level specifications of the solenoid valves previously described. The relays chosen were produced by Crydom Co. (Digi-Key part number CC1590-ND, manufacturer part number DC60S3-B) and had an input voltage range of 3.5-32 Vdc, a load voltage range of 3-60 Vdc, and a load current maximum of 3 A (Digi-Key, 2008). These specifications exceeded the power levels necessary to activate the solenoid valves (12 Vdc and 8 W load, resulting in 2/3 A current load), and had a sufficiently low input

voltage level to be compatible with USB-powered control commands (which operate at 5 Vdc) (HWB, 2008). An example of these relays is included in Figure 53.



Figure 53: Example of a Crydom solid state relay, taken from (Digi-Key, 2008)

The wiring configuration used to connect the relays to the USB controller and to the solenoid valves is included in Figure 54.

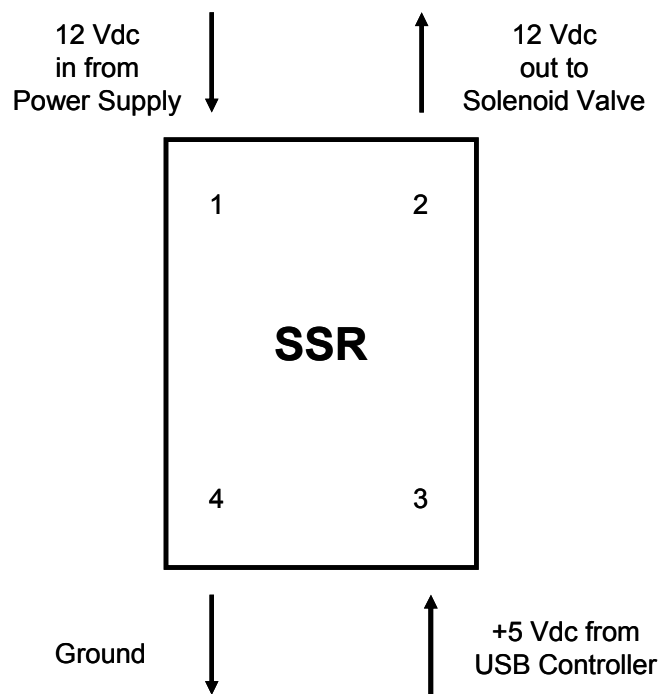


Figure 54: Solid state relay wiring configuration

3.3.8 – DC Power Supplies

Two variable DC power supplies were used to independently power the pressure sensors and solenoid valves. Because the three pressure sensors were part of the same sensor family (and thus required the same input voltage, 8 Vdc regulated) all three sensors were successfully wired in parallel to one power supply. The same configuration was employed to power the two solenoid valves (at 12 Vdc) using the second power supply.

3.3.9 – Data Acquisition/Control Architecture

As previously discussed, the data acquisition/control subsystem architecture was comprised of two main components: a laptop computer capable of running real-time data processing and control algorithms; and an external DAQ board capable of receiving analog voltage data from the pressure transducers, communicating this data via USB to the laptop control software, and sending digital control signals from the control software to the solid state relay/solenoid valve subsystem.

Several USB DAQ boards exist with this type of capability (analog, digital, and analog/digital combination boards are relatively common devices). However, only two candidate software packages could be found that were both capable of custom data processing/control and within the project's limited budget (ignoring the prospect of developing software from scratch) – LabView, or MATLAB and Simulink using the Data Acquisition Toolbox. Preliminary testing of both software packages led to the decision to use MATLAB and Simulink over LabView. This was based on both familiarity/ease of use and specific technical capability of the software. Based on this decision, the number of candidate DAQ boards decreased significantly, as a new constraint (compatibility with the MATLAB Data Acquisition Toolbox) was introduced.

The development of the processing and control algorithm using this software, as well as the DAQ board selection and implementation method, are described in detail in the following sections.

3.3.10 – Data Acquisition Board (DAQ)

A DAQ board by Measurement Computing Corp. was selected based on its compatibility with the MATLAB Data Acquisition Toolbox as well as its ability to simultaneously collect analog input data and send digital output data. The DAQ board selected (USB-1408FS) featured eight analog inputs, 16 digital I/O, and USB 2.0 connectivity. An example of this DAQ board is included below as Figure 55.



Figure 55: USB-1408FS DAQ board from Measurement Computing Corp., taken from (Measurement Computing, 2008)

The three pressure sensors were connected to three independent analog input channels, and the two SSRs were connected to two independent digital output channels.

3.3.11 – MATLAB Data Acquisition Toolbox and Simulink Modeling

The MATLAB Data Acquisition Toolbox (MATLAB version R2007a) was selected for its capability to provide analog input and digital output through the Simulink block-diagram interface (MathWorks, 2008). Once a supported DAQ (like the USB-1408FS) was properly installed and calibrated, developing a real time control system using Simulink was straightforward using the following blocks and method (see Figures 56a-h):

1. Open Simulink and select the “Data Acquisition Toolbox”, which provides the user with the following blocks: “Analog Input”, “Analog Output”, “Digital Input”, and “Digital Output”.

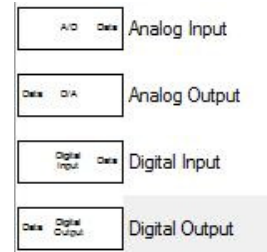


Figure 56a: Data Acquisition Toolbox blocks

2. Import the desired input block into a Simulink model (“Analog Input” in this case), and the software will automatically detect any compatible data acquisition devices connected to the system, allowing the user to select the desired device to be controlled.

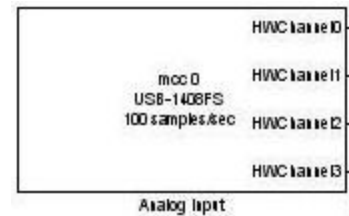


Figure 56b: USB-1408FS analog input block

3. Select the number of input channels desired (3 in this case – one each for the primary chamber pressure sensor, HPR sensor and LPR sensor), and use the appropriate blocks from the “Math Operations” tab in the standard “Simulink” block-set to convert each input voltage signals to pressure signals (as prescribed by the sensor voltage-pressure calibrations).

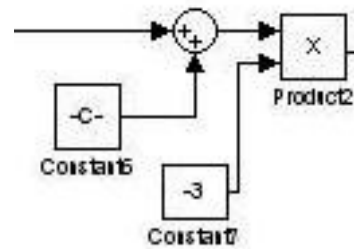


Figure 56c: Voltage signal conversion blocks

- Log each pressure signal to file using a “To File” block from the “Sink” tab in the standard “Simulink” block-set (for data analysis purposes).

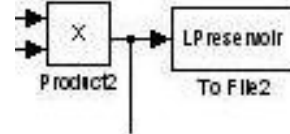


Figure 56d: Sink block

- Create the control architecture for the two output signals (one for each valve/reservoir) using the “Switch” block from the “Signal Routing” tab in the standard “Simulink” block-set, and connect the primary chamber pressure signal to the middle input of each “Switch” block. Because digital outputs are desired (value = 1 or value = 0), connect the upper and lower inputs of each “Switch” block to appropriate “Constant” Source blocks.

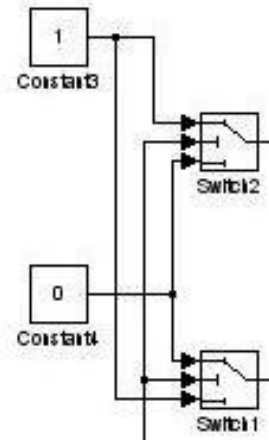


Figure 56e: Switch blocks

- Set the activation threshold (the signal value at which the switch triggers) for each switch by double clicking on the “Switch” block and setting the “Threshold” value as desired (for the regulator prototype, the threshold was set to ± 0.35 kPag, or 0.05 psi, based on system requirements demanding the regulator be at least as good as the current pressure regulation system).

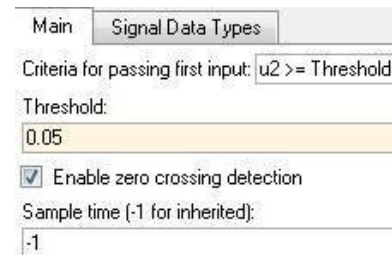


Figure 56f: Switch threshold menu

7. Import the desired output block from the “Data Acquisition Toolbox” (“Digital Output”, in this case), and again the software will automatically detect any compatible data acquisition devices connected to the system, allowing the user to select the desired device to be controlled.



Figure 56g: USB-1408FS digital output block

8. Connect the two “Switch” output signals to independent channels of the “Digital Output” block.

9. Set the desired run time in the main model toolbar (15 s or 30 s in this case, as will be described in the next section), and click on the “Start Simulation” button to run the model.



Figure 56h: Run time menu and “Start Simulation” button

Figures 56a-h: Catalog of pertinent Simulink control blocks

An overview of the final Simulink control model is represented below as Figure 57.

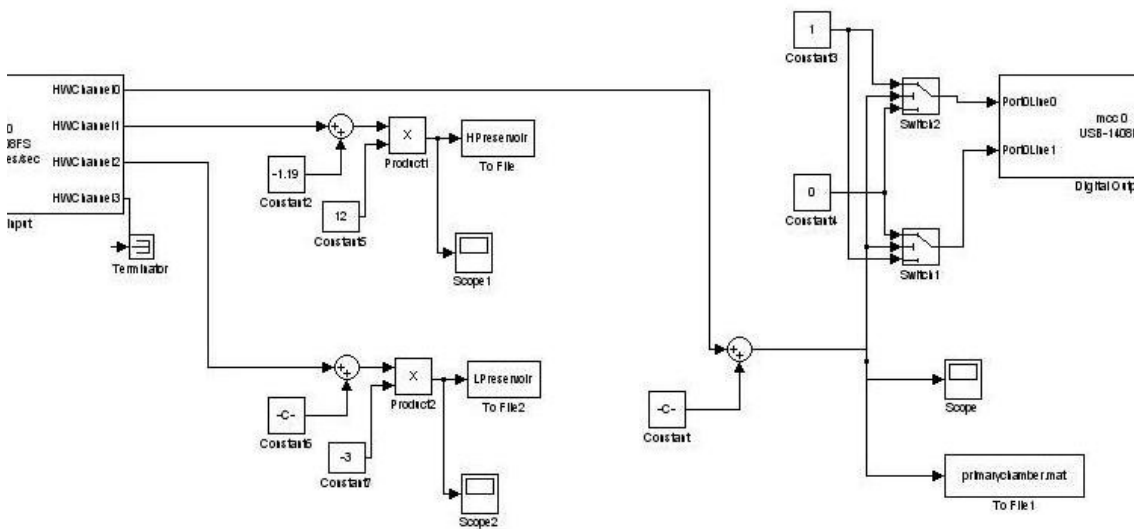


Figure 57: Final Simulink control diagram

3.3.12 – Vacuum Pump and Air Compressor

In order to charge the HPR and LPR to their initial pressure differentials, both a vacuum pump and air compressor were necessary. The same vacuum pump used to evacuate the MVL vacuum chamber was used to create the initial LPR pressure differential (previously discussed in Section 2.2.2). A portable air compressor capable of producing up to 689 kPa (100 psi) positive pressure was used to create the initial HPR pressure differential. These two devices were only used to create initial charges for the reservoirs – after that point they were disconnected, leaving the system physically independent from all equipment (with the exception of the external power supplies and laptop computer).

3.3.13 – System Integration

These components were integrated to form a fully functioning pressure regulation prototype system. This system is presented in Figure 58.

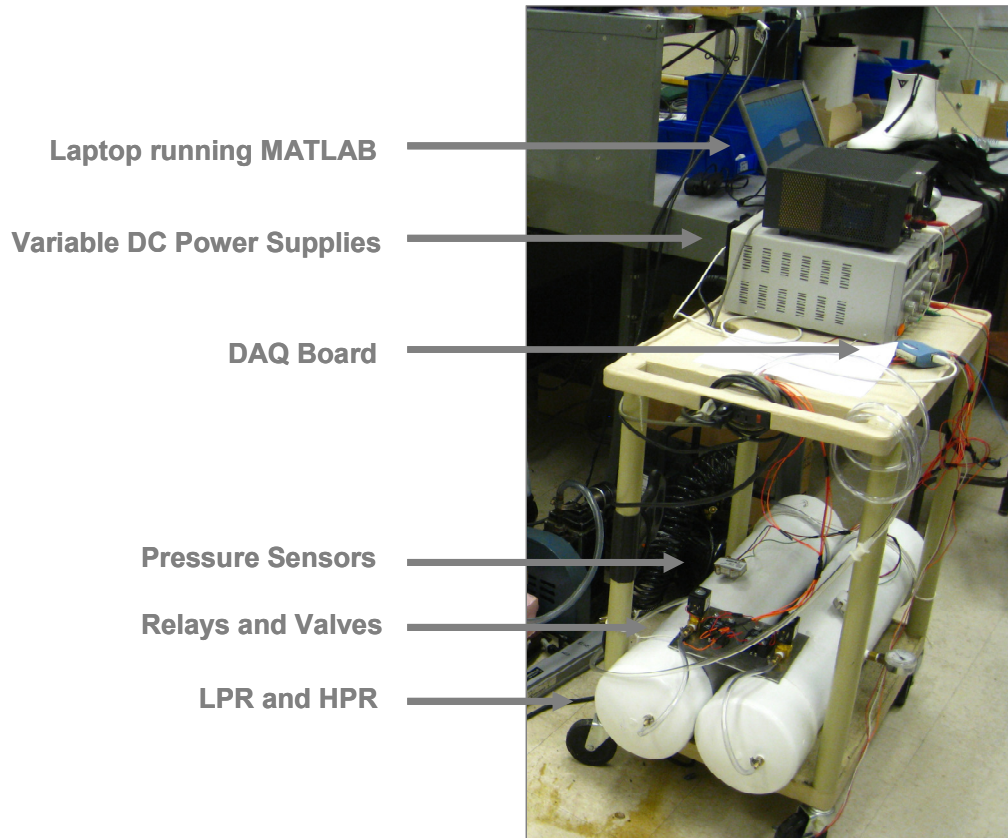


Figure 58: Fully integrated pressure regulation system prototype

3.4 - EXPERIMENTAL TEST PLAN AND METHODS

3.4.1 – System Initialization and Calibration

A first-time system initialization/calibration was necessary to bring the regulator system online. In addition to these first time steps, a number of start-up steps were necessary each time the regulator system was used. These steps are detailed in Appendices G and H, respectively.

3.4.2 – Syringe for Precise Primary Chamber Volume Change Control

Because the system was designed to counteract pressure spikes caused by changes in internal volume, a method for repeatably and precisely inducing controlled volume changes in the primary chamber was developed. An oversized (600 cm^3 , or approximately 2.07% of the primary chamber volume) air-tight veterinary syringe was purchased and modified to include a rubber hose pipe fitting on its nozzle. This syringe, which was the largest syringe commercially available, reasonably approximated an adiabatic compression/expansion (minus heat generated by friction), and was attached to the primary chamber using rubber hose. It is represented in Figure 59.



Figure 59: 600 cm^3 syringe used for precise control of changes in internal volume (with the primary chamber visible at the bottom of the image)

3.4.3 - Test Plan Overview

Using the pressure regulator prototype and test syringe previously described, a test plan was devised to characterize the regulator system response (pressure vs. time) for a number of volume change conditions. Four tests were defined to accomplish these goals.

The four tests were defined as follows:

1. Test 1 (volume change with no regulation): pressure vs. time response of the primary chamber when subjected to a complete syringe compression stroke and complete syringe expansion stroke without active pressure regulation, to characterize the baseline, worst-case-scenario chamber response
2. Test 2 (volume change with active regulation): an identical test to that performed in test 1, except the active pressure regulation prototype was enabled, to characterize the system's ability to mitigate pressure changes stemming from both positive and negative volume changes
3. Test 3 (multiple volume changes with active regulation): a repeat of test 2, except instead of only one compression/expansion cycle, multiple cycles were performed in quick succession, to characterize the system's ability to mitigate multiple volume changes in a short time (this test simulated situations where the internal operating volume of the suit is constantly changing, for example, during running/loping, or during complex multi-joint movements)
4. Test 4 (multiple volume changes with active regulation and a slower stroke rate): an identical test to that performed in test 3, only with a reduced stroke rate (approximately 75% slower), to characterize the effect of stroke rate on total system performance

Using these four tests as a framework, a test matrix (Table 12) was developed to structure the testing procedure. Syringe compression/expansion timing and rate, as well as the presence (or lack-thereof) of active pressure regulation, served as the independent variables for each test condition. Primary chamber pressure (as a function of time) served as the dependent variable (with HPR and LPR pressures also recorded). LPR and

HPR pressure differentials were loosely controlled as test parameters (though their exact starting values had minimal effect on the system performance).

Table 12: Prototype Pressure Regulation System Study Test Matrix

	No Regulation	Active Pressure Regulation
One Compression Cycle	Test 1	Test 2
Multiple Compression Cycles (Fast)	N/A	Test 3
Multiple Compression Cycles (Slow)	N/A	Test 4

The specific test methods used for each test condition are described in the next section.

3.4.4 - Test Method 1: Volume Change with No Regulation

The following protocol was implemented for the volume change test with no regulation:

1. Initialize the pressure sensors and DAQ system using the method described in Appendix H, except do not connect the relays/valves to a power supply
2. Set the test syringe to its maximum volume state (plunger at maximum expansion) and connect the syringe to the primary chamber
3. Set the test duration to 15 s, and begin the simulation
4. At time $t = 5$ s, compress the syringe as fast as reasonably possible (which was empirically determined to be approximately $770 \text{ cm}^3/\text{s}$)
5. Hold the syringe in this compressed position for 5 s
6. At time $t = 10$ s, extend the syringe as fast as reasonably possible back to its starting state (full expansion)
7. Hold the syringe in this extended position for the remaining 5 s
8. Retrieve and save the newly created data file from the MATLAB output directory

3.4.5 - Test Method 2: Volume Change with Active Regulation

The following protocol was implemented for the volume change test with active pressure regulation:

1. Initialize the pressure sensors and data acquisition system using the method described in Appendix H, pressurizing the HPR and LPR to ± 69 kPag (± 10 psi), respectively
2. Set the test syringe to its maximum volume state (plunger at maximum expansion) and connect the syringe to the primary chamber
3. Set the test duration to 15 s, and begin the simulation
4. At time $t = 5$ s, compress the syringe as fast as reasonably possible (which was empirically determined to be approximately $770 \text{ cm}^3/\text{s}$)
5. Hold the syringe in this compressed position for 5 s
6. At time $t = 10$ s, extend the syringe as fast as reasonably possible back to its starting state (full expansion)
7. Hold the syringe in this extended position for the remaining 5 s
8. Retrieve and save the newly created data files from the MATLAB output directory

3.4.6 - Test Method 3: Multiple Volume Changes with Active Regulation

The following protocol was implemented for the multiple volume changes test with active pressure regulation:

1. Initialize the pressure sensors and data acquisition system using the method described in Appendix H, pressurizing the HPR and LPR to ± 69 kPag (± 10 psi), respectively
2. Set the test syringe to its maximum volume state (plunger at maximum expansion) and connect the syringe to the primary chamber
3. Set the test duration to 15 s, and begin the simulation
4. At time $t = 0$ s, compress the syringe as fast as reasonably possible
5. As soon as the system fully mitigates the induced pressure spike (i.e. as soon as primary chamber pressure returns to 0 kPag), extend the syringe as fast as reasonably possible back to its starting state (full expansion)
6. As soon as the system fully mitigates the induced pressure spike, repeat steps 4-5
7. Continue repeating the compression/expansion cycles at full speed until the simulation ends at $t = 15$ s
8. Retrieve and save the newly created data files from the MATLAB output directory

3.4.7 - Test Method 4: Multiple Volume Changes with Active Regulation, Reduced Stroke Speed

The following protocol was implemented for the multiple volume changes test with active pressure regulation and slower compression/extension stroke speed:

1. Initialize the pressure sensors and DAQ system using the method described in Appendix H, pressurizing the HPR and LPR to ± 69 kPag (± 10 psi), respectively
2. Set the test syringe to its maximum volume state (plunger at maximum expansion) and connect the syringe to the primary chamber
3. Set the test duration to 30 s, and begin the simulation
4. At time $t = 0$ s, compress the syringe at a rate of $210 \text{ cm}^3/\text{s}$ (approximately 1/3 of the total syringe volume per second)
5. As soon as the system fully mitigates the induced pressure spike (i.e. as soon as primary chamber pressure returns to 0 kPag), extend the syringe at the same slowed rate back to its starting state (full expansion)
6. As soon as the system fully mitigates the induced pressure spike, repeat steps 4-5
7. Continue repeating the compression/expansion cycles at the slowed rate until the simulation ends at $t = 30$ s
8. Retrieve and save the newly created data files from the MATLAB output directory

3.5 - RESULTS

3.5.1 - Test 1: Volume Change with No Regulation

The first test, pressure vs. time of the primary chamber system when subjected to changes in volume without any pressure regulation, aimed to characterize the unmitigated effects of volume change on a closed environment representing a pressurized, occupied EMU. The results of this test are included below as Figure 60.

The pressure response of the primary chamber is shown during a -600 cm^3 volume change at time $t = 5 \text{ s}$, and $+600 \text{ cm}^3$ volume change at time $t = 10 \text{ s}$. This compression represents a -2.07% change in total operating volume. The compression and expansion strokes were both conducted at a rate of approximately $770 \text{ cm}^3/\text{s}$ (which was the fastest rate achievable by an operator manually compressing the piston in the syringe). The compression stroke induced a spike of 2.82 kPag (an increase of 2.78%) that remains unchanged until an equal and opposite expansion approximately returns the chamber pressure to its starting condition of 0 kPag (the chamber pressure actually returns to a value slightly below 0 kPag , which is attributable to a minor leak in the system).

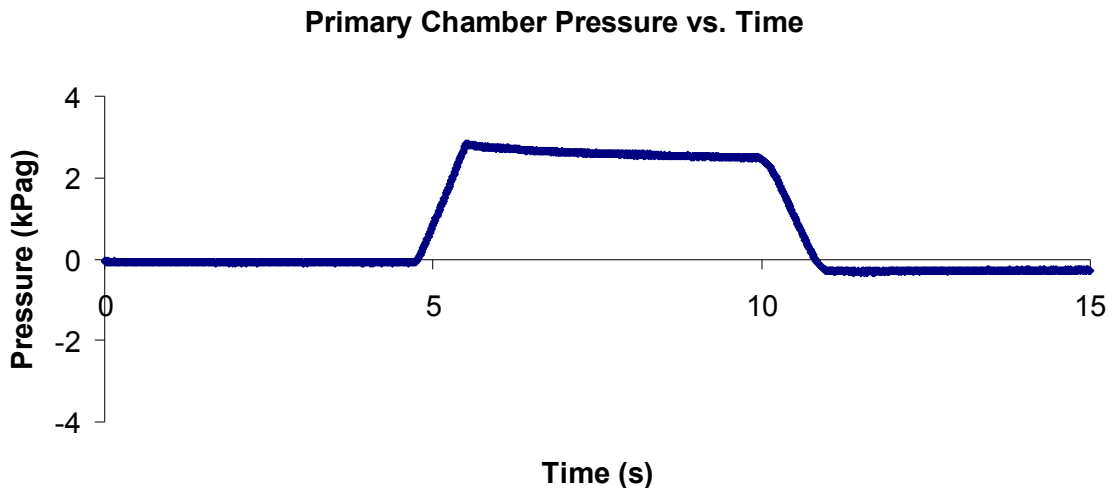


Figure 60: Pressure vs. time of the primary chamber without active regulation

3.5.2 - Test 2: Volume Change with Active Regulation

The second test, pressure vs. time of the primary chamber system when subjected to changes in volume with the prototype active pressure regulation system enabled, aimed to characterize the effects of volume change on a closed environment representing a pressurized, occupied EMU when the internal pressure was actively monitored and controlled. The results of this test are included below as Figure 61.

The same compression/expansion cycle used in test 1 was repeated (at the same rate of $770 \text{ cm}^3/\text{s}$) with the pressure regulation system enabled. For this identical cycle, the active pressure regulation system reduced the amplitude of the initial pressure spike by 34% (to 1.86 kPag from 2.82 kPag). Unlike in test 1, this pressure increase was a transient spike rather than a sustained shift - the primary chamber pressure returned to its starting condition of 0 kPag only 1.49 s after the initiation of the compression stroke. At time $t = 10 \text{ s}$, when the expansion stroke was initiated, a similar transient negative pressure spike was induced (of magnitude -1.07 kPag). The regulation system responded as before, and returned the system to its starting condition 1.33 s after the initiation of the expansion stroke.

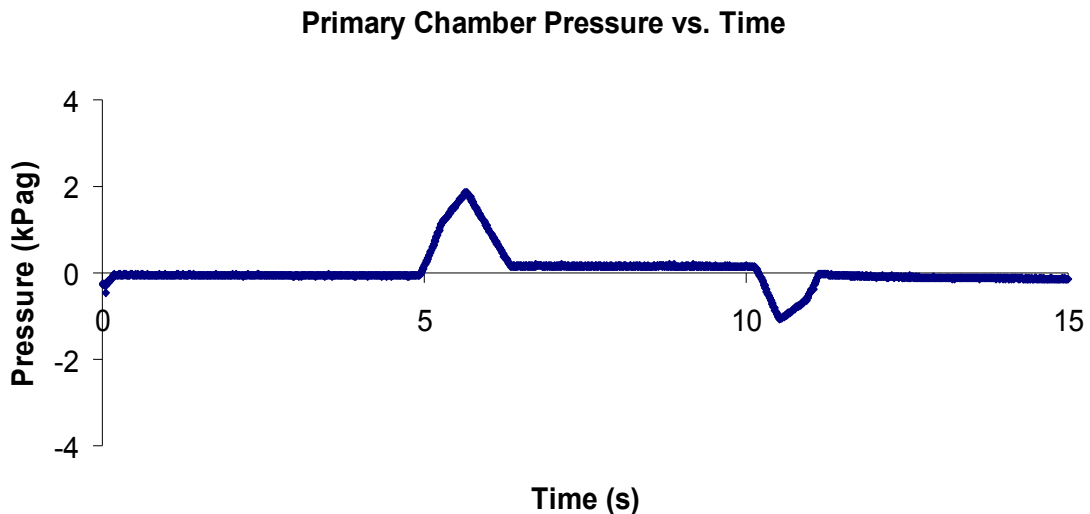
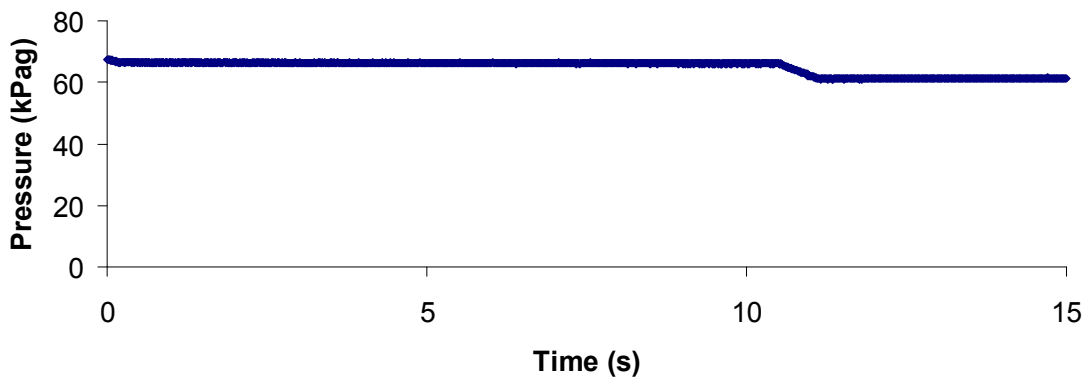


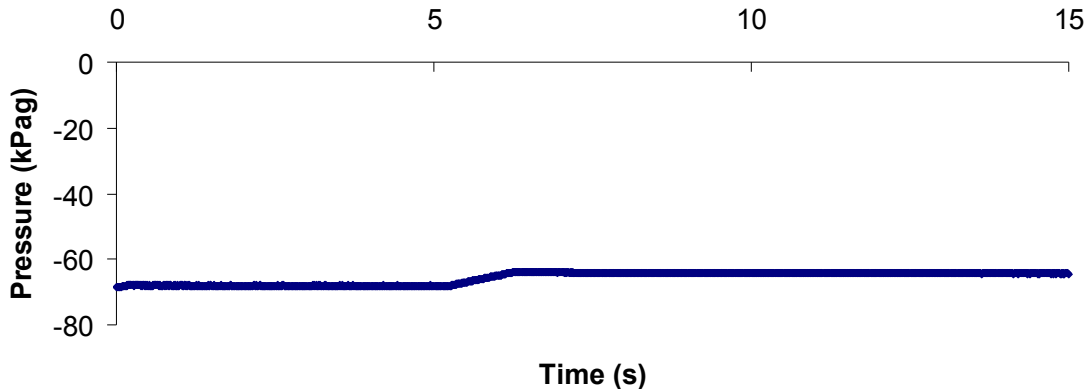
Figure 61: Pressure vs. time of the primary chamber with active regulation

For this test, the HPR and LPR were charged to ± 69 kPag, respectively – these levels were selected as a compromise between increased system performance (higher pressure differentials between the reservoirs and the primary chamber would decrease mixing time required to mitigate pressure spikes) and system safety (excessively high pressure differentials could exceed the material strength of the PVC reservoirs). Pressure vs. time histories of these reservoirs are included below as Figures 62a-b.

(c) HPR Pressure vs. Time



(b) LPR Pressure vs. Time



Figures 62a-b: Pressure vs. time of the HPR and LPR during active regulation

At $t = 5$ s, the LPR acted to mitigate the positive pressure spike caused by the compression stroke, resulting in a decrease in reservoir pressure of 3.88 kPag. Similarly, at $t = 10$ s, the HPR acted to mitigate the negative pressure spike caused by the expansion stroke, resulting in a decrease in reservoir pressure of 4.85 kPag.

3.5.3 - Test 3: Multiple Volume Changes with Active Regulation

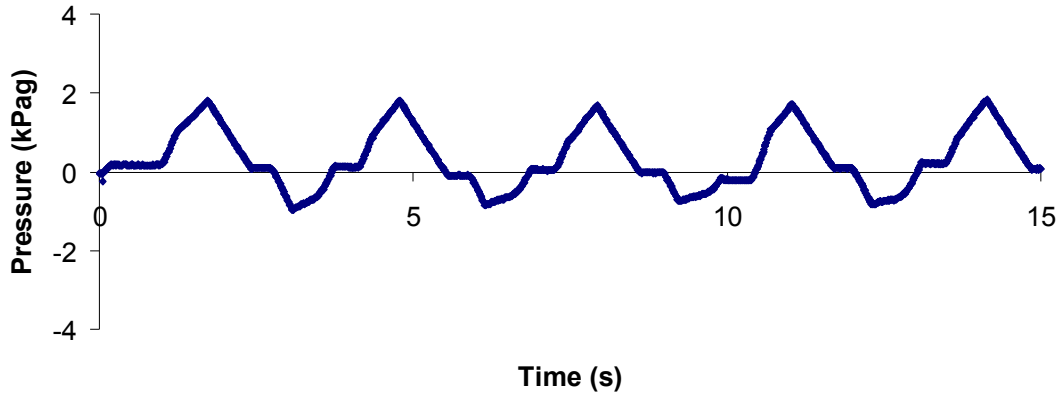
The third test, pressure vs. time of the primary chamber system when subjected to repeated changes in volume with the prototype active pressure regulation system enabled, aimed to characterize the ability of the prototype system at mitigating multiple pressure spikes over time. The primary chamber was subjected to a sequence of five compression/expansion cycles, one immediately following another. The compression/expansion strokes were performed at the same rate as tests 1 and 2 (770 cm³/s), and the HPR and LPR were both initially charged to the same pressure differentials (± 69 kPag). The HPR and LPR were not recharged between compression/expansion cycles. Plots of the primary chamber response vs. time, as well as the responses of the HPR and LPR vs. time, are included as Figure 63a-c.

The system mitigated each compression/expansion cycle in similar fashion to test 2: positive and negative transient pressure spikes (of magnitude $\leq \pm 1.848$ kPag) were created at the moment of compression/expansion, and these spikes decayed to zero shortly thereafter (average decay time $t = 1.23$ s). Each transient decay corresponded to the activation (and pressure differential degradation) of either the HPR or LPR.

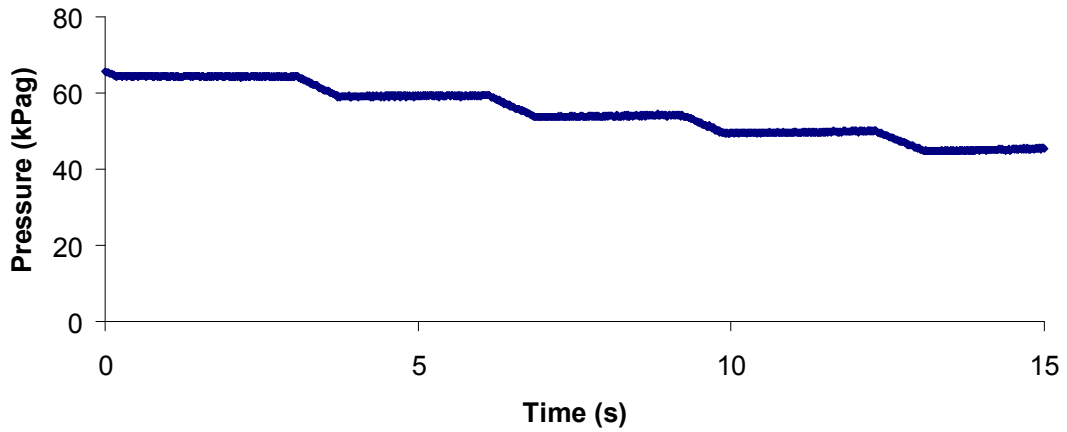
3.5.4 - Test 4: Multiple Volume Changes with Active Regulation, Reduced Stroke Speed

The fourth and final test, pressure vs. time of the primary chamber system when subjected to a more slowly occurring series of volume changes with the prototype active pressure regulation system enabled, aimed to characterize the effect of stroke rate on overall system performance. A series of three compression/expansion cycles were conducted at a stroke rate of 210 cm³/s (73% slower than previous tests). Because the stroke rate was reduced, the simulation time was set to twice the length of previous tests (30 s vs. 15 s). Again, the HPR and LPR were charged to the same pressure differentials (± 69 kPag), and were not recharged between compression/expansion cycles. Plots of the primary chamber response vs. time, as well as the responses of the HPR and LPR vs. time, are included as Figure 64a-c.

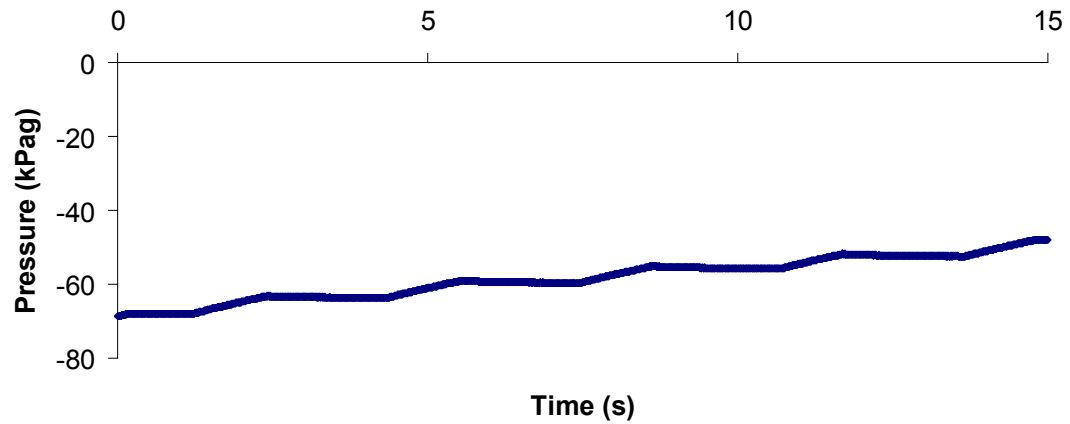
(a) Primary Chamber Pressure vs. Time



(b) HPR Pressure vs. Time

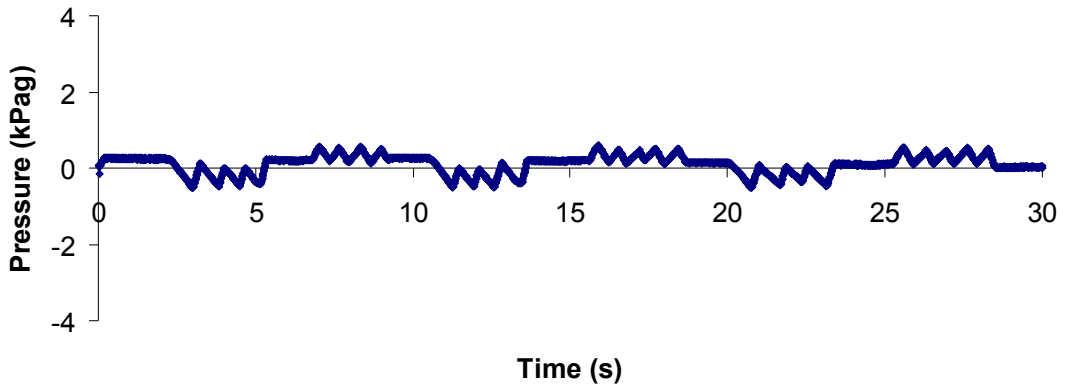


(c) LPR Pressure vs. Time

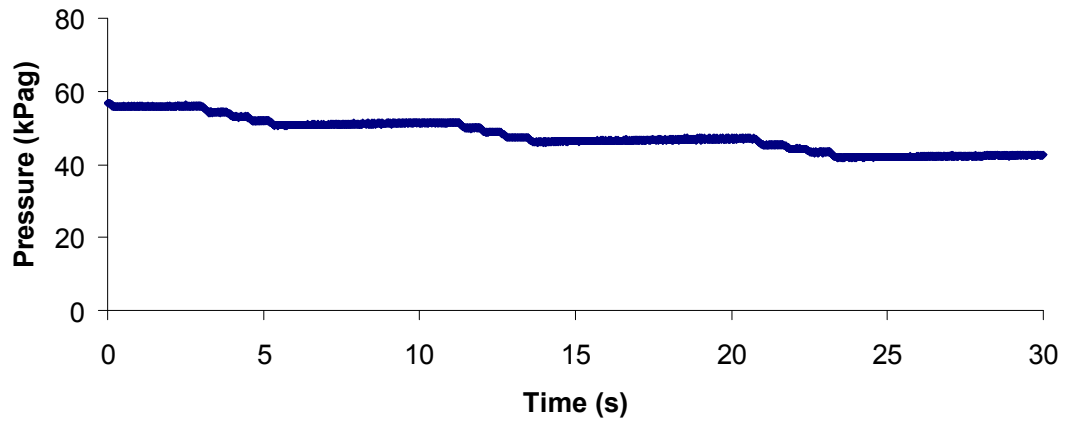


Figures 63a-c: Primary chamber, HPR and LPR pressure vs. time for 770 cm³/s stroke rate compression cycles (test 3)

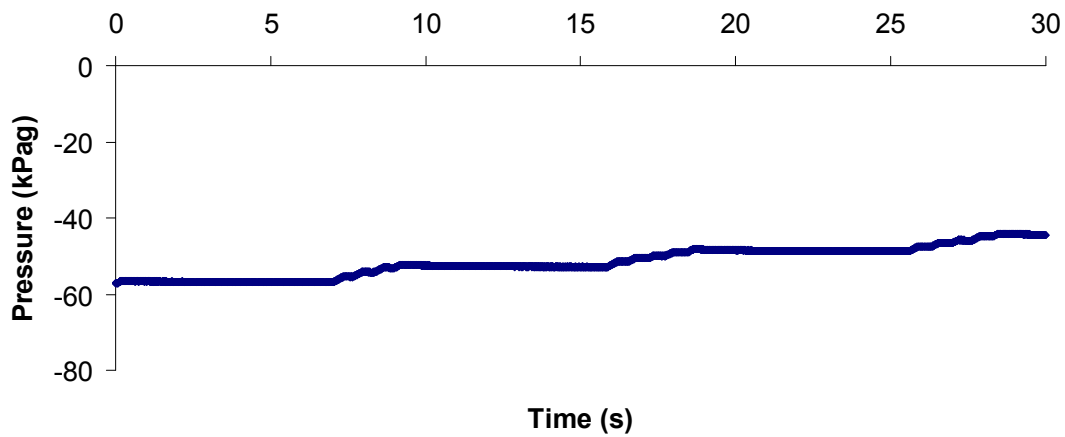
(a) Primary Chamber Pressure vs. Time



(b) HPR Pressure vs. Time



(c) LPR Pressure vs. Time



Figures 64a-c: Primary chamber, HPR and LPR pressure vs. time for 210 cm³/s stroke rate compression cycles (test 4)

3.6 – DISCUSSION

Tests 1 and 2 demonstrate the improvement in primary chamber pressure response to significant changes in operating volume provided by the active pressure regulation system prototype for identical compression/expansion cycles (34% reduction in initial pressure spike magnitude, and an immediate return to the initial pressure state that does not occur in the unregulated condition). These improvements suggest that the prototype pressure system is sufficiently powerful to maintain constant pressure (minus decaying transients) in a closed volume environment with unstable internal volume (i.e. a gas pressurized space suit). Additionally, during 4.5 consecutive compression and expansion cycles, the system was capable of consistently maintaining primary chamber pressure within the levels seen during a single cycle (± 1.848 kPag). Qualitatively, the system response to each of the cycles closely resembled that of the single compression/expansion cycle. This demonstrates that the system can maintain its initial regulation performance throughout a series of significant changes in primary chamber volume.

When compared to repeated cycles at a fast stroke rate, the primary chamber pressure response to repeated cycles at a slower stroke rate was considerably different. Rather than causing one large spike and corresponding decay, each compression or expansion stroke caused several spikes/decays of much smaller magnitude in immediate succession. This difference was an interesting outcome. For tests using the fast ($770 \text{ cm}^3/\text{s}$) stroke rate, the primary chamber pressure changed more quickly than the system could mitigate, meaning that even after system activation (the point where chamber pressure crosses the detection threshold, identifiable symptomatically by a change in slope of the transient pressure spike), primary chamber pressure continued to rise for the duration of each compression stroke (or fall for each expansion stroke). Once each compression/expansion stroke ended, with the system still activated, the pressure spike then decayed to zero. This behavior resulted in a single large spike (with a discontinuity in slope during the growth of the spike) and subsequent rapid decay upon completion of the stroke. This behavior can be seen graphically as follows in Figure 65:

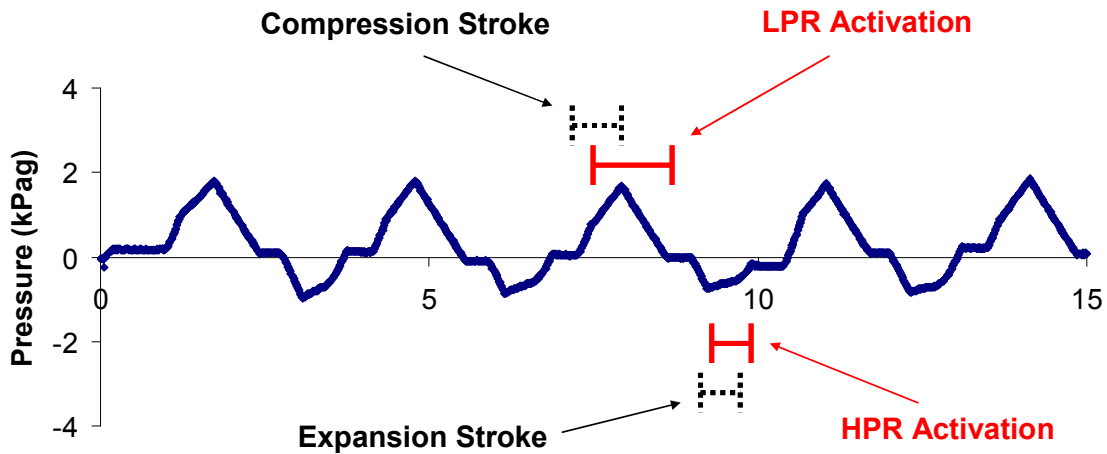


Figure 65: Relationship of 770 cm³/s stroke to HPR and LPR system activation for one cycle, leading to single large spike behavior (test 3)

For the slower (210 cm³/s) stroke rate, however, the system acted more quickly than the rate of change of primary chamber pressure, meaning that once activated the system would drive the pressure back to zero very quickly and then deactivate (and this would happen in a fraction of the time required to complete one compression/expansion stroke). As a result, this activation/deactivation behavior would occur multiple times per compression/expansion stroke. This resulted in a series of miniature pressure spikes. This behavior can be seen graphically as follows in Figure 66:

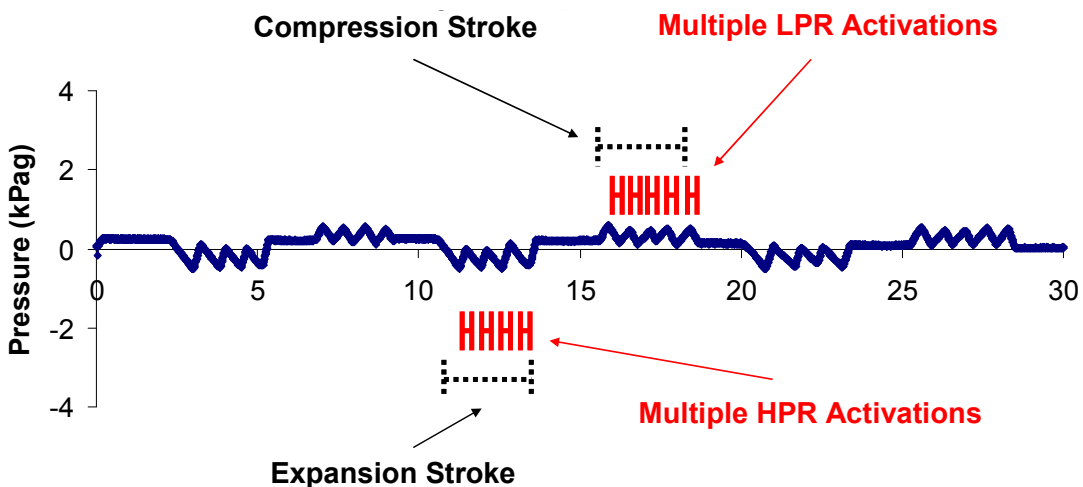


Figure 66: Relationship of 210 cm³/s stroke to HPR and LPR system activation for one cycle, leading to multiple small spike behavior (test 4)

A comparison between Figures 63b-c and 64b-c demonstrates that the HPR and LPR qualitatively behaved similarly regardless of stroke rate. Most importantly, though, is the fact that the regulator system was able to maintain a tighter control on primary chamber pressure for the slower stroke rate test run (± 0.55 kPag vs. ± 1.86 kPag, representing a bandwidth reduction of 70.4%). And, compared to the case with no regulation, the slower stroke rate test run reduced pressure bandwidth by 80.5% while maintaining constant primary chamber pressure (minus transients). This demonstrates that the pressure bandwidth can be significantly reduced despite changes in operating volume, and this reduction can be magnified if the user is willing to slow the rate at which he or she induces the changes in volume.

The HPR and LPR plots provide a complete system understanding of the prototype's behavior. Every time the regulator was activated (in response to both positive and negative pressure spikes), it was possible to map the corresponding primary chamber pressure decay to a specific activation of the LPR/HPR. These activations each resulted in a degradation of the initial pressure charge of the respective reservoir. Every time a positive pressure spike was mitigated, on average a 4.41 kPag reduction in LPR pressure differential was measured. Similarly, every time a negative pressure spike was mitigated, on average a 5.03 kPag reduction in HPR pressure differential was measured. These tests showed that, as expected, without intervention the regulating reservoirs will eventually lose their starting pressure differentials, leading to a degradation of system performance and ultimately to total loss of system capability. It is for this reason that the prototype design calls for an in-line pump between the HPR and LPR (though this pump was not implemented in the prototype for these tests).

3.6.1 - Hypothesis Assessment and Conclusions

The hypothesis proposed in this study, that active pressure regulation can mitigate pressure effects despite changes in internal volume, was not directly assessed, but was implicitly supported. Active pressure regulation proved capable of maintaining very tight control of primary chamber pressure despite significant and repeated changes in internal

volume. Pressure control was further enhanced by decreasing the compression/expansion stroke rate. Although no tests were conducted to directly assess the effectiveness of the prototype regulator system at reducing torque contributions from pressure effects, the fact that the system was capable of mitigating pressure spikes due to volume changes implies that it would prove successful at mitigating pressure effects-induced torque.

There is added potential for the prototype pressure regulator to serve as a sort of “volume accommodator”. The system could be used to reduce the human workload associated with volume effects by moving the internal gas using pressure gradients rather than astronaut effort. If volume effects (which were previously determined to be the dominant contributor to total suit rigidity) could be reduced or eliminated using this system, this could allow engineers to focus on lighter, more comfortable joint designs and relax the requirement of constant volume joints.

Further refinement of this system, including optimization for power consumption, mass minimization, and component hardening and miniaturization could potentially lead to the development of a viable mobility enhancement system for future space suits.

3.6.2 – Limitations

There are aspects of the tests conducted for this study that limit the applicability of the conclusions discussed. First, the primary chamber was maintained at 101.325 kPa and the working gas used was air. The EMU (and likely future space suits) will not operate at this high pressure, or with air as its gas (Abramov et al., 1994). This has implications specifically for the LPR. In this study the LPR was charged to -69 kPag. If the system were attached to a suit pressurized to approximately 30kPa (like the EMU) it would be physically impossible to maintain the LPR at pressures lower than -30kPag. The system performs better when the differentials between the primary chamber and reservoirs are large: this constraint is therefore a very real limitation of the current design. And, because this was a proof of concept test, the system was designed without consideration

for mass, power consumed, or size/bulkiness. If this system were further developed, these design considerations will increase significantly in importance.

3.6.3 - Future Work

Simple hardware improvements to this system, including increasing the number and flow capacity of solenoid valves, and implementing the HPR/LPR pump as called for in the system schematics, could significantly improve performance without excessive cost or development. Furthermore, it would be useful to rig the prototype pressure regulator system to a full EMU to assess the practical improvements to suit mobility that may be gained as a result of active pressure regulation (measured explicitly in terms of torque vs. angle reduction for different joint articulations). Developing the concept of a “volume accommodation” system based on this design may lead to significant reductions in both pressure and volume effects.

A reservoir-based pressure regulation system provides additional freedoms regarding real-time modifications of internal suit pressure. Previous studies have shown that for different gravity regimes and activity levels, there exists varying optimal suit stiffnesses for minimized energy expenditure (Carr, 2005). It would therefore be energetically advantageous to be able to modify the stiffness of the suit at will depending on the nature of the task at hand. This regulator system could be easily expanded to include control over suit stiffness by varying internal pressure – the possibilities related to this concept warrant future study.

Finally, the development of active pressure regulation to improve suit mobility could lead to tighter fitting, smaller diameter and less bulky gas-pressurized suits. There are many benefits to pursuing such suit designs if the mobility problems associated with decreasing the internal operating environment and relaxing the requirement of constant-volume operation can be overcome.



PART IV

US Planetary Protection Policy Analysis for the Private Spaceflight Industry

Every one of us is precious in the cosmic perspective. If a human disagrees with you, let him live. In a hundred billion galaxies, you will not find another.

- Carl Sagan

4.1 – INTRODUCTION

The search for evidence of past and/or present extra-terrestrial life is one of the primary motivations for continued robotic and human exploration of the Solar System. One of the most challenging aspects of this search for life is preventing biological contamination of celestial bodies by terrestrial life forms (carried by the spacecraft itself). Such contamination would permanently confound our ability to definitively assess the origin of any biological material that may be discovered on bodies other than Earth – if we were to find life forms on the surface of Mars, for example, and the spacecraft responsible for discovering these life forms was not biologically sterilized prior to launch, it would be impossible to say with certainty that the newly discovered life forms were unique and extra-terrestrial in origin. Additionally, if unique extra-terrestrial life did exist, and a “dirty” spacecraft were to land and contaminate its environment with Earth-based life, the results could be highly destructive.

Of similar concern is the threat of biological contamination of Earth by potential extra-terrestrial life brought back by spacecraft that have visited celestial bodies (either through sample return, or simply through incidental interaction with the vehicle hardware). While such contamination would not confound the search for life in the Solar System, it could significantly affect Earth life and ecosystems that are unprepared for the introduction of potentially destructive foreign biological agents. Such contamination could have incredibly serious consequences, up to and potentially including threatening the survival of all Earth life.

These threats of biological contamination of the solar system (dubbed “forward-contamination” in the case of Earth life contaminating extra-terrestrial bodies, and “back-contamination” in the case of extra-terrestrial life contaminating Earth) are of such concern that international policies have been in development since the 1960s to prevent or minimize them from occurring (COSPAR, 2002). These policies, and the practices related to enforcing these policies, are collectively known as Planetary Protection.

4.1.1 – Legal Basis for US Planetary Protection Obligations

The concept of Planetary Protection was introduced as a tenet of the 1967 United Nations Treaty on Principles Governing the Activities of States in the Exploration and Use of Outer Space, Including the Moon and other Celestial Bodies (commonly referred to as the UN Outer Space Treaty of 1967). Article IX of this treaty officially states:

States Parties to the Treaty shall pursue studies of outer space, including the Moon and other celestial bodies, and conduct exploration of them so as to avoid their harmful contamination and also adverse changes in the environment of the Earth resulting from the introduction of extraterrestrial matter, and where necessary, shall adopt appropriate measures for this purpose (UN, 1967)

The United States signed and ratified this treaty in 1967, and to date 98 states have done the same (State.gov, 2001) (UN, 1967). While the original treaty necessitating Planetary Protection is now more than 40 years old, these policies are continually evolving at the international level based on recommendations from the UN Committee on Space Research (COSPAR). At the national level, NASA has independently and autonomously taken on the responsibility of ensuring continued compliance with US Planetary Protection obligations as specified by COSPAR since the signing of the treaty during the Apollo era – this has been (and continues to be) accomplished by NASA civil servants working in concert across multiple centers, and is headed by NASA’s single Planetary Protection Officer (currently Dr. Catharine Conley) (COSPAR, 2002) (NASA, 2008). NASA describes the nature and purpose of Planetary Protection as follows:

“[Planetary Protection] is the practice of protecting solar system bodies (planets, moons, comets, and asteroids) from contamination by Earth life, and protecting Earth from possible life forms that may be returned from other solar system bodies. Planetary protection is essential for several important reasons: to preserve our ability to study other worlds as they exist in their natural states; to avoid contamination that would obscure our ability to find life elsewhere—if it exists; and to ensure that we take prudent precautions to protect Earth's biosphere in case it does” (NASA, 2008)

4.1.2 – Categories of Planetary Protection

Not all Solar System bodies are “created equal” from a Planetary Protection standpoint. Depending on the nature of the body of interest, as well as the type of mission being considered, the relative importance of the prevention of biological contamination varies. For example, a mission to the Sun (where it is believed that no life exists and that no life could exist) requires no Planetary Protection countermeasures. Missions to bodies that may have harbored life (or could currently harbor life), however, require significant contamination countermeasures (with missions involving direct interaction with the body in question, like a lander/rover mission, having more stringent requirements than indirect missions, like orbiters/fly-bys). Missions that return hardware/samples to Earth after visiting an extra-terrestrial body are of particular concern from a contamination standpoint, and a specific set of regulations have been developed by COSPAR to govern such missions. As a result, depending on the body of interest and nature of the mission, the Planetary Protection requirements of a specific mission design will fall under one of five categories, outlined below (NASA, 2008) (COSPAR, 2002):

Category I: Missions to the Sun, Mercury, and other bodies of no biologic interest or risk

- Planetary Protection mitigation strategies required: none

Category II: Missions to bodies of interest related to chemical evolution/origin of life, but no real risk of contamination jeopardizing future study (e.g. the Moon, Venus, Jupiter, outer Solar System planets, comets)

- Planetary protection mitigation strategies required: simple documentation

Category III: Flyby/Orbiter missions to bodies of interest related to the chemical evolution/origin of life where the chance of contamination is significant and could jeopardize future study (e.g. Mars, Europa, Titan, Enceladus)

- Planetary Protection mitigation strategies required (some or all of the following): documentation, trajectory biasing, clean room assembly and bioburden reduction

Category IV: Entry Probe/Lander/Rover missions to bodies of interest related to the chemical evolution/origin of life where the chance of contamination is significant and could jeopardize future study (e.g. Mars, Europa, Titan, Enceladus)

- Planetary Protection mitigation strategies required: documentation, bioassays, trajectory biasing, clean room assembly, bioshield implementation, partial and/or complete sterilization

Category V: Return Missions to Earth, differentiated between “unrestricted” and “restricted”, depending on whether the target body is deemed capable of supporting life

- “Unrestricted” return Planetary Protection mitigation strategies required: typically Category I or II outbound requirements, no inbound requirements
- “Restricted” return Planetary Protection mitigation strategies required: Category IV requirements, plus additional requirements concerning prevention of destructive impact and sample containment

It is important to note that the categorization of celestial bodies is based upon the best current understanding of its past/present capability of supporting life. As a result, a certain body could have its official category changed if new information comes to light that changes this understanding (as was the case for the Moon, which in 2008 was elevated from Category I to Category II) (COSPAR, 2008).

4.1.3 – Research Motivation

As previously stated, the responsibility for US Planetary Protection compliance has been undertaken independently and autonomously by NASA since the Apollo era. Consequently, NASA has spent the past four decades developing in-house operating procedures, technologies, infrastructure and workforces to comply with COSPAR policies and to tackle the challenge of domestic Planetary Protection for deep-space exploration missions. This in-house, autonomous regulatory and enforcement architecture for domestic Planetary Protection has always made sense – to this point, any US mission requiring Planetary Protection control would necessarily have been

developed by NASA (to date no such domestic missions have ever been conducted outside of NASA) so granting NASA the authority to enforce Planetary Protection requirements autonomously has always minimized bureaucratic interference. And given NASA's track record of success at self policing in this regard, this regulatory architecture has been generally accepted as sufficient (Buxbaum, 2010).

While this regulatory architecture has historically been sufficient, the US is entering a new era of private and commercial spaceflight that could create serious long-term Planetary Protection regulation and enforcement problems. In the not-too-distant future (and for the first time in the history of the American space program), private entities outside of NASA will have both the independent capability to send objects into orbit and beyond, and the interest in doing so. Companies like Virgin Galactic, Orbital Sciences and SpaceX are developing both the technologies and underlying business models to promote private access to space from US soil (see Figure 67), and efforts like the Google Lunar X-Prize are actively promoting initiatives to privately land objects on extra-terrestrial bodies (Orbital, 2010) (SpaceX, 2010) (VirginGalactic, 2010) (X-Prize, 2010).



Figure 67: Orbital Sciences Taurus II and SpaceX Falcon 9 launch vehicles, designed to provide commercial access to space (photo credit: Orbital Sciences Corp., 2010, and SpaceX Corp., 2010)

Given the recent cancellation of the Constellation program by President Obama, which is now scheduled to be replaced by a new vision for NASA that includes increased support for the commercial spaceflight industry, the development of the private spaceflight sector (and thus, private access to space) is likely to accelerate (Bolden, 2010). Specifically, studies have been conducted to quantitatively predict the expansion of the suborbital tourism spaceflight industry based on current and future consumer demand. A study published by the Futron Corporation in 2002 and revised in 2006 predicts consumer demand for suborbital space tourism to reach nearly 14,000 passengers by 2021 (a fourteen-fold increase in demand since 2006) (Futron Corp, 2002) (Futron Corp, 2006). This predicted demand is presented in Figure 68:

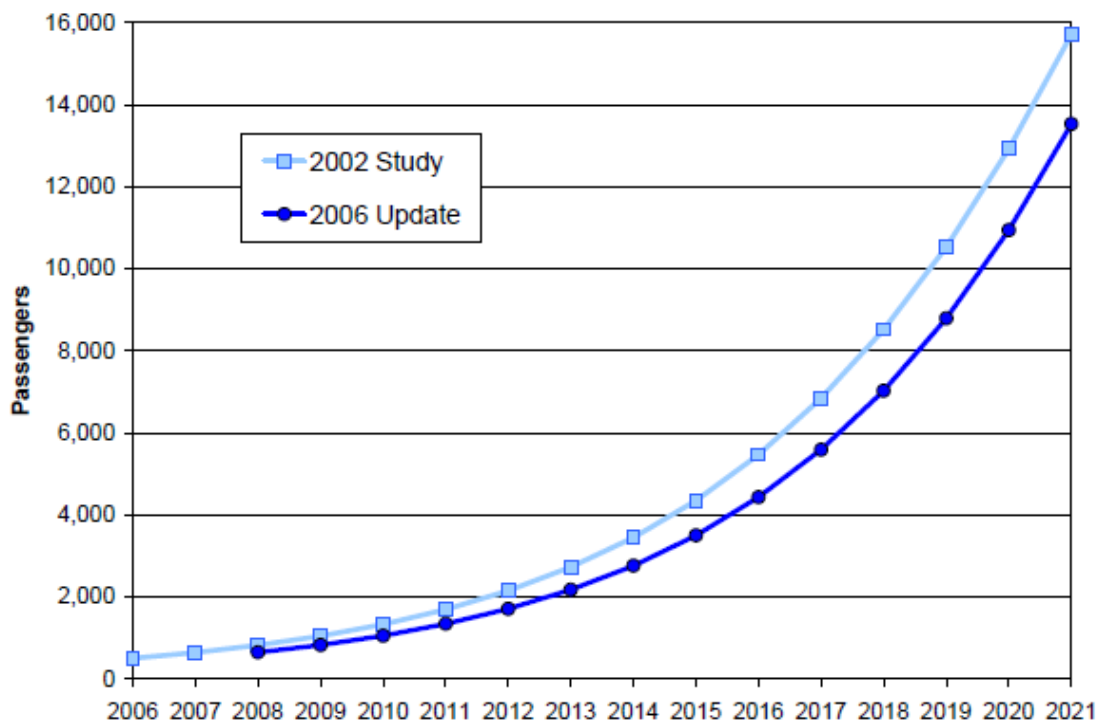


Figure 68: Predicted growth of passenger demand for suborbital space tourism, taken from “Suborbital Space Tourism Revisited” (Futron Corp, 2006)

While this figure shows a downward shift in demand based on a 2006 revision to the study (stemming from an increased estimate of initial ticket prices due to updated business models), the trend is still clear: as an industry, suborbital space tourism is

expected to grow exponentially in the next decade. It is predicted that revenue from this industry will reach nearly \$700 million by 2021 (Furtron Corp, 2006).

Suborbital space tourism does not pose any direct Planetary Protection threats, because no person/spacecraft will ever leave Earth orbit (thus no contamination risk exists). However, the maturation of this industry represents the ushering in of a new paradigm in which US access to space is no longer fully controlled by NASA and the public sector. While these private capabilities have not yet fully matured, and the current business model for these companies is limited to Earth-based space tourism, it is conceivable (and, some would argue, inevitable) that private entities will eventually develop viable technologies and business models to send robotic and/or human spacecraft to land on celestial bodies. It is this possibility, the possibility of direct physical interaction of extra-terrestrial bodies by non-NASA US entities, which poses a significant problem for the current NASA-run US Planetary Protection regulatory architecture: simply stated, since there has never been a need for US Planetary Protection policies or mechanisms for non-NASA entities, none currently exist.

Compounding the problem is the fact that Planetary Protection is both a costly and time consuming endeavor, yet it adds no tangible business value to the final product. At NASA, Planetary Protection is viewed by many hardware engineers as a distraction. For many, it represents a “hoop that must be jumped through”, and it is “tolerated” but not generally embraced (Buxbaum, 2010). For example, the direct, traceable costs associated with Planetary Protection compliance for the Mars Exploration Rovers (MER) totaled between \$3-5M, and these expenses did not contribute in any way to increased functionality of the rovers. Furthermore, this cost estimate does not include the indirect costs of compliance stemming from delays in hardware development and integration, altering of mission requirements, etc., so the actual total cost of Planetary Protection for the MER program is undoubtedly higher than this value. The Planetary Protection costs of a Mars sample return mission are currently estimated at 5-10% of the total mission cost (which could exceed \$100M on a \$1B mission) (Buxbaum, 2010).

For private companies, Planetary Protection will likely be even less well received than it is at NASA, as it represents a real and explicit burden that acts contrary to the primary goal of earning profits. As a result, these private, profit-driven entities may be less inclined than an organization like NASA to independently and voluntarily comply with US Planetary Protection obligations, meaning that explicit policies and enforcement mechanisms governing their behavior to ensure compliance may very well be necessary. At the very least, this reality illustrates the fact that the current US Planetary Protection regulatory architecture appears to be incomplete, as it does not provide an adequate framework to address the issues that will stem from the emergence of the domestic private spaceflight industry.

4.1.4 – Private Obligation to Uphold International Commitment

While some may argue that private US companies would not be responsible for complying with the Planetary Protection requirements described in the UN Outer Space Treaty because they are not state actors and thus not bound by treaties governing the behavior of state actors, there are several arguments against such a notion. First, because the private spaceflight industry is receiving (and will likely continue to receive) significant public financial support, it would be difficult to entirely separate private spaceflight actors from their public counterpart (the distinction between “public” and “private” in this sense is being blurred by the transfer of seed resources from the government to the commercial sector) (Bolden, 2010). In such a situation, a credible legal argument could be made that “private” US entities are not in fact entirely private, and as such are subject to the legal obligations of US state actors and would therefore be bound by the Outer Space Treaty.

Additionally, and perhaps more importantly, legal precedent already exists in the realm of space law ascribing legal responsibility to national governments for certain space-based activities occurring within their borders, regardless of the nature (public or private) of the entity conducting said activities. According to the Convention on International Liability for Damage Caused by Space Objects (commonly known as the Space Liability

Convention, which has been ratified by 86 states including the US), “A State from whose territory or facility a space object is launched ... shall be absolutely liable to pay compensation for damage created by its space object on the surface of the Earth or to aircraft flight” (UN, 1971). This means that the US government is internationally responsible for the actions of all space organizations within its borders, regardless of their public/private status (at least from a liability standpoint). It could thus be argued that this legal precedent demands that other US international obligations (such as Planetary Protection compliance) be also upheld by all entities operating within its borders, regardless of their public/private status. Such an argument invalidates the notion that commercial space entities are exempt from the international Planetary Protection rules that govern NASA simply because they are private actors.

4.1.5 – Problem Statement

The fundamental problem statement that forms the basis of this research effort is as follows: current US Planetary Protection policies are ill-equipped to deal with the changing face of the American space industry, as there are no protocols or policies for ensuring private space entities comply with US international Planetary Protection obligations.

4.1.6 – Research Questions and Intended Audience

To address this problem statement, the following research questions were formulated:

- What type of policy architectures will ensure commercial spaceflight compliance with US Planetary Protection obligations?
- Which architecture will do so with the least interference to both NASA and private spaceflight industry development?

The answers to these questions are important for several groups involved in US national policymaking groups: space policymakers at NASA headquarters; congressional

members of states whose constituencies have a vested interest in long-term public and private space development; the Department of State (due to the foreign policy implications of compliance with international treaties); the Department of Commerce; and both current and future Presidential Administrations responsible for setting budgets and agendas for NASA.

4.1.7 – Research Methods and Assumptions

This research effort, which seeks to answer the preceding research questions, is based upon two fundamental assumptions:

1. Planetary Protection, both in the public and private space flight industries, is necessary, therefore compliance by both sectors is critical (i.e. the tenets of the UN Outer Space Treaty related to Planetary Protection, the US decision to sign this treaty, and the implied obligation of private US companies to comply with this treaty, will not be challenged)
2. The development of the commercial spaceflight industry is beneficial to the US, and as a result Planetary Protection policies governing private behavior should be designed in a way that guarantees compliance without undue hindrance to economic development of the industry

Given these assumptions, NASA's current Planetary Protection practices were analyzed with a specific focus on how these practices might be applied to the commercial spaceflight industry. This analysis involved a series of interviews with NASA's Planetary Protection community, and a cost and functionality analysis of the Planetary Protection technologies, infrastructures, and workforce currently employed by NASA to carry out its Planetary Protection practices. Based on these analyses, policy architecture options for the commercial space industry were evaluated with regard to several metrics of interest (including compliance, cost, efficiency, and autonomy). These metrics and policy architectures will be discussed in detail in Section 4.3.

4.2 – NASA PLANETARY PROTECTION METHODS

To comply with US Planetary Protection obligations under the UN Outer Space Treaty, NASA has developed and refined a set of operating procedures and technologies specifically designed to assess and reduce the presence of viable biological agents on spacecraft leaving Earth orbit. These procedures and technologies are presented in the following sections, followed by analysis of NASA’s methods as it relates to the burgeoning US commercial spaceflight industry.

4.2.1 – Probabilistic Approach to Planetary Protection

Original attempts at Planetary Protection in the early era of space exploration (1960-70s) relied upon a probabilistic method for determining the likelihood of forward contamination for a given mission, and explicit values for maximum allowable probabilities of contamination were specified by COSPAR and dictated to each space agency, including NASA (COSPAR, 1969). The following equation was established to calculate the probability of forward contamination:

$$P_C = N_0 * R * P_S * P_I * P_R * P_G \quad \text{eq. 15}$$

Where:	P_C	–	Total probability of contamination
	N_0	–	Total number of organisms initially present on spacecraft
	R	–	Bioburden reduction factor
	P_S	–	Probability of surviving space exposure
	P_I	–	Probability of off-nominal impact
	P_R	–	Probability of microbial release
	P_G	–	Probability of Earth microbial growth upon release

COSPAR originally specified that P_C could not cumulatively exceed 10^{-3} for all missions to Mars (countries capable of sending objects to Mars were allocated a fraction of this total contamination probability), and similar limits were established for other Solar System bodies of biological interest (NRC, 2006) (COSPAR, 1969). This method for determining contamination risk was criticized by many, because the uncertainties in

several of the input variables were large, and in some cases their values were subjectively determined and debated (making the final calculated value essentially meaningless) (NRC, 2006) (NRC, 1992).

These criticisms ultimately led to a movement away from explicit probability calculations for Planetary Protection compliance (instead setting sterilization requirements based on the mission categories discussed in section 4.1.2), though current practices still focus on “many of the same variables that were the focus of earlier Planetary Protection policies” (NRC, 2006). The original equation for total contamination probability is still valid (despite the change in official policy), and as a result is still highly useful because it correctly identifies the specific aspects of each spacecraft/mission design that affect the overall contamination risk posed by a given mission. By examining this equation, it is clear which aspects of mission design, development, and hardware integration can and should be focused on to reduce total contamination risk: pre-launch bioburden reduction (R), altered mission trajectories to encourage exposure to harsh space environments and prevent off-nominal impact (P_S and P_I), and strategic spacecraft design to prevent microbial release (and P_R). As is shown in the next sections, it is exactly these aspects that NASA focuses on when implementing Planetary Protection countermeasures.

4.2.2 – NASA Planetary Protection Methods

NASA uses multiple methods to reduce the risk of forward contamination of the Solar System by US-launched spacecraft. These methods will be outlined in the following subsections, and include (but are not limited to) pre-launch microbial reduction, bio-shielding to prevent re-contamination up to and including launch, and trajectory and orbit biasing post-launch.

Pre-launch Microbial Reduction. Preventing forward biological contamination begins first and foremost with reducing the quantity and potency of any microbial entities (referred to as a spacecraft’s “bioburden”) on NASA spacecraft hardware before launch (i.e. reducing the value of the quantity “ R ” in equation 15). This is accomplished through a number of methods. All spacecraft are cleaned, assembled, and tested in clean-room

environments by specially trained and outfitted personnel, which provides an initial series of opportunities to reduce the bioburden on the surfaces of the craft (NRC, 2000). Depending on the level of Planetary Protection required, clean-room assembly may be followed by an additional sterilization technique at adjacent facilities known as dry-heat cycling (NRC, 2006). As the name would imply, dry-heat cycling sterilization subjects hardware to temperatures reaching 230 degrees Fahrenheit for extended periods of time (≥ 30 hours), and this process is repeated (NASA, 2008). The spacecraft components are essentially “baked” in a large oven, and this process kills a sufficiently high number of active microbes on and in the spacecraft to satisfy the mission-specific Planetary Protection requirements. However, because certain highly sensitive spacecraft components cannot survive such treatment, other forms of sterilization such as hydrogen-peroxide cycling, alcohol wiping, and exposure to beta/gamma radiation are also used depending on the types of components and/or types of microbial spores involved (though these methods require additional verification to ensure that proper sterilization has taken place) (NRC, 2006). An example of dry-heat sterilization is provided in Figure 69:



Figure 69: Dry-heat sterilization of a Viking Lander (photo credit: NASA, 2008)

Due to the previously mentioned sensitivity of certain components to high temperature environments, spacecraft rarely undergo complete dry-heat sterilization cycling in their fully assembled state (NRC, 2000). This poses challenges from a Planetary Protection certification standpoint, as it necessitates post-sterilization integration and testing (which increases the likelihood of re-contamination).

Verification of Post-Sterilization Bioburden Reduction. It is necessary to verify the effectiveness of sterilization procedures on bioburden reduction of a given spacecraft prior to launch. To do so, biological assays are conducted to measure the microbial density on all accessible spacecraft surfaces (samples are heat shocked, and “the surviving cells are cultured to determine the number of colony-forming units”) (NRC, 2000). Surfaces that are found to be insufficiently sterilized are flagged for additional cleaning, which would then be followed by additional assays for verification.

While this method is adequate for assessing the effectiveness of sterilization techniques on the internal and external surfaces of the spacecraft, it cannot be used to determine the amount of “encapsulated” bioburden (active microbes embedded inside components of the spacecraft that are not directly accessible). Although these microbes pose a less-significant threat to planetary contamination, as they would only interact directly with the surface of the target body under some form of off-nominal circumstance (a destructive landing for example), they must still be accounted for when certifying the cleanliness level of a sterilized spacecraft. To estimate the level of encapsulated bioburden, portions of the spacecraft likely to be harboring microbial material are assigned parameter values based on standards developed by the Planetary Quarantine Advisory Panel (NRC, 2006).

Prevention of Re-contamination. Once assembled and sterilized, NASA spacecraft are maintained in a clean-room environment until immediately before launch to prevent re-contamination, assuming the clean-room environment itself is sufficiently sterile. For missions that require higher levels of sterilization than can be provided by a standard clean-room environment, spacecraft are placed within a protective bio-shield casing (which may or may not contain additional countermeasures like positive-pressure barriers and high-efficiency particulate air [HEPA] filtration) that will protect the craft prior to and during launch (NRC, 2006). In some cases this positive-pressure defense barrier will be maintained through the full launch phase, and the casing will only be jettisoned once the craft has reached sufficient altitude to guarantee no further contamination risk from atmospheric gases. Additional countermeasures to prevent re-contamination, like

mandatory sterilization of all internal surfaces of launch fairings, are scheduled to be implemented for future robotic exploration missions (NRC, 2006).

Trajectory Biasing. In addition to sterilization techniques undertaken prior to spacecraft launch, it is possible to reduce the bioburden of a vehicle after launch by modifying its interstellar trajectory and final orbit (i.e. reducing the value of the quantity “ P_s ” in equation 15). This is possible because the space environment is hazardous to Earth-based life – in particular, ionization caused by Solar radiation is known to damage DNA, meaning that extended exposure to such radiation will lead to a reduction in viable microbial life carried by a spacecraft. It is estimated that on a single interstellar trip to Mars, a spacecraft would experience 500 times as much Solar radiation as it would for a comparable time spent on the surface of the Earth (Buckey, 2006). Thus, by extending the length of time it takes a spacecraft to travel to its destination, or by altering its interstellar trajectory such that it experiences higher doses of Solar radiation, it is possible to passively sterilize a spacecraft during its transit phase (COSPAR, 2002).

However, intentionally biasing a spacecraft trajectory or orbit can have several negative consequences – for example, exposing sensitive equipment to excessive radiation can cause irreversible damage, and delaying the spacecraft’s arrival at the target body can shorten the useful lifespan of the vehicle. Using such a strategy thus requires careful consideration of these tradeoffs. Further, because it is not possible to verify or certify the effectiveness of this type of sterilization after the fact, it would be unwise to solely rely on this method to satisfy bioburden reduction requirements.

4.2.3 – NASA Planetary Protection Workforce

Equally as important to NASA’s Planetary Protection efforts are the highly trained civil servants dedicated to the cause. This workforce is headed by NASA’s single Planetary Protection officer, who is responsible for agency-wide policy generation and enforcement (Buxbaum, 2010). Reporting to this officer are several civil servants, spread across multiple centers, who are active both at the mission/hardware level and the conceptual

mission design level, and who have been specially trained in the policies/procedures required to carry out NASA's Planetary Protection strategy (Buxbaum, 2010).

The size of NASA's Planetary Protection workforce fluctuates depending on the phase of a given mission. The demand for Planetary Protection resources is low during the early development phases, and understandably increases during the hardware assembly, test, and launch operations (ATLO) phases, when active cleaning, sterilization and assaying take place (though a consistent need for Planetary Protection analysis always exists at a high level for long-term mission planning and conceptual design) (NRC, 2006).

For example, the Planetary Protection team at NASA's Jet Propulsion Laboratory (JPL) included nearly 25 members at its peak during the MER development cycle, and now has dwindled to approximately half that size (Buxbaum, 2010). The employees that choose to leave the team are generally not lost from NASA, but instead move internally to other teams and take on more traditional engineering responsibilities. While this migration is natural given the varying demand for Planetary Protection resources, it does pose challenges down the road because many of these individuals choose not to return to Planetary Protection tasks once the demand for such resources increases again. This cyclic outflux of corporate knowledge is costly, as it forces NASA to commit significant up-front resources to train a new class of Planetary Protection employees each time a new mission moves into the ATLO phase (Buxbaum, 2010).

4.2.4 – European Planetary Protection Methods

It is worthwhile to examine the Planetary Protection methods of other international space agencies to provide a point of comparison for the aforementioned NASA strategy. Take for example the European Space Agency (ESA), composed of several constituent European nations who have agreed to the same set of rules outlined by the 1967 UN Outer Space treaty as the United States (UN, 1967). As signatories of this treaty, the ESA is obligated to satisfy identical Planetary Protection requirements as NASA for all deep-space exploration missions, and unsurprisingly has chosen similar methods for

achieving compliance. ESA bioburden reduction is achieved using dry-heat cycling, except in cases where such cycling would damage spacecraft components (in which case alternative methods like alcohol wiping, hydrogen peroxide plasma exposure, or exposure to radiation are employed) (ESA, 2002). Other comparable mitigation strategies, such as clean-room assembly, post-assembly bio-shielding, and trajectory biasing/orbit modification are also implemented (ESA, 2002) (Debus, 2008).

4.2.5 – Analysis and Summary

NASA's Planetary Protection strategy is multi-faceted, and is comparable in approach to other space agencies with similar exploration capabilities. Since the inception of domestic Planetary Protection policy, NASA has modified its methods as necessary to accommodate changing COSPAR recommendations and to match the constantly evolving technological state of the art. These efforts have resulted in considerable agency-level investment in both human capital and sterilization infrastructure/technologies. NASA's methods have been generally considered successful, evidenced by the fact that there has never been a need for external inspection or enforcement mechanisms within the US to ensure domestic compliance with international Planetary Protection obligations: NASA's autonomous approach has proven itself to be trustworthy and effective (Buxbaum, 2010).

However, because the demand for Planetary Protection services is highly variable based on the quantity and type of active deep-space missions (and also on the phase of said missions), NASA's resources in this regime at times go under-utilized, and corporate knowledge is periodically lost as personnel transition (sometimes permanently) to other fields. Consequently, this under-utilization of NASA's resources represents a significant opportunity for partnerships with future private domestic space organizations: such organizations will require similar technologies, infrastructure, and expert personnel to achieve Planetary Protection compliance, and NASA is well positioned to lend its resources and expertise to this effort. As will be demonstrated in the following section, an effective Planetary Protection policy architecture for the commercial space sector should leverage this opportunity for collaboration.

4.3 – POLICY ARCHITECTURE ANALYSIS

4.3.1 – Policy Options and Metrics of Interest

As previously stated, the policy analysis that follows is based upon two fundamental assumptions: that Planetary Protection compliance is necessary for both public and private US space organizations; and that the development of the private US spaceflight industry should not be unduly hindered by policies designed to ensure said compliance. With these assumptions in mind, three policy architecture options for Planetary Protection compliance in the emerging US commercial space sector were evaluated. While not intended to be an exhaustive set, these architecture options span (at a high level) the general policy trade-space surrounding this issue. These architecture options, which vary based on the levels of autonomy granted to each sector, are as follows (and will be covered in greater detail in subsequent sections):

- Policy Architecture 1: NASA continues to administer Planetary Protection procedures independently autonomously, and the private space sector is given identical autonomy to police itself
- Policy Architecture 2: NASA continues to administer Planetary Protection procedures independently autonomously, and its authority is extended to oversee, support and regulate Planetary Protection efforts in the private space sector
- Policy Architecture 3: An independent Planetary Protection oversight entity is created to support and police the efforts of both NASA the private space sector

In order to evaluate these architectures, four metrics were identified that capture the critical policy and business considerations that are tied to this decision. These metrics were ranked in order of relative importance, and are as follows: **compliance**; **cost**; **efficiency**; and **organizational autonomy**.

- The first metric, “compliance”, refers to the likelihood of both public and private space organizations maintaining full compliance with US Planetary Protection obligations under a given policy architecture. This metric was identified as the most important evaluation metric because it targets the specific behavioral

outcome that these policies are designed to induce (compliance). Put another way, it was decided this metric must be held above all else, because if a policy fails to induce compliance then it will have failed its primary purpose (and thus should not be evaluated against any other metric).

- The second metric, “cost”, is self explanatory, referring to the relative financial burden incurred en route to compliance for both the public and private sector (i.e. how much will compliance cost?). This was ranked as the most important metric (after compliance) because it could directly affect the development of the private sector (policy architectures that impose significant financial burdens on the private sector could preemptively sink the industry).
- The third metric, “efficiency”, is also self explanatory, and is closely related to cost. This metric is meant to capture the impact of a given policy architecture on the day-to-day efficiency (i.e. time/energy required to achieve compliance) of both the public and private sectors. It was ranked below cost in terms of importance, because it was deemed “slow-but-cheap” policy architectures should be preferred over “quick-but-costly” architectures (due to the already high costs/slim profit margins predicted for initial private space business models, it was believed that an such organizations would prefer schedule slips over cost overruns, though this belief is open to debate).
- The final metric, “organizational autonomy”, refers to an individual organization/industry’s ability to police itself without outside interference. While autonomy is generally desired (nobody prefers to lose power of self-governance), a loss of autonomy represents the least severe potential consequence (i.e. if compliance can be achieved cheaply and quickly, but doing so requires a loss of autonomy, such an outcome would likely be deemed acceptable).

One of three “grades” (*positive, negative, or mixed*) was assigned to summarize the general net effect of each policy option with respect to a given metric. This assessment method is adapted from a similar space policy analysis conducted by MIT researchers Newsome et al., which was presented at the AIAA Space 2009 conference (Newsome et al., 2009).

4.3.2 – Policy Evaluation: NASA and the Private Sector Operate Autonomously

In this policy architecture, NASA and the private space sector are both granted independent autonomy to implement Planetary Protection procedures in accordance with US international compliance obligations. This architecture represents no significant change to NASA’s current operating procedure (as NASA has autonomously policed itself from a Planetary Protection standpoint for over four decades). It does, however, represent a laissez-faire approach to regulating the private space sector, as each private organization is given the freedom (and responsibility) to develop internal policies and technologies to comply with COSPAR regulations. Such a strategy employs a Chicago school of economics philosophy (which emphasizes hands-off open-market economics) and minimizes the level of external bureaucracy, the merits of which are open to both political and philosophical debate (Viscusi, 1995).

A simple schematic representing this policy architecture is presented in Figure 70.

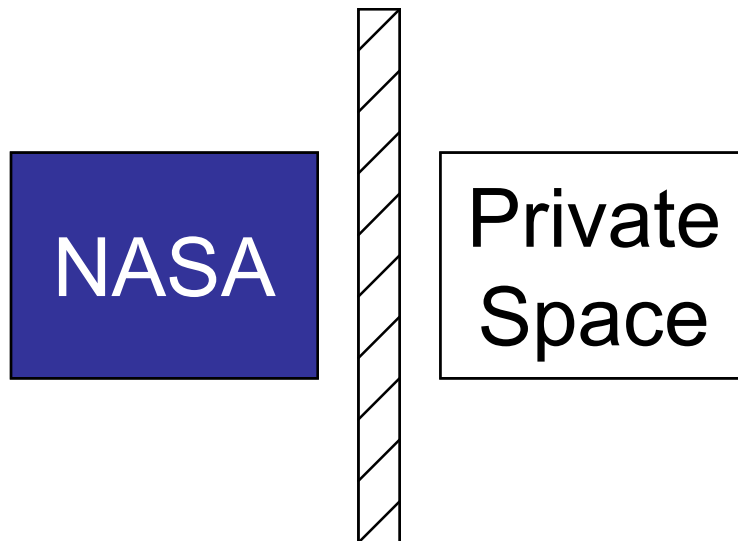


Figure 70: Schematic of a proposed policy architecture where NASA and the private sector each independently and autonomously oversee their respective Planetary Protection responsibilities

This policy architecture is evaluated as follows:

1. Compliance – Negative

Though NASA has proven itself capable at policing itself from a Planetary Protection standpoint without the need for an explicit or external enforcement mechanism, it is unlikely that the private sector will prove itself equally responsible. The primary distinction between NASA and the private sector in this regard is the issue of underlying motivation. Planetary Protection compliance is costly and takes time, impeding progress without providing tangible reward. For public organizations such as NASA that are not profit-seeking, Planetary Protection might be viewed as a nuisance, but it does not threaten their fundamental operating models. Private organizations, however, have far less incentive to autonomously comply with Planetary Protection obligations, because the resources spent to achieve compliance produce no material return and provide no opportunity for profit or business growth.

Proponents of the hands-off approach to private sector regulation argue that sufficient mechanisms exist to ensure regulatory compliance (litigation in the event failure causing public or private harm, fear of brand/reputation damage, etc.) therefore the imposition of external review is not necessary. Ignoring the multitude of examples of corporations ignoring or cutting corners with regard to regulatory compliance, such an argument is even less compelling when applied to Planetary Protection because failure to prevent biological contamination of celestial bodies does not have the same material and tangible effect as failures in more traditional scenarios (for example, failure to properly sterilize medical equipment represents a similar type of compliance failure, but with far greater material consequences than “celestial contamination”). Simply stated, if a private company fails to comply with Planetary Protection regulations and consequently contaminates Mars with a spacecraft, the outrage (and thus threat of legal retribution) will be far less than if poorly sterilized medical equipment leads to widespread health issues and/or loss of life. The threat of retribution is far less severe when dealing with Planetary Protection compliance, therefore it is unlikely that it would serve as an effective deterrent against bad corporate behavior.

2. Cost – Mixed

Because resources and expertise would not be shared between NASA and the private sector under this policy architecture, up-front costs would likely be very high for each private organization (including resources spent to develop and refine operating procedures, capital expenditures for infrastructure and hardware, and costs associated with recruiting and training qualified personnel). Additionally, since this policy would not take advantage of potential partnerships with NASA, it could prove more costly for NASA than other policies that promote collaboration. This is true because NASA's current operating procedures result in periods of under-utilization of its own personnel and resources, thus by maintaining the status quo this policy architecture is perhaps more costly than implementing changes that promote partnership and resource sharing.

However, a primary criticism of government organizations like NASA is that the lack of competition causes unnecessary cost and schedule overruns. It is conceivable that private, profit-seeking organizations could eventually develop better, cheaper methods for achieving Planetary Protection compliance than those currently employed at NASA if left to their own volition. In such a scenario, freeing the private sector to tackle Planetary Protection compliance using their own methods could ultimately prove to be the least costly option (once the high start-up costs are overcome).

3. Efficiency – Mixed

Using similar arguments as provided for cost, the effect of this policy architecture on total time spent by both NASA and the private sector is mixed. Because the expertise and infrastructure of NASA would not be shared with the private sector, the initially-steep learning curve associated with policy/procedure development will likely lead to temporary losses in business efficiency. However, if the private sector does develop new methods that are superior to NASA's strategy, efficiency could ultimately be improved.

4. Organizational Autonomy – Positive

This policy is unambiguously positive from an organizational autonomy standpoint. Both NASA and the private sector are free to operate as they see fit, which represents a maximization of overall organizational autonomy.

4.3.3 – Policy Evaluation: NASA Controls All Domestic Planetary Protection Efforts

In this policy architecture, NASA is placed in charge of all domestic Planetary Protection efforts. NASA continues to operate independently and autonomously with regard to its own internal Planetary Protection strategy, and NASA’s authority is also extended to oversee, support, and regulate Planetary Protection efforts in the private space sector. This architecture is designed to leverage the fact that Planetary Protection is already a core competency of NASA, and prevents the private space sector from both having to reinvent the wheel with regards to policy/procedure development and from needlessly spending money on redundant technologies and infrastructure (especially given the fact that NASA’s resources are at times under-utilized). The exact details of the relationship that would exist between NASA and the private sector in this scenario are open to debate (including the extent to which resources are shared and work is outsourced). At the very least, though, NASA would assume the role of a regulatory body with regard to Planetary Protection compliance in the private sector, and would be responsible for ensuring private compliance with COSPAR policies. A simple schematic representing this policy architecture is presented in Figure 71.

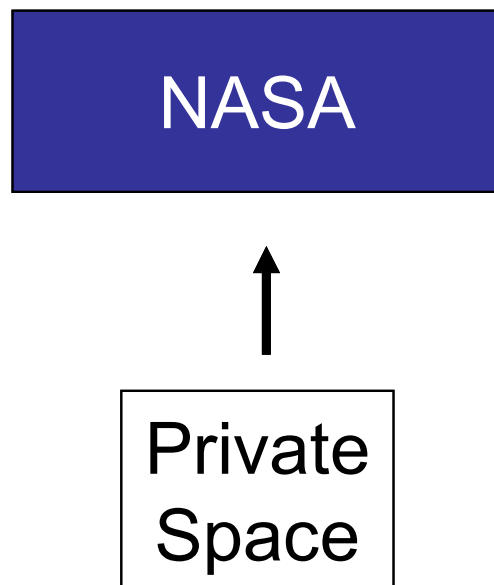


Figure 71: Schematic of a proposed policy architecture where NASA controls all domestic Planetary Protection efforts

This policy architecture is evaluated as follows:

1. Compliance – Positive

The likelihood of successful compliance under this architecture is high. By creating an explicit oversight process headed by NASA, the private sector would be unambiguously monitored (and if necessary, policed) to ensure compliance with Planetary Protection regulations. And given NASA's expertise and experience with the subject, they are well equipped to take on this responsibility.

2. Cost – Positive

This architecture enables and encourages resource sharing between NASA and the private sector. Not only does it remove the significant up-front costs that each private organization faces, but it also provides an opportunity for these organizations to outsource Planetary Protection tasks to the most capable and experienced group in the country. NASA would likely welcome these additional responsibilities, because it represents an opportunity for additional revenue streams, and it would also provide a steadier stream of work that aligns perfectly with one of its core competencies (thus avoiding the brain drain that stems from periods of low demand).

It could be argued that this architecture may be costlier in the long run, because NASA might not conduct Planetary Protection operations as cheaply as competition-driven, profit-seeking private organizations. While explicit cost numbers could not be obtained for this analysis, the fact that this architecture avoids the need for individual, private procurement of technologies/infrastructure that would be redundant in many ways to NASA's resources (and would also likely go under-utilized) suggests that private organizations would benefit financially by operating under this architecture.

3. Efficiency – Mixed

It is difficult to assess the net effect of this architecture on efficiency. NASA's workload and responsibilities will undoubtedly increase due to their additional roles in supporting and regulating the private sector. It could be argued, though, that this will actually

increase efficiency at NASA, because it allows resources to be more fully utilized (and could specifically prevent human resource losses within an otherwise-under-engaged Planetary Protection workforce, which will save NASA from having to spend time and energy to train new employees down the line). However, if these additional responsibilities push NASA beyond its capacity, and additional resources are not made available to accommodate this increase in workload, it could force an internal reallocation of resources that negatively affects other aspects of NASA's work.

In the private sector, similar tradeoffs on efficiency exist under this architecture. By outsourcing Planetary Protection work to NASA, private organizations will certainly experience time savings by avoiding the burden of initial policy/procedure development and employee training (i.e., they won't have to "reinvent the wheel" internally). However, these time savings might be lost due to the increased bureaucracy of having to report to / be certified by NASA for each deep space mission. Additional inefficiencies may be also introduced if NASA's resources and infrastructure are directly used by multiple private organizations - not only will it take time to physically transport private hardware to NASA's facilities, but organizations may find themselves competing with each other (or with NASA itself) for sufficient access to resources. This could place private organizations at the mercy of NASA's mission schedule, which could lead to significant schedule delays.

4. Organizational Autonomy – Mixed

Under this architecture, NASA's internal autonomy is unchanged, and its authority is also increased to include regulatory power over the private sector. This increase in power, though, represents a loss of autonomy in the private sector, as these organizations would be subjected to external review and regulation.

4.3.4 – Policy Evaluation: NASA and the Private Sector are both Subject to External Review

In this policy architecture, a new, independent and external review board is established to exclusively monitor all domestic Planetary Protection issues. This board would oversee the actions of both NASA and the private space sector, and would provide a centralized, unambiguous, hierarchal enforcement mechanism for ensuring compliance. All missions requiring Planetary Protection mitigation strategies, regardless of source (public or private), would be subject to review and approval/modification based on recommendations from the board. This architecture, while introducing the most bureaucracy of the three architectures presented, also represents the most egalitarian approach to the problem of Planetary Protection regulatory compliance. The exact composition of this review board and whether it would function within an already existing government agency (like the FAA) or would require the creation of a new government body, are details open to debate and will not be addressed in this analysis. A simple schematic representing this policy architecture is presented in Figure 72.

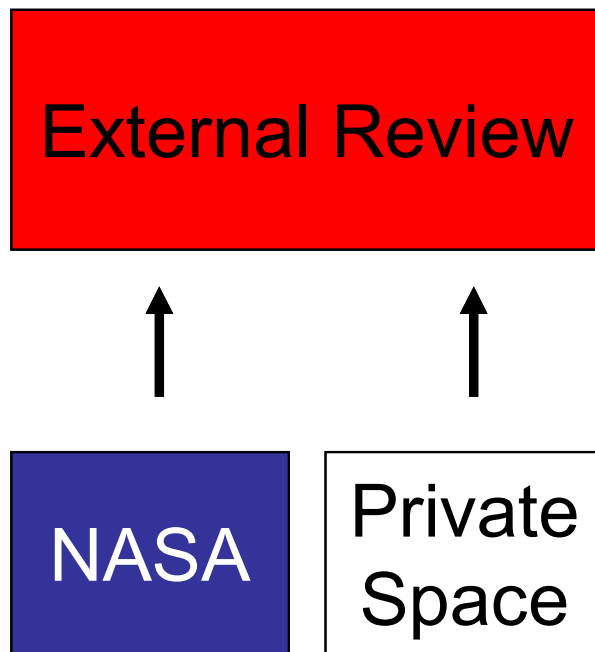


Figure 72: Schematic of a proposed policy architecture where NASA and the private sector are both subject to external Planetary Protection review

This policy architecture is evaluated as follows:

1. Compliance – Positive

Similar to the previous policy architecture, the likelihood of successful compliance under this architecture is high. The creation of an explicit, independent and external review board guarantees that both NASA and the private sector are unambiguously monitored to ensure compliance with Planetary Protection regulations (though NASA likely does not need such monitoring).

2. Cost – Mixed

This policy architecture is costly for NASA, because it will require the agency to restructure both its workforce and current operating procedures to reflect the loss of agency-level regulatory autonomy (i.e., any arrangement that forces NASA to report to an outside agency for Planetary Protection approval will necessarily increase costs over the status quo of independent and autonomous operation). The effects of this policy on costs for the private sector are less clear, because simply reporting to an outside review board does not necessarily preclude the private sector from independently partnering with NASA to reduce total costs (which as previously argued is likely the best choice from a cost perspective). On the other hand, because this architecture does nothing to facilitate or encourage a public-private partnership, the bureaucracy and organizational inertia of an agency like NASA might be too large for partnerships with the private sector to form organically (i.e., a catalyst in the form of explicit policy might be necessary, but more analysis here is required). When compared to the policy architecture that places NASA in charge, at best this architecture could be slightly more costly (due to the forced restructuring of NASA), and at worst could be significantly more costly (if an effective partnership with NASA cannot be crafted voluntarily).

3. Efficiency – Mixed

This architecture requires a restructuring of NASA's current methods, which as previously discussed is not necessary (NASA's independent and autonomous approach to Planetary Protection has been considered sufficient for four decades). Therefore this policy represents a step back in efficiency for NASA. Regarding the private sector,

reporting to an outside review board does increase bureaucracy over a hands-off approach (therefore inefficiencies will inevitably be created). However, these inefficiencies will not be significantly greater than those that arise in the scenario where the private sector is forced to report to NASA: it is the act of obtaining outside approval, rather than the nature of the agency issuing the approval, that causes inefficiencies. Additionally, depending on the nature of the public-private relationship in this scenario (i.e. do they share resources or act independently?) additional inefficiencies may arise.

4. Organizational Autonomy – Negative

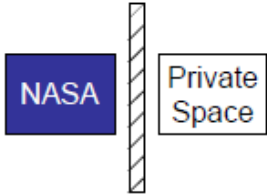
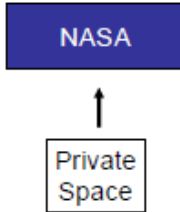
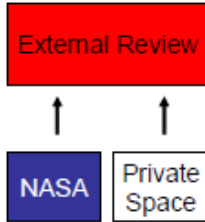
This policy architecture creates the most bureaucratic interference of all architectures presented, as it requires all organizations to report to an outside entity (regardless of public or private status). Not only is the private sector prevented from policing itself, but NASA will have its previously existing independence and autonomy revoked (something that NASA will likely heavily resist).

4.4 – CONCLUSIONS

Given this analysis, the policy architecture that is best suited to ensure Planetary Protection compliance while still encouraging the development of the private space industry is one in which NASA is placed in charge of all US Planetary Protection efforts, serving as an oversight, support, and regulatory authority over the private space industry. This architecture places complete authority with those who are most experienced with Planetary Protection (NASA) without significant restructuring, allows NASA to maintain its internal status quo (which has proven to be reliable), and creates opportunity for public-private partnerships that could provide mutual cost savings by eliminating existing under-utilization of NASA resources. While this architecture will reduce the autonomy of the private sector, it represents a small price to pay to maximize the likelihood of total and continued domestic Planetary Protection compliance.

A summary of the policy analyses presented in Section 4.3 is included as Table 13.

Table 13: A summary of US policy options regarding NASA-private space Planetary Protection regulatory architectures

	US Policy Options Regarding NASA-Private Space Planetary Protection Regulatory Architectures		
Metrics	 Public and Private Autonomy	 NASA in Charge	 External Review
Compliance	Negative	Positive	Positive
Cost	Mixed	Positive	Mixed
Efficiency	Mixed	Mixed	Mixed
Organizational Autonomy	Positive	Mixed	Negative

4.4.1 – Limitations and Recommendations for Future Work

This study provides a first attempt at analyzing the Planetary Protection policy landscape as it applies to the emerging private spaceflight sector. While it provides qualitative analysis of several high-level policy architectures that might be implemented in the future to regulate the private space industry, this study leaves some questions unanswered and would benefit from additional analysis based on quantitative modeling. Specifically, a quantitative analysis of the cost-savings that could be achieved through resource-sharing between NASA and private space organizations would significantly strengthen the

analysis and conclusions presented herein. Additionally, investigations of more detailed versions of these policy architectures (rather than the high-level structures used for this study) would help make this analysis more practical and implementable. Further, because the private space industry is still in its infancy, it is impossible to fully predict either the timeline of its growth or the structure it will ultimately adopt – as a result, this policy analysis will need to evolve to match the ever changing face of the industry. Additionally, this analysis does not consider multinational companies (with US registration) – such companies may require more complicated regulatory architectures, and a study specifically focusing on Planetary Protection policies for these entities is necessary. Finally, it would be constructive to bring together Planetary Protection officials from NASA, representatives from the private space industry, and also national space policymakers for a collaborative discussion using this initial analysis as a starting point.

Planetary Protection compliance with regard to the US private space industry might not seem like a critical issue currently, because the industry has significant business and technological hurdles to overcome before private spacecraft will actually leave Earth orbit. Even so, the current policy landscape is not equipped to deal with this issue once it becomes a real threat. The analysis presented here is a first attempt at addressing this specific (and impending) policy problem, and will hopefully initiate a discussion that will lead to actual and implementable policy solutions.

THESIS SUMMARY AND CONTRIBUTIONS

In Part I, the concept of pressure effects was introduced, and it was hypothesized these effects represent a third, and not well studied, contributor to gas-pressurized space suit rigidity (in addition to volume and structural effects). A simple model was developed to estimate the relative influence of pressure effects relative to volume effects under isentropic, adiabatic conditions. This concept was experimentally tested in Part II, where a Class III EMU elbow joint was pressurized and flexed through its complete range of motion to determine the relative influence of all three contributing effects (pressure, volume and structural effects). The results suggested that structural effects dominate at low flexion angles, volume effects dominate at high flexion angles, and pressure effects become significant at high flexion angles where constant volume behavior breaks down. In Part III, an active pressure regulation system designed to mitigate pressure effects in future space suits was successfully developed and tested.

The hypotheses that pressure effects contribute to gas-pressurized space suit rigidity, and that these effects are a statistically significant contributor to total torque of the EMU elbow joint, were partially supported by the data collected. Pressure effects were found to contribute to total torque of the EMU elbow joint, but only when the arm was capped at the shoulder (fixing the internal volume at approximately 25% of the total EMU volume). This suggests that these effects, while not significant in the elbow joint when tested using a representative volume, will affect larger diameter joints that are not as well-optimized for constant volume operation. The third hypothesis, that active pressure regulation can mitigate pressure effects within a space suit despite changes in internal volume, was implicitly supported by the data collected. The regulator system proved capable of mitigating repeated pressure spikes stemming from compressions of a closed volume of gas, suggesting that this system would eliminate pressure effects when connected to a space suit by eliminating the pressure spikes that stem from joint articulation.

These findings have three main implications for space suit mobility: first, they demonstrate that current gas-pressurized space suit modeling efforts (that focus only on volume effects and/or structural effects) do not fully capture the mechanisms that affect total rigidity; second, they illustrate that structural, volume, and pressure effects do not contribute equally to total torque of the EMU elbow joint, and that the relative roles of these effects are likely specific to each joint depending on its size and its volume vs. angle behavior; and third, these findings demonstrate that active pressure regulation is a viable method for reducing joint torque in future gas-pressurized space suit designs.

Additionally, in Part IV, a policy analysis was conducted to determine the best regulatory architecture for ensuring the newly emerging US private spaceflight sector complies with international Planetary Protection obligations. This study determined that a policy architecture that places NASA in charge of all domestic Planetary Protection operations will guarantee private spaceflight Planetary Protection compliance with the least negative impact on industry development.

The major contributions of this thesis include:

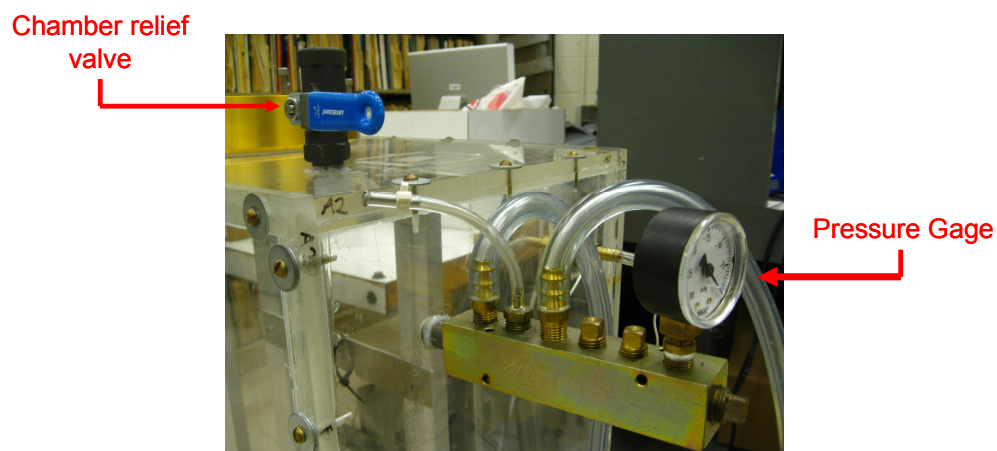
1. The introduction of a previously unstudied contributor to gas-pressurized space suit rigidity (pressure effects) and a first attempt at modeling these effects (Part I)
2. The first documented experimental assessment of volume change behavior of the EMU elbow joint (Part II)
3. The first documented experimental assessment of the effect of volume change on internal space suit pressure, and the effect of these changes on total suit stiffness (Part II)
4. An experimental assessment of historical modeling efforts that reveals volume, structural and pressure effects each contribute to total torque, and the relative magnitude of these effects changes throughout the flexion envelope (Part II)
5. Indirect evidence that overall suit mobility could be increased by introducing active pressure regulation (Part III)
6. A first-attempt at developing Planetary Protection policy to regulate the emerging private spaceflight sector (Part IV)

APPENDICES

Appendix A – Pressure Chamber Control Method

The following method was used to maintain constant pressure in the MVL chamber:

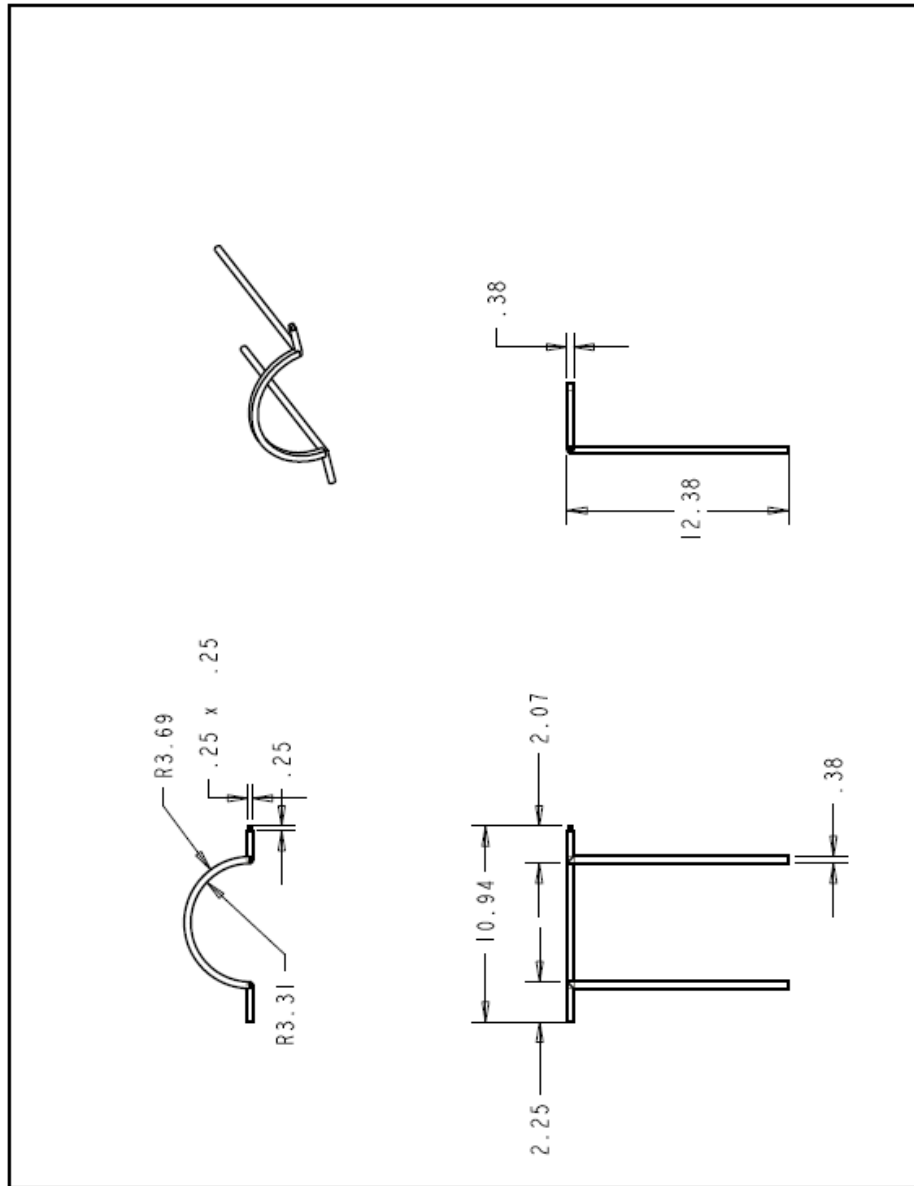
1. Close the chamber relief valve and ensure that the elbow articulation rig access point is either occupied by the wrench adapter or is plugged
2. Turn on both vacuum pumps (labeled “red” and “blue” on the power strip – note the “red” pump is twice as powerful as the “blue” pump)
3. Allow the chamber pressure to decrease to approximately -8.5” hg differential
4. Disable the “red” vacuum pump by turning off its switch on the power strip
5. Monitor the chamber pressure gage to see if the pressure remains constant at -8.5” hg
6. Do one of the following actions, depending on the outcome of step 5:
 - a. If pressure continues to increase with only the “blue” vacuum pump activated, then incrementally open the chamber relief valve until the chamber pressure levels off at the desired value - leave the valve open to this position
 - b. If pressure remains constant, do nothing
 - c. If pressure begins to drop, then disable the “blue” vacuum pump and enable the “red” pump – this will certainly cause the pressure to increase beyond -8.5 in hg, so it will be necessary to incrementally open the chamber relief valve until the pressure levels off at the desired value - leave the valve open to this position



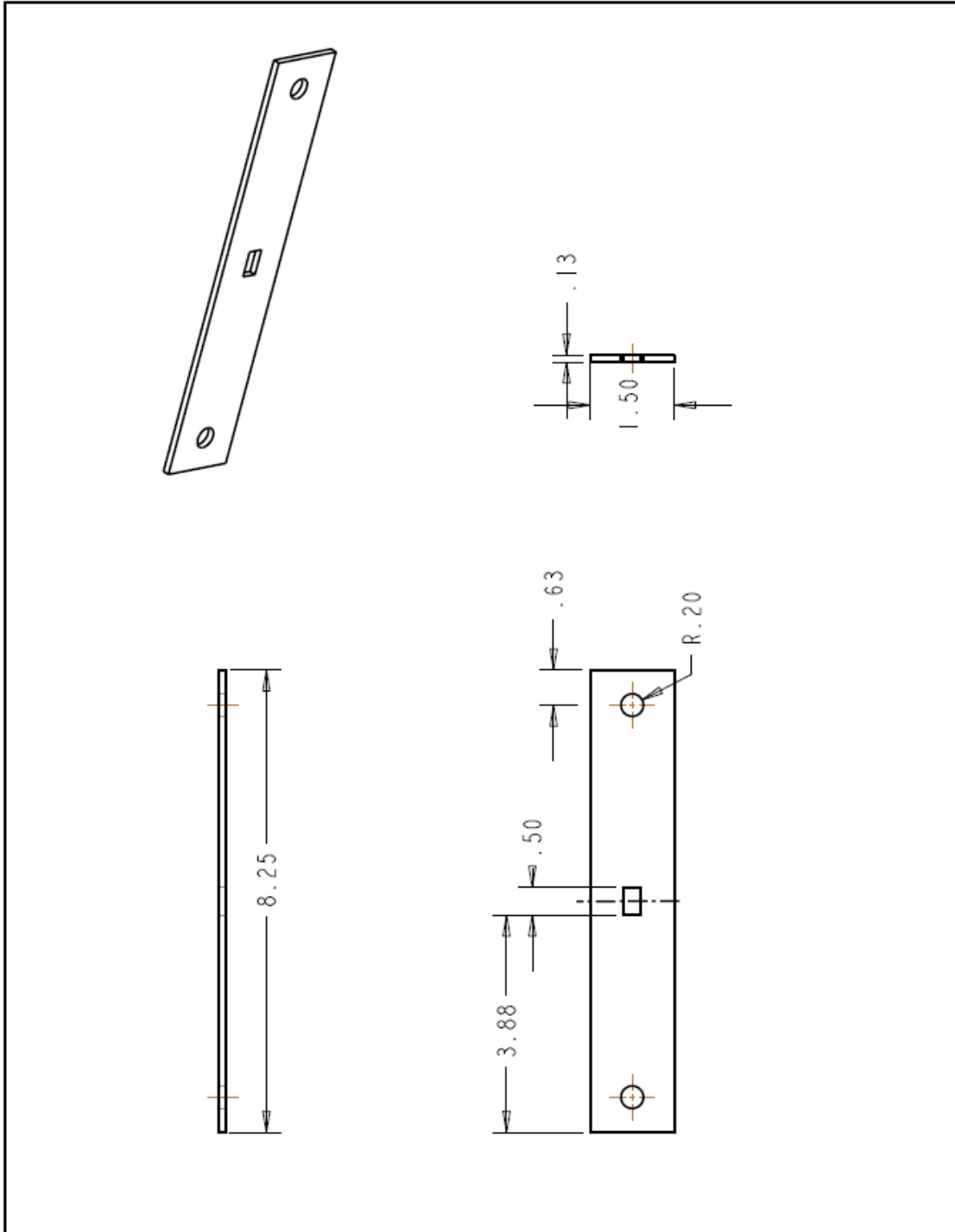
Pressure chamber relief valve and pressure gage

Appendix B – Engineering Drawings of Articulation Rig

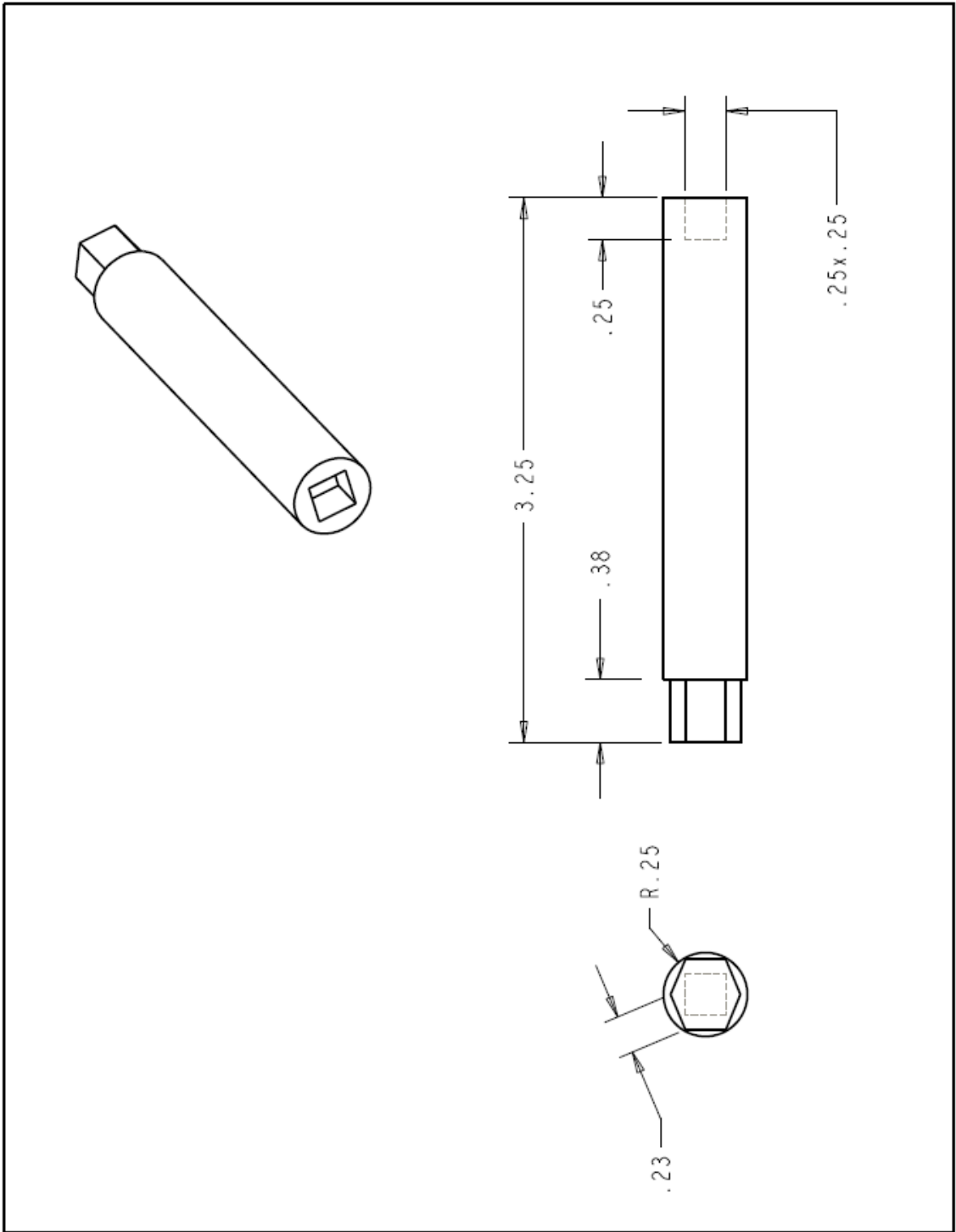
Three-dimensional models of the components of the elbow articulation rig were created (one each for the brace, the wrist plate, and the wrench adapter). These models were created using Pro/ENGINEER design software, and engineering drawings were produced from those models. These drawings are included in this appendix (all dimensions are in inches).



Engineering drawing of the EMU articulation rig brace



Engineering drawing of the EMU articulation rig wrist plate



Engineering drawing of the EMU articulation rig wrench adapter

Appendix C – Torque Wrench Data Collection and Retrieval Methods

The following methods were used to collect and retrieve data using the TECHMEMORY™ TECH1FRM240 electronic torque wrench:

Data Collection (the wrench can store up to 1,000 data points at one time):

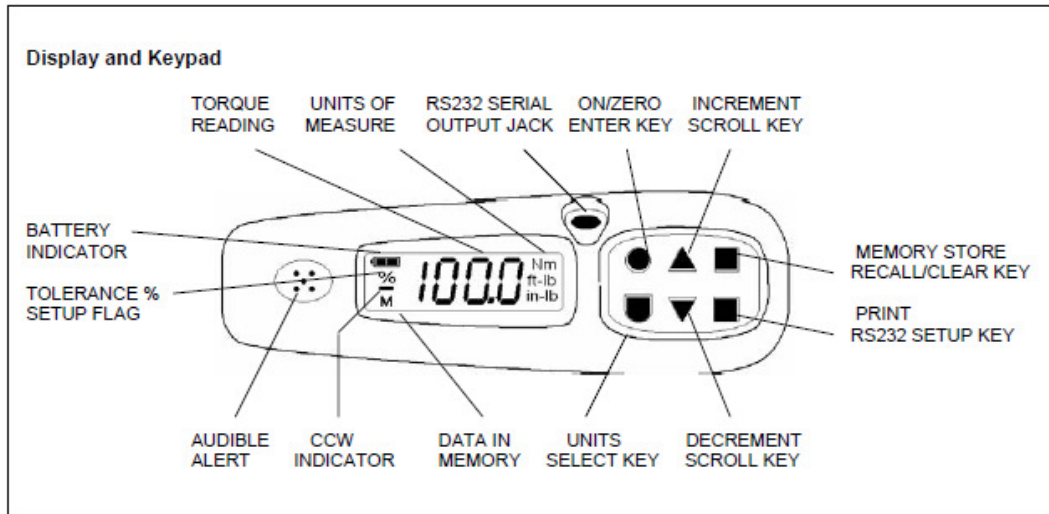
1. Attach a 7/16” socket to the wrench’s ¼” drive
2. Turn on the wrench by pressing the upper-left button on the wrench display (“I”)
3. Mount the wrench to the arm articulation rig
4. Flex the arm to the desired angle, then release the load (the display should read a static value representative of the peak torque reached) – DO NOT reapply torque, as this will cause the previous peak value to be erased
5. Store the torque data by pressing the upper-right button on the wrench display (“M”) while the peak torque value is still displayed

Data Retrieval:

1. Install the included TORQLOG™ software on a Microsoft Office-ready PC
2. Open a new Excel spreadsheet
3. Open the TORQLOG™ program – a small window should appear on screen
4. Connect the TECH1FRM240 wrench to the PC using the included serial port cable
5. Turn on the wrench by pressing the upper-left button on the wrench display (“I”)
6. Select the cell in the spreadsheet where you would like the data to begin (make sure you have at least 3 columns and enough rows free for each data point to be retrieved, as they will overwrite any existing data in those cells)
7. Press the lower-right button on the wrench display (the icon resembling a piece of paper) to copy all stored data points to the spreadsheet
 - a. Three pieces of information will be recorded for each data point – data point number, torque value, and torque units

More detailed operator instructions are included below, and were provided by SnapOn.com (Snap-On, 2008):

OPERATOR INSTRUCTION MEMORY MODELS



1. POWER ON - With no torque applied, push the "ON/ZERO" key – the wrench will self-test and then show the torque preset value.

On "D" models the torque preset value is shown for two seconds and then the display shows "0000."

2. UNITS SELECT - Push the **UNITS** key – to select "Nm," "ft lb," or "in lb."

3. PRESET ADJUST - Use the **INCREMENT** and **DECREMENT** keys to set the torque preset value. (Display will roll-over at each end).

*On "D" models, momentarily push the **ON/ZERO** key while holding down the **INCREMENT** key until the display flashes the torque preset value. Use the **INCREMENT** and **DECREMENT** keys to change the torque preset value. Push the **ON/ZERO** key to enter the new torque preset value and return to measurement mode.*

4. TOLERANCE ADJUST ("D" models only)

*Momentarily push the **ON/ZERO** key while holding down the **DECREMENT** key until the display flashes tolerance percent. Use the **INCREMENT** and **DECREMENT** keys to change the tolerance value between 1% and 16%. Push the **ON/ZERO** key to enter the new tolerance value and return to measurement mode.*

5. APPLY TORQUE SLOWLY until **audible** alert is heard and **vibration** alert is felt in the handle. **DO NOT APPLY LOAD TO THE ENDCAP.** The display will **TRACK** applied torque until load is released.

6. On load release, the **PEAK** torque value is displayed, flashing, for 10 seconds or until torque is re-applied or any key is pushed.

7. To **STORE** the PEAK reading, momentarily push the **MEMORY** key while the **PEAK** display is flashing.

MEMORY FUNCTION DETAIL

The **TECHMEMORY™** wrench will store, recall and download data to a computer or printer via RS232 true standard. A download software disk is included with the wrench for use with an IBM PC running WINDOWS or NT operating system. Refer to the **TORQLOG™** disk for PC installation instructions. Refer to your serial printer instruction manual for installation instructions - see *Setup serial baud rate* below.

Two Excel templates are provided on the **TORQLOG™** disk for user convenience. These should be copied and renamed, and are intended to be changed to suit the user's needs. NOTE: *Snap-on Tools does not provide technical support for these templates.* Use the **DOWNLOAD** Template to print the previously stored data list from the wrench. The **PRINT** function of the wrench sends out the number of the reading, the torque value and the units of measure. Use the **DATE-TIME** Template to automatically create a **DATE** and **TIME** stamp for each reading, while the wrench is connected to the computer. Individual readings are both stored in the wrench and are sent out the serial port simultaneously. Only the torque value and the units of measure are sent out during the store function.

STORE - Momentarily push the **MEMORY** key to store PEAK readings captured on the flashing display. The audible alert will sound once and the reading will be stored and numbered in memory and the reading will be sent out the RS232 port simultaneously. The "**M**" indicator will turn on when at least one reading is stored in memory.

RECALL - To review the data in memory, push and hold the **MEMORY** key for three seconds. The last reading will be displayed alternating with its memory location number. Use the **INCREMENT** and **DECREMENT** keys to scroll through the data list. Push **ON/ZERO** key to return to measurement mode.

CLEAR - To clear a reading, enter the **RECALL** mode as above. Scroll to the memory location number that you want to clear and hold the **MEMORY** key for three seconds. The display will show "**CLr**" for one second and decrement to the next reading. If this was not the last reading stored, all subsequent readings will shift down one memory location. Push **ON/ZERO** key to return to measurement mode.

CLEAR ALL - To clear the entire data list, enter the **RECALL** mode as above. Hold the **MEMORY** key and the **INCREMENT** key simultaneously for three seconds. The "**M**" indicator will turn off and the wrench will revert to measurement mode.

PRINT - To send the entire data list out the RS232 port, push the **PRINT** key momentarily. The audible alert will sound twice and the display will read "**SEnd**" until the data stream is finished. The wrench will then revert to measurement mode.

Setup serial baud rate:

Note: RS232 protocol is true, 8 data bits, 1 stop bit, carriage return delay is 600 mS and character delay is 14 mS. Default is 9600 baud. Push the **ON/ZERO** key to exit the setup mode at any time without changing previous baud setup.

To change output baud rate, push and hold the **PRINT** key for three seconds to enter setup mode. Display shows previously programmed baud rate flashing and **UNITS** display is off. Use the **INCREMENT** and **DECREMENT** keys to select the required baud rate, "0012"=1200, "0024"=2400, "0048"=4800, "0096"=9600 or "0192"=19.2K. Push the **PRINT** key momentarily to accept the new baud rate. Audible alert will sound once and display will revert to measurement mode.

Appendix D – Specifications of TECHMEMORY™ TECH1FRM240 SnapOn Torque Wrench

The specifications for the TECHMEMORY™ TECH1FRM240 electronic torque wrench used to determine the EMU elbow torque vs. angle relationships, including its certificate of calibration, are included in this appendix (Snap-On, 2008):

SnapOn TECH1FRM240 Specifications

Product Specifications	
Stock #	TECH1FRM240
Name	Torque Wrench, Electronic, TECHWRENCH, Flex Ratchet, 24 to 240 in. lbs., 1/4" drive
Price**	\$689.00
Brand	Snap-on
Country Of Origin	USA
Square Drive, inches	1/4
Head Type	Flex Head
Gear Teeth	36
Gear Action	10°
Range, in. lb.	24-240
Range, ft. lb.	2-20
Range, N•m	2.7-27.12
Head Depth, inches	7/16
Head Width, inches	7/8
Operating Temperature	40-110°F (5-42°C)
Storage Temperature	0 to 122°F (-20 to 50°C)
Humidity	up to 90% non-condensing
Housing Color	Red
Ratchet Service Kit	RKRT936
Memory Capacity	1,000 peak reading - reading number, torque value, units of measure
Torque Setting Resolution	0.1 ft. lb. (0.1 N•m, 1 in. lb.)
Digital Download	RS232 (True) - selectable 1200 to 19.2K Baud
Power	3 "AA" batteries (included)
Overall Length, inches (mm)	15 (381)
Weight, lbs. (kg)	1.7 (.77)

TECHMEMORY™ SPECIFICATIONS MEMORY MODELS

Display Capacity and Resolution

Model	Square Drive	Range ft-lb	in-lb	Nm
TECH1M	1/4in	2.00-20.00	24.0-240.0	2.80-28.00
TECH2M	3/8in	5.0-100.0	60-1200	6.7-135.6
TECH3M	1/2in	25.0-250.0	300-3000	33.9-339.0
TECH4M	3/4in	60.0-600.0	720-7200	81.3-813.6

Note: "SJ" models display Nm units of measure only

Display Modes SETUP (PRESET), TRACK, PEAK HOLD, MEMORY RECALL

Accuracy (72°F)	CW	CCW
Fixed or Flex	+/-1%	+/-1.5% of reading, 20% to 100% of full scale
Ratchet Head (non-flexed)	+/-2%	+/-3% of reading, 10% to 19% of full scale
	+/-4%	+/-8% of reading, 5% to 9% of F.S. (TECH2 only)
	CW	CCW
J, Y, X, and Z Interchangeable Tool Heads	+/-4%	+/-6% of reading, 20% to 100% of full scale
	+/-8%	+/-12% of reading, 10% to 19% of full scale
	+/-16%	+/-20% of reading, 5% to 9% of F.S. (TECHY only)

Torque Setting Resolution	TECH1M	TECH2M	TECH3M	TECH4M
	0.1 ft-lb, 0.1 Nm, 0.01 in-lb	1.0 ft-lb, 1.0 Nm, 1 in-lb.	1.0 ft-lb, 1.0 Nm, 1 in-lb.	1.0 ft-lb, 1.0 Nm, 1 in-lb.

Tolerance Setting fixed* at -2% of torque setting (all except "D" models)
adjustable (+ and -) 1 to 16% of torque setting ("D" models)
*Output alert occurs 2% below setting for ergonomic compensation

Output Alert	Audible tone and Vibrating Handle
Memory Capacity	1000 readings - Reading number, torque value, units of measure
Digital Download	RS232 (True) - selectable 1200 to 19.2K Baud

Sealed Key Pad

ON/ZERO - auto self check (not a calibration check) - zero tare

UP - increments torque setting, tolerance and scrolls memory

DOWN - decrements preset torque setting and scrolls memory

UNITS - selects Nm, ft-lb, or in-lb, display

MEMORY - store, recall and clear peak readings

PRINT - RS232 download to computer or serial printer and port setup

Operating Temperature - 5 to 42°C (40 to 110°F)

Storage Temperature - -20 to 50°C (-1 to 122°F)

Humidity - up to 90% non-condensing

Dimensions -	length	weight	length	weight (w/o tool head)
TECH1FRM	15 in	1.7 lbs.	TECH1JM	13.5 in 1.6 lbs.
TECH2FRM	17 in	2.2 lbs.	TECH2YM	15.5 in 1.9 lbs.
TECH3FRM	26 in	3.7 lbs.	TECH3XM	23.5 in 2.9 lbs.
TECH4FRM	48 in	10.0 lbs.	TECH4ZM	45.5 in 7.0 lbs.

Battery - three "AA" Alkaline cells, up to 80 hours continuous operation.

Auto Shut-off - after 2 minutes idle

Appendix E – Detailed Pressure Sensor Specifications

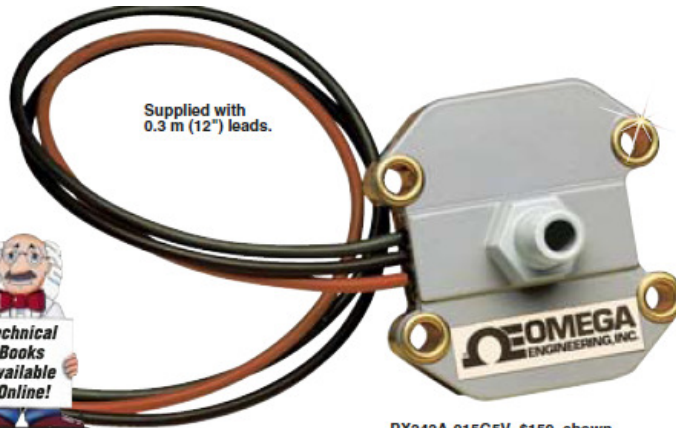
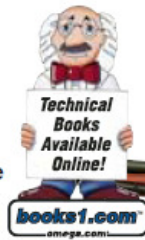
The detailed specifications for the pressure sensors used in the prototype active pressure regulation system are included in this appendix (Omega.com, 2008):

PX240A Series
5 to 250 psig
0.5 to 16 bar

Starts at
\$149
Imperial
Ranges



- ✓ Silicon Diaphragm
- ✓ Stainless Steel Case
- ✓ Buna-N Seals
- ✓ 8 Vdc Excitation
- ✓ 0.3 m (12") Lead Wires
- ✓ -40 to 85°C (-40 to 185°F)
- ✓ 1 to 6 Vdc Output
- ✓ Temperature Compensated



PX242A-015G5V, \$159, shown close to actual size.

SPECIFICATIONS

Excitation: 8 Vdc regulated, 7 to 16 Vdc

Output: 1 to 6 Vdc @ 8 Vdc into 800 Ω min

Linearity: ±0.25% linearity and hysteresis combined

Repeatability: ±0.1%

Zero Balance: 1.0 Vdc ±0.05; PX243, 3.5 Vdc ±0.05

Compensated Temperature Range: -27 to 63°C (-17 to 145°F)

Operable Overpressure: 2x FS

Response Time: 1 ms

Gage Type: Solid state piezoresistive

Body Material: Stainless steel

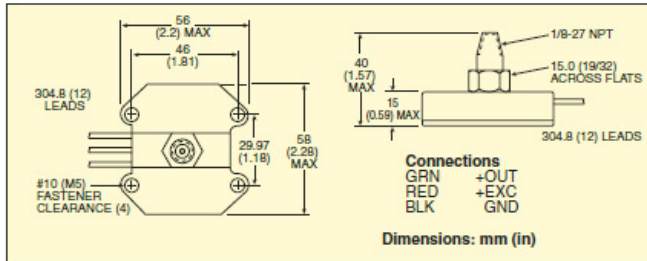
Diaphragm Material: 2.5 mm (0.10") square silicon sensor chip with Buna-N O-ring

Media Compatibility: Limited to non-caustic media that will not attack stainless steel, silica, borosilicate glass or Buna-N seal

Pressure Port: 1/8-27 NPT male

ACCESSORY

MODEL NO.	PRICE	DESCRIPTION
PE-1001	\$250	Reference Book: Instrumentation and Control Fundamentals and Applications



Connections
GRN +OUT
RED +EXC
BLK GND

Dimensions: mm (in)

☐ MOST POPULAR MODELS HIGHLIGHTED!

To Order (Specify Model Number)

RANGE		MODEL NO.	PRICE	COMPATIBLE METERS*
-15 to 0 psig	-1 to 0 bar	PX241A-15NG5V	\$159	DPiS8, DP41-E, DP25B-E
0 to 5 psig	0 to 0.34 bar	PX242A-005G5V	159	DPiS8, DP41-E, DP25B-E
0 to 15 psig	0 to 1.0 bar	PX242A-015G5V	159	DPiS8, DP41-E, DP25B-E
0 to 30 psig	0 to 2.1 bar	PX242A-030G5V	159	DPiS8, DP41-E, DP25B-E
0 to 60 psig	0 to 4.1 bar	PX242A-060G5V	159	DPiS8, DP41-E, DP25B-E
0 to 100 psig	0 to 6.9 bar	PX242A-100G5V	149	DPiS8, DP41-E, DP25B-E
0 to 150 psig	0 to 10.3 bar	PX242A-150G5V	149	DPiS8, DP41-E, DP25B-E
0 to 250 psig	0 to 17.2 bar	PX242A-250G5V	149	DPiS8, DP41-E, DP25B-E
±2.5 psig	±0.17 bar	PX243A-2.5BG5V	159	DPiS8, DP41-E, DP25B-E
±5.0 psig	±0.34 bar	PX243A-05BG5V	159	DPiS8, DP41-E, DP25B-E
±15 psig	±1.0 bar	PX243A-15BG5V	159	DPiS8, DP41-E, DP25B-E

Comes with complete operator's manual.

* See section D for compatible meters.

Ordering Examples: PX242A-015G5V, stainless steel transducer with 0 to 15 psig range and 1/8 NPT fitting, \$159.

B-71

(Omega.com, 2008)

Appendix F – Detailed Solenoid Valve Specifications

The detailed specifications for the solenoid valves used to control the prototype active pressure regulation system are included in this appendix (Omega.com, 2008):



OMEGA-FLO® 2-WAY GENERAL PURPOSE SOLENOID VALVES





SV3308, \$67, shown larger than actual size.



- Ideal for Compressed Air, Inert Gas, Water and Synthetic Oils
- Available in Normally Open or Normally Closed
- Process Temperature to 137°C (280°F)
- 120 Vac Standard (DC Coils are Optional)
- All Coils are CE

SV-3300 Series 2-way solenoid valves are direct-acting valves featuring brass, stainless steel construction and Viton® seal material. The temperature range from -10 to 137°C (14 to 280°F) is ideal for neutral media such as compressed air, inert gases, water, and synthetic oils.

Electrical connection options are a 13 mm (½") conduit plug or strain relief connector.

SPECIFICATIONS

Mounting Position: Any (preferably with solenoid system upright)

Maximum Process Temperature: 137°C (280°F) due to Viton® O-ring

Maximum Ambient Temperature: Coil dependent (see ratings on coils)

Voltage Tolerance: ±10%

Opening Time (msec):
AC: 10 to 20,
DC: 20 to 80 depending on orifice and pressure

Closing Time (msec):
AC and DC: 20 to 30 approximately

Cycling Rate: Approx 1000 cpm

Duty Cycle: Continuous (100%)

Coil Molding Material:
Black Polyester (Class F):
 SV8COIL-115AC
 SV8COIL-24DC/60HZ
 SVC0IL-24AC/50 to 60Hz
 SV8COIL-220AC
Black Polyamide (Class F):
 SV8COIL-12DC, SV8COIL-24DC,
 all 12 W coils



SV-CC, \$7, ½" conduit connector, shown larger than actual size.

SV-CGC, \$7, cable grip connector, shown larger than actual size.

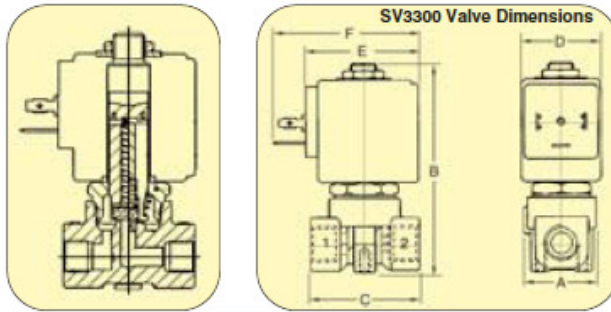
Black Polyphenylsulfide (Class H):
 SV8COIL-115/60HZ

Black Epoxy Resin (Class H):
 All 14 W coils

COIL SPECIFICATIONS		
WATT	INRUSH VA	HOLDING VA
8	25	14.5
12	36	23
14	43	27

MATERIALS OF CONSTRUCTION	
Body	Brass
Armature Tube	Stainless steel 300
Fixed Core	Stainless steel 400
Plunger	Stainless steel 400
Spring	Stainless steel 300
Shading Ring	Copper
Orifice	≤¼" Stainless steel 300
	>¼" brass

C-127



VALVE DIMENSIONS			
NPT SIZE	A	B	C
1/8"	1 3/32"	1 1/16"	1 1/8"
1/4"			

COIL DIMENSIONS			
WATT	D	E	F
8	1 3/16"	1 21/32"	2 1/8"
12	1 1/8"	1 9/16"	2 3/8"
14	2 1/16"	2 7/32"	2 21/32"

To Order (Specify Model Number)

MOST POPULAR MODELS HIGHLIGHTED!

							OPERATING PRESSURE				
NORMALLY CLOSED		NORMALLY OPEN					COILS		M.O.P.D.*		
MODEL NO.	PRICE	MODEL NO.	PRICE	PIPE SIZE	ORIFICE SIZE	CV FLOW FACTOR	POWER (watt)	OPTIONAL COIL	MIN psi	AC psi	DC psi
SV3301	\$67	SV3301-NO	\$92	1/8"	1/16"	0.10	8	—	0	435	260
SV3302	67	SV3302-NO	92	1/8"	3/64"	0.14	8		0	315	230
				1/8"	3/64"	0.14		12/14	0	505	435
SV3303	67	SV3303-NO	92	1/8"	1/32"	0.22	8		0	200	130
				1/8"	3/32"	0.22		12/14	0	435	360
SV3304	67	SV3304-NO	92	1/8"	1/16"	0.28	8		0	145	85
				1/8"	1/16"	0.28		12/14	0	360	290
SV3305	67	SV3305-NO	92	1/8"	3/16"	0.45	8		0	70	20
				1/8"	3/16"	0.45		12/14	0	170	85
SV3306	67	SV3306-NO	92	1/4"	1/16"	0.10	8	—	0	435	260
SV3307	67	SV3307-NO	92	1/4"	3/64"	0.14	8		0	315	230
				1/4"	3/64"	0.14		12/14	0	505	435
SV3308	67	SV3308-NO	92	1/4"	3/32"	0.22	8		0	200	130
				1/4"	1/32"	0.22		12/14	0	435	360
SV3309	67	SV3309-NO	92	1/4"	1/16"	0.28	8		0	145	85
				1/4"	1/16"	0.28		12/14	0	360	290
SV3310	67	SV3310-NO	92	1/4"	3/16"	0.45	8		0	70	20
				1/4"	3/16"	0.45		12/14	0	170	85
SV3311	67	SV3311-NO	92	1/4"	1/32"	0.63	8		0	50	10
				1/4"	1/32"	0.63		12/14	0	100	40

Comes with complete instruction sheet and cable grip connector.
 * Maximum operational pressure differential. † BSP threads. In most cases BSP and NPT are interchangeable in this size.
 Ordering Examples: SV3309, 1/4" NPT normally closed valve, \$67. SV3303-NO: 1/8" normally open valve, \$92.

ACCESSORIES

MODEL NO.	PRICE	DESCRIPTION
CONNECTORS		
SV-CGC	\$7	Cable grip connector
SV-CC	7	1/2" conduit connector
COILS		
SV8COIL-115AC	16	Replacement 8W coil for 110 to 120 Vac/50 to 60 Hz 154°C (310°F) (Class F)
SV8COIL-12DC	16	8W coil for 12 Vdc 154°C (310°F) (Class F)
SV8COIL-24DC	16	8W coil for 24 Vdc 154°C (310°F) (Class F)
SV8COIL-24AC/60HZ	16	8W coil for 24 Vac/50 to 60Hz 182°C (360°F) (Class F)
SV8COIL-220AC	16	8W coil for 220 to 240 Vac/50 to 60 Hz 154°C (310°F) (Class F)
SV8COIL-115/60HZ	23	8W coil for 115 Vac/60 Hz 182°C (360°F) (Class H)
SV12COIL-120/60HZ	23	12W coil for 120 Vac/60 Hz 154°C (310°F) (Class F)
SV12COIL-12DC	50	12W coil for 12 Vdc 154°C (310°F) (Class F)
SV12COIL-24DC	23	12W coil for 24 Vdc 154°C (310°F) (Class F)
SV14COIL-24DC	50	14W coil for 24 Vdc 182°C (360°F) (Class H)
SV14COIL-24/50-60HZ	50	14W coil for 24 Vdc/50 to 60Hz 182°C (360°F) (Class H)
SV14COIL-12DC	50	14W coil for 12 Vdc 182°C (360°F) (Class H)
FW-306	125	Reference Book: Valve Handbook

C-128

(Omega.com, 2008)

Appendix G – First-time Regulator System Initialization and Calibration

The following steps were taken to initially prepare and calibrate the pressure regulator system:

Internal calibration of the DAQ board:

1. Install the Instacal software package included with the Measurement Computing USB-1408FS DAQ board on the laptop to be used for system control.
2. Connect the DAQ board to the PC (it should be recognized by Windows and/or the Instacal software).
3. Start the Instacal software.
4. If the USB-1408FS does not automatically appear on the list of detected PC boards, add it using the toolbar button.
5. Navigate the “Calibrate” and “Test” menus to calibrate and test the board (making sure to follow all instructions issued by the software).
6. Close the Instacal software.

Simulink signal calibration of the pressure sensors:

1. Connect the pressure sensors and valve/relay subsystems to the appropriate analog input and digital output channels of the DAQ board, and connect the board to the laptop.
2. Connect the sensors (in parallel) and valve/relay subsystems (in parallel) to the two variable DC power supplies, ensuring the power supplies are in the off position.
3. Turn on the power supplies, and set them to the appropriate voltage levels (8V DC for the pressure sensors, 12V DC for the relays/valves).
4. Open MATLAB and Simulink on the laptop, and load the control model.
5. Set the voltage-pressure conversion block values to their theoretical values (for example, the HPR outputs between 1-6V DC which corresponds to 0-60 PSI,

- meaning that to convert the signal from voltage to pressure the signal must first be subtracted by 1, then multiplied by 12). Do this for all 3 input signals.
6. Run the simulation, and check the output pressure signals of each channel: if any of the signals do not read 0 PSI, then physically modify the input voltage until the signal approaches this value.
 7. If modification of the input voltage does not rectify the discrepancy, it will be necessary to modify the signals using the Simulink model (it might be the case that modification of the input voltage corrects one signal while shifting another away from the desired value). These modifications can be accomplished by tweaking the constant source values used to convert each voltage signal.
 8. Check the calibration of the sensors by pressurizing the HPR and LPR using the air compressor and vacuum pump and comparing the values recorded in Simulink to those of the physical pressure gauges installed on both reservoirs. If there is a discrepancy, troubleshoot as necessary.

Appendix H – Regular Pressure Regulator Start-Up Steps

Assuming the regulator system has been properly initialized and calibrated (using the steps described in Appendix G), the following steps should be followed each time the regulator is to be used:

1. Make sure the sensors and valves/relays are connected to the DAQ board, and that the DAQ board is connected to the laptop
2. Make sure the sensors and valves/relays are connected to the variable DC power supplies
3. Open MATLAB and Simulink on the laptop, and load the control model.
4. Turn on the power supplies, and make sure the voltage is set to the calibrated values determined when the system was initially calibrated.
5. Run the model once to verify the calibration is still correct (if it is not, repeat steps 7 and 8 of Appendix G to resolve the calibration discrepancy).
6. If the calibration is still correct, then pressurize the HPR and LPR to the desired values, using the physical gauges on the reservoirs as guides.
7. Run the model again to verify the reservoir sensors are functioning properly
8. Double check to ensure that all openings to the primary chamber are plugged, that all release valves are closed, and that the test syringe is connected and in the desired starting position (either extended or compressed).
9. Input the test duration (in seconds) to the model menu, and click the “Start Simulation” button to begin the test.
10. Physically perform the desired test using the test syringe.

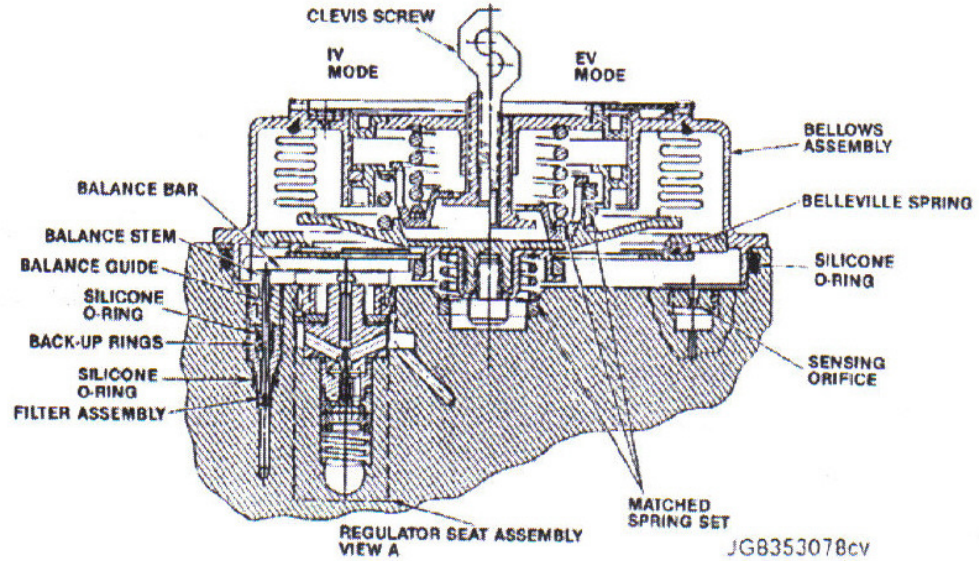
Appendix I – Current EMU Pressure Regulator

A schematic of the dual mode pressure regulator currently used in the EMU is included in this appendix.

ITEM 113D

DUAL MODE REGULATOR

Controls suit pressure to 0.9 ± 0.5 or 4.3 ± 0.1 psig as desired.



(Hamilton-Sundstrand, 2003)

BIBLIOGRAPHY

Abramov, I., Stoklitsky, A., Barer, A., and Filipenkov, S. (1994). "Essential Aspects of Space Suit Operating Pressure Trade-Off". International Conference on Environmental Systems. Friedrichshafen, Germany, Society of Automotive Engineers.

Annis, J., and Webb, P. (1971). "Development of a Space Activity Suit". N. C. R. CR1891.

Bolden, C. (2010). "Statement by Charlie Bolden, NASA Administrator." NASA Budget Press Conference Retrieved March 20, 2010, from http://www.nasa.gov/pdf/420994main_2011_Budget_Administrator_Remarks.pdf.

Buckey, J. (2006). Space Physiology. New York, NY, Oxford University Press.

Buxbaum, K. (2010). Personal Communication. Cambridge, MA

Carr, C. (2001). "Distributed Architectures for Mars Surface Exploration". Cambridge, MA, Massachusetts Institute of Technology. S.M Thesis.

Carr, C. (2005). "The Bioenergetics of Walking and Running in Space Suits". Cambridge, MA, Massachusetts Institute of Technology. ScD Thesis.

Corner, R., and Levy, S. (1963). "Deflections of an inflated circular cylindrical cantilever beam." AIAA Journal 1(7): 1652-1655.

COSPAR (1969). COSPAR DECISION No. 16, COSPAR Information Bulletin. **50**: 15-16.

COSPAR (2002). COSPAR Planetary Protection Policy, COSPAR/IAU Workshop on Planetary Protection.

COSPAR (2008). Amendments to COSPAR Planetary Protection Policy, COSPAR/IAU Workshop on Planetary Protection. Retrieved from <http://cosparhq.cnes.fr/Scistr/PPPpolicy%2820-July-08%29.pdf>

Debus, A. (2008). "Planetary Protection for Sample Return Missions", CNES Planetary Protection.

Digi-Key. (2008). "Crydom Proportional Controller." Retrieved July 9, 2008, from <http://rocky.digikey.com/weblib/Crydom/Web%20Photos/10PCV24.jpg>

Digi-Key. (2008). "Relay SSR PNL MNT - DC60S3-B." Retrieved July 8, 2008, from <http://parts.digikey.com/1/parts/758250-relay-ssr-pnl-mnt-dc60s3-b.html>.

Dionne, S. (1991). "AX-5, Mk III, and Shuttle Space Suit Comparison Test Summary". Moffett Field, CA, NASA EVA Technical Document 91-SAE/SD-004.

Emerson Industrial. (2009). "Engineering Information: Flow data, flow factor and orifice size." Retrieved June 3, 2009, from http://detector-gas-systems.web.cern.ch/detector-gas-systems/downloads/kv_calc_doc.pdf.

Engineering Toolbox. (2005). "PVC Pipes - Pressure Ratings." Retrieved February 8, 2009, from http://www.engineeringtoolbox.com/pvc-cpvc-pipes-pressures-d_796.html.

ESA. (2002). "No bugs please, this is a clean planet!" Retrieved April 1, 2010, from http://www.esa.int/esaCP/ESAUB676K3D_index_0.html

Fay, J., and Steele, C. (1999). "Forces for rolling and asymmetric pinching of pressurized cylindrical tubes." *Journal of Spacecraft and Rockets* 36(4): 531-537.

Fay, J., and Steele, C. (2000). "Bending and symmetric pinching of pressurized tubes." *International Journal of Solids and Structures* 37: 6917-6931.

Frazer, A., Pitts, B., Schmidt, P., Hoffman, J., Newman, D. (2002). "Astronaut Performance: Implications for Future Spacesuit Design." International Astronautical Federation.

Futron Corp. (2002). "Space Tourism Market Study: Orbital Space Travel & Destinations with Suborbital Space Travel". Bethesda, MD, Futron Corporation.

Futron Corp. (2006). "Suborbital Space Tourism Demand Revisted". Bethesda, MD, Futron Corporation.

Hamilton-Sundstrand (2003). "NASA Space Shuttle Extravehicular Mobility Unit (EMU) Life Support Subsystem (LSS) and Space Suit Assembly (SSA) Data Book (Rev. H)."

Harris, G. (2009). Personal Communication. Savannah, GA.

Hodgson, E. (2008). Personal Communication. Cambridge, MA.

Hoffman, J. (2008). Personal Communication. Cambridge, MA.

HWB. (2008). "Universal Serial Bus (USB)." Retrieved July 9, 2008, from http://www.hardwarebook.info/Universal_Serial_Bus_%28USB%29.

Iberall, A. (1964). "The Use of Lines of Nonextension to Improve Mobility in Full-Pressure Suits." Aerospace Medical Research Laboratories, Wright Patterson Air Force Base, Ohio.

- Iberall, A. (1970). "The experimental design of a mobile pressure suit." *Journal of Basic Engineering* (June, 1970): 251-264.
- Jordan, N., Saleh, J., Newman, D. (2006). "The extravehicular mobility unit: A review of environment, requirements, and design changes in the US spacesuit." *Acta Astronautica* 59(12): 1135-1145.
- Judnick, D. (2007). "Modeling and Testing of a Mechanical Counterpressure BioSuit System". Cambridge, MA, Massachusetts Institute of Technology. S.M Thesis.
- Kozloski, L. (1994). "U.S. Space Gear: Outfitting the Astronaut". Smithsonian Institution Press, D.C..
- Larson, W. J., Ed. (1999). "Human Spaceflight Mission Analysis and Design". Space Technology Series, McGraw-Hill.
- Lukasiewicz, S., and Glockner, P. (1985). "Stability of lofty air-supported cylindrical membranes." *Journal of Structural Mechanics* 12(4): 543-555.
- Main, J. (1993). "Analysis and design of inflatable aerospace structures". Nashville, TN, Vanderbilt University. PhD Thesis.
- Main, J., Peterson, S., and Strauss, A. (1995). "Beam-type bending of space-based inflatable structures." *Journal of Aerospace Engineering* 8(2): 120-125.
- MathWorks. (2008). "Data Acquisition Toolbox 2.16." Retrieved July 9, 2008, from <http://www.mathworks.com/products/daq/>.
- Matty, J., and Aitchison, L. (2009). "A Method for and Issues Associated with the Determination of Space Suit Joint Requirements". International Conference on Environmental Systems. Savannah, GA, Society of Automotive Engineers.
- Measurement Computing. (2008). "USB-1408FS - 14-Bit USB Multifunction Module with 8 Analog Inputs." Retrieved July 9, 2008, from <http://www.mccdaq.com/usb-data-acquisition/USB-1408FS.aspx>.
- Menendez, V., Diener, M., and Baez, J. (1994). "Performance of EVA Suit Soft Flat Pattern Mobility Joints". International Conference on Environmental Systems. Friedrichshafen, Germany, Society of Automotive Engineers.
- Morgan, D., Wilmington, R., Pandya, A., Maida, J., and Demel, K. (1996). "Comparison of Extravehicular Mobility Unit (EMU) Suited and Unsuited Isolated Joint Strength Measurements". NASA TP-3616. Houston, TX.
- NASA. (1969). "Buzz Aldrin on the Moon (Apollo 11)." Retrieved March 30, 2010, from http://starchild.gsfc.nasa.gov/docs/StarChild/space_level2/aldrin.html.

NASA. (1972). "Astronaut Falling Down on Lunar Surface." Retrieved March 25, 2010, from http://history.msfc.nasa.gov/saturn_apollo/videos.html.

NASA. (1988). "AX-5 Space Suit (Hardsuit) attached to donning stand." Retrieved March 29, 2010, from <http://ails.arc.nasa.gov/>

NASA. (2008). "Spacesuits and Spacewalks." Retrieved March 30, 2010, from http://www.nasa.gov/audience/foreducators/spacesuits/home/clickable_suit_nf.html.

NASA. (2008). "Planetary Protection: All of the Planets, All of the Time." Retrieved March 3, 2010, from <http://planetaryprotection.nasa.gov/pp/index.htm>.

NASA. (2009). "Spacewalk!" Retrieved March 25, 2010, from <http://aerospacescholars.jsc.nasa.gov/HAS/Modules/Shuttle-to-Station/3/6.cfm>.

Newman, D. and Barratt, M (1997). Chapter 22: "Life Support and Performance Issues for Extravehicular Activity (EVA)," *Fundamentals of Space Life Sciences*, S. Churchill, ed., Krieger Publishing Co., Melbourne, Florida, 1997.

Newman, D., Pitts, B., Brensinger, C., Saleh, J., Carr, C., Schmidt, P. (2001). "Astronaut Bio-Suit for Exploration Class Missions". NIAC Phase I Report. Cambridge, MA, MIT.

Newman, D., Hoffman, J., Bethke, K., Carr, C., Jordan, N., Sim, L., Campos, N., Conlee, C., Smith, B., Wilcox, J., and Trotti, G. (2005). "An Astronaut 'Bio-Suit' System for Exploration Missions. NIAC Annual Meeting". Broomfield, CO.

Newsome, S., Yamamoto, N., Grindle, A., Holschuh, B., Ono, M., Weigel, A. (2009). "Analysis of US Policy Options for the Future of the International Space Station". AIAA Space 2009, Pasadena, CA.

NRC (1992). "Biological Contamination of Mars: Issues and Recommendations". Washington, D.C., National Academy Press.

NRC (2000). "Preventing the Forward Contamination of Europa". Washington, D.C., National Academy Press.

NRC (2006). "Preventing the Forward Contamination of Mars". Washington, D.C., National Academy Press.

Omega.com. (2008). "Low Pressure, Bi-Directional Pressure and Vacuum Sensors." Retrieved February 8, 2009, from <http://www.omega.com/ppt/pptsc.asp?ref=PX242&Nav=preb03>.

Omega.com. (2008). "Valves, Regulators and I/P Converters." Retrieved June 3, 2008, from <http://www.omega.com>

- Orbital. (2010). "Taurus II Fact Sheet." Retrieved March 25, 2010, from <http://www.orbital.com/TaurusII/>
- Scheuring, R. (2007). *The Apollo Medical Operations Project: Recommendations to Improve Crew Health and Performance for Future Exploration Missions and Lunar Surface Operations*". NASA/TM-2007-214755: 6-9.
- Schmidt, P. (2001). "An Investigation of Space Suit Mobility with Applications to EVA Operations". Cambridge, MA, Massachusetts Institute of Technology. PhD Thesis.
- Schmidt, P., Newman, D., and Hodgson, E. (2001). "Modeling Space Suit Mobility: Applications to Design and Operations". International Conference on Environmental Systems. Orlando, FL, Society of Automotive Engineers.
- Skoog, A., Abramov, I., Stoklitsky, A., and Doodnik, M. (2002). "The Soviet-Russian Space Suits: A Historical Overview of the 1960s". *Acta Astronautica* 51(1-9): 113-31.
- Snap-On. (2008). "Torque Wrench, Electronic, TECHWRENCH, Flex Ratchet, 24 to 240 in. lbs., 1/4" drive " Retrieved March 23, 2010, from <http://buy1.snapon.com>
- SpaceX. (2010). "Falcon 9 Overview." Retrieved March 25, 2010, from <http://www.spacex.com/falcon9.php>
- State.gov. (2001). "Narrative: Treaty on Principles Governing the Activities of States in the Exploration and Use of Outer Space, Including the Moon and Other Celestial bodies." Retrieved March 20, 2010, from <http://www.state.gov/www/global/arms/treaties/space1.html>
- UN. (1967). "Treaty on Principles Governing the Activities of States in the Exploration and Use of Outer Space, including the Moon and Other Celestial bodies." Retrieved March 25, 2010, from <http://www.oosa.unvienna.org/oosa/SpaceLaw/outerspt.html>
- UN. (1971). "Convention on International Liability for Damage Caused by Space Objects." Retrieved March 25, 2010, from http://www.unoosa.org/oosa/en/SpaceLaw/gares/html/gares_26_2777.html
- VirginGalactic. (2010). "Overview." Retrieved March 25, 2010, from <http://www.virgingalactic.com/overview/>
- Viscusi, K. (1995). *Economics of Regulation and Antitrust*. Cambridge, MA, MIT Press.
- Waldie, J. (2008). Personal Communication. Cambridge, MA.
- X-Prize. (2010). "Google Lunar X Prize." Retrieved March 25, 2010, from <http://www.googlelunarxprize.org/>



From the Russian Children's Book *Neznaika Na Lune* (*Neznaika on the Moon*)
(Kozloski, 1994)